Thermochronometric constraints on the thermal anatomy and evolution of an extensional accommodation zone and implications on exploration for extensional-type geothermal systems

By

Kyle E. Gorynski

Submitted to the graduate degree program in Geology and the Graduate Faculty of the University of Kansas in partial fulfillment of the requirements for the degree of Master of Science.

_____

Daniel F. Stockli (Co-Chairperson)

_____

J. Douglas Walker (Co-Chairperson)

_____

Anthony W. Walton

Date Defended: May 4th, 2011

The Thesis Committee for Kyle E. Gorynski

certifies that this is the approved version of the following thesis:

Thermochronometric constraints on the thermal anatomy and evolution of an extensional accommodation zone and implications on exploration for extensional-type geothermal systems

_____

Daniel F. Stockli (Co-Chairperson)

_____

J. Douglas Walker (Co-Chairperson)

Date approved: May 12th, 2011

ABSTRACT

Thermochronometric constraints on the thermal anatomy and evolution of an extensional transfer zone and implications on exploration for extensional-type geothermal systems

The northern Basin and Range province is characterized by a significantly elevated heat flow and geothermal gradient as a result of shallow volcanism and lithospheric stretching and thinning occurring in tandem throughout the Cenozoic. Along the western margin of the northern Basin and Range, in west-central Nevada, early to middle Miocene volcanism immediately preceded large-magnitude extension, which is accommodated by high degrees of footwall rotation in normal faults. The Wassuk Range (WR) footwall is one such example, where Miocene and younger extension was preceded by the extrusion of the ~15 Ma Lincoln Flat andesite, and subsequent extension resulting in footwall rotation (≥ 60°), as recognized in $^{40}Ar/^{39}Ar$ dated, pre- and syn-extensional Neogene volcanic and sedimentary rocks. The structural architecture of the southern WR is that of a terminating extensional fault system in that the degree of tilting and extension decreases southward into a series of right-lateral faults of the Mina Deflection (MD) accommodation zone. Apatite (AHe) and zircon (ZHe) thermochronologic data from ~9 – 4 km exhumed and exposed upper-crustal sections in the central and southern WR footwall preserve the thermal and tectonic evolution of the southern WR and MD accommodation zone. The entire WR and MD region underwent slow cooling (< 2 – 2.5° C/Ma) during the earliest Cenozoic related to the slow denudation of Mesozoic basement rocks. Middle Miocene heating overprinted much of the Paleogene cooling history towards the southernmost WR which was anomalously hot (≥ 65 ± 20 °C/km), and was the result of magmatic advection focused along the MD. The onset of rapid footwall exhumation in the Wassuk Range began at ~15 Ma, due to Basin and Range extension and again at ~3 – 4 Ma related to Walker Lane transtensional faulting.

Pliocene to recent Walker Lane transtensional structures are associated with a number of extensional-type geothermal systems. AHe ages along the modern WR range front and from a ~1.4 km deep borehole in the hanging-wall basin show evidence of young (< 3 Ma) hydrothermal reheating (85° - 135° C) and correlate with the location of a known geothermal anomaly. Thermal modeling of hydrothermally reset AHe ages from the modern range front suggests that the geothermal likely has been active for ~0.1 – 1 Ma, while borehole AHe ages in the hanging-wall basin suggests that its current plumbing system and manifestation as a geothermal anomaly is likely very young and that the borehole is not in conductive thermal equilibrium. This study demonstrates that thermochronometry can be an effective geothermal exploration tool to detect young and blind geothermal resources.

ACKNOWLEDGEMENTS

This research was funded primarily through a research grant from the Navy Geothermal Program Office at China Lake, CA. Additional funding was provided from EnCana Corporation, the Geology Associates Program of the University Of Kansas Department Of Geology, the American Association of Petroleum Geologists, and the Geological Society of America. Thank you to all of the students, staff and professors who work in the University of Kansas' Isotope Geochemistry Lab. Specifically, thank you to my advisors and committee members Danny Stockli, Doug Walker and Anthony W. Walton, my wife Bree, and my family. I truly appreciate all of the help and friendship from my lab and class mates and specifically my office mates, Josue Pujols-Vazquez and Evan Bargnesi, who have been a tremendous help throughout this project. Additional help came from Andy Sabin and Frank Monastero from the Navy Geothermal Program Office at China Lake, CA; John Peterson from the Hawthorne Ammunitions Depot in Hawthorne, NV; John Lee and Mike Cosca from the USGS $^{40}Ar/^{39}Ar$ lab in Denver, CO; and Roman Kislitsyn and Chris Hager, from the University of Kansas.

LIST OF TABLES AND FIGURES **PAGE**

[Page left intentionally blank]

CHAPTER 1: INTRODUCTION

The Walker Lane (Figure 1) is a zone of northwest-oriented right-lateral faults that resides between the highly extended Basin and Range province and stable Sierra Nevada block (Stewart, 1980; Hardyman and Oldow, 1991; Oldow, 1992; Wesnousky, 2005a; 2005b). Much of the Walker Lane was affected by two episodes of Cenozoic extension. Large-magnitude, Basin and Range extension began in the Miocene (e.g., John et al., 1989; Seedorff, 1991; Dilles and Gans, 1995; Wernicke et al., 1988; Dubendorfer and Simpson, 1994; Stockli et al., 2002; 2003; Surpless et al., 2002; Stewart, 1998) and was tied to a southwestward sweep of Cenozoic igneous activity and the steepening descent of the Farallon Slab (Coney and Reynolds, 1977; Christiansen and Yeats, 1992). Large-magnitude extension in the Basin and Range of west-central Nevada was primarily accommodated by large-offset normal faults and footwall rotation (e.g., Proffett, 1977; Dilles and Gans, 1993; 1995; Stockli et al., 2002; Surpless et al., 2002). Tilt-domain boundaries and accommodation zones in the Basin and Range province are thought to have formed during this time to accommodate opposite polarity or differentially tilted footwall blocks (Dilles and Gans, 1995; Stewart, 1998; Stockli et al., 2003). A second episode of extension and transtension began in the late Miocene to early Pliocene and was associated with the onset of right-lateral shearing in the Walker Lane due to a change in plate motion between the Pacific and North American Plates (Atwater and Stock, 1998; Faulds and Henry, 2008). Tilt domain boundaries also evolved during the onset of Walker Lane transcurrent deformation and now commonly act as transfer zones and releasing bends between misaligned strike-slip and transtensional faults (e.g., Stockli et al., 2003; Oldow et al., 2008).

The Mina Deflection (Ryall and Priestly, 1975) defines a series of east-northeast-striking sinistral and transcurrent faults that mark the location of an active, regional-scale structural step over/releasing bend between north-northwest -oriented faults in the central and southern Walker Lane belt (Figure 1)

(Oldow, 1992; Oldow et al., 1994; 2008; Stockli et al., 2003). Like many of the structures in the Walker Lane, the Mina Deflection has been reactivated throughout the Neogene and is the successor to a middle-late Miocene accommodation zone that accommodated a reversal in fault polarity between structures to its north and south, including the oppositely dipping Wassuk Range and White Mountains footwalls (Oldow, 1992; Oldow et al., 1994; Stockli et al., 2003; Tincher and Stockli, 2009). While many of the tilt-domain boundaries and transfer zones may have developed during this time (i.e., Stewart, 1998), the spatial concordance between the Mina Deflection and other crustal and isotopic boundaries (e.g., Kistler and Peterman, 1973; Oldow et al., 1989; Burchfiel et al., 1992) suggests a long-lived structural and lithospheric discontinuity (Oldow et al., 2008). Thus, the Mina Deflection and associated structures likely played a major role in the focusing of Miocene arc volcanism immediately prior to the onset of large-magnitude extension, and influenced the structure of propagating extensional systems.

The Wassuk Range is composed of rocks in the footwall of a ~90 km-long, north-south trending, east-dipping normal fault on the western margin of the Great Basin (Figures 1, 2). Like many places throughout the Walker Lane and Basin and Range province, Wassuk Range extension was immediately preceded by volcanism and an increase in the geothermal gradient (Dilles and Gans, 1995; Stockli et al., 2002; Surpless et al., 2002). Subsequent extension and tilting are variable along strike and decrease towards the south into the Mina Deflection accommodation zone, where the northerly striking range-front normal-fault system becomes linked to east-northeast-oriented sinistral faults in the Mina Deflection, via a curvilinear fault trace at Whisky Flat. The southern Wassuk Range is an ideal location to study the thermal anatomy and evolution of the Mina Deflection accommodation zone and tilt-domain boundary. Extension and tilting throughout the Cenozoic exhumed kilometer-thick upper-crustal sections now exposed in the southern Wassuk Range footwall. These exposed sections provide a unique opportunity to study the thermal structure of the crust and its evolution immediately prior to and during

large-magnitude extension (e.g., Foster et al., 1991; 1994; Foster and John, 1999; Miller et al., 1999; Reiners et al., 2000; Stockli et al., 2000; 2002; 2003; Surpless et al., 2002).

Characterization of the thermal structure and evolution of accommodation zones is not only important in an academic sense, but also has practical application in guiding geothermal exploration efforts. This is especially true in Walker Lane, where geothermal systems are commonly associated with Neogene extensional and transtensional structures (e.g., Faulds et al., 2006). In recent years, genetic occurrence models for geothermal resources (e.g., Blewitt et al., 2002; 2003; Coolbaugh et al., 2002; Walker et al., 2005; Sabin et al., 2005) have been developed to help find "blind" geothermal systems (Sass et al., 1971) that lack obvious surface manifestations (e.g., geysers, fumaroles, mud pots, tuffa deposits, etc.). For extensional-type geothermal systems, where heat is sourced from rapidly exhumed footwalls in normal faults, these models have focused geothermal exploration efforts to areas of recent faulting, earthquakes, and high strain rates because they tend to be zones of localized, increased structurally enhanced permeability and isotherm advection (Koenig and McNitt, 1983; Glazner et al., 1994; Caskey and Wesnousky, 2000; Blewitt et al., 2002, 2003, 2005; Coolbaugh et al., 2002; Coolbaugh and Shevenell, 2004; Walker et al., 2005; Kreemer et al., 2006; Bell and Ramelli, 2007, 2009; Hammond et al., 2007; Hickman et al., 2009). The southern Wassuk Range is ideal for studying this relationship, as it hosts a moderate-temperature extensional-type geothermal system in its hanging-wall basin.

The second chapter is a journal manuscript titled *(U-Th)/He Thermochronometrically Constrained Evolution and Anatomy of a Miocene Extensional Transfer Zone and Tilt Domain Boundary: The Southern Wassuk Range, Nevada*, and will be submitted to the journal *Tectonics* with co-authors Daniel F. Stockli and J. Douglas Walker. This chapter pairs detailed structural mapping of west-tilted volcanic and sedimentary rocks on the western flank of the southern Wassuk Range, with zircon (ZHe) and apatite (AHe) (U-Th)/He thermochronologic data from the exposed upper-crustal sections in the

southern Wassuk Range footwall (Figure 2) in order to quantify the timing and degree of footwall rotation during episodic extension throughout the Cenozoic. Furthermore, pre-extensional geothermal gradient estimates gleaned from thermochronologic data are used to evaluate the pre- and syn-extensional thermal anatomy of the Mina Deflection accommodation zone. Inverse-model derived time-temperature histories are used to assess the timing, style, and lateral variability of heating and cooling in the upper crust associated with pre-extensional volcanism and subsequent footwall exhumation during extension.

The third chapter is a journal manuscript titled; *Apatite (U-Th)/He Thermochronometry as an Innovative Geothermal Exploration Tool: A Case Study from the Southern Wassuk Range, Nevada*, and will be submitted to the journal *Volcanology and Geothermal Research,* with co-authors J. Douglas Walker, Daniel F. Stockli, Andrew Sabin, and Ben Surpless. AHe ages from the southern Wassuk Range footwall and from a ~1.4 km deep geothermal borehole in the hanging-wall basin are used to address the temperature, distribution and longevity of geothermal anomalies and their plumbing systems. Furthermore, the utility of the AHe thermochronometer as a regional-scale geothermal exploration tool is evaluated here, and is used to identify zones of increased footwall advection and areas of hydrothermal fluid migration along the footwall range front and within the geothermal borehole. Geothermal borehole samples and temperature data were generously supplied by the Navy Geothermal Program Office at China Lake, CA.

The research presented here was primarily funded by a research grant awarded to Daniel F. Stockli and J. Douglas Walker, from the Navy Geothermal Program Office at the Naval Air Warfare Center at China Lake, CA. Additional research grants from EnCana Corporation, University of Kansas, Geological Society of America and the American Association of Petroleum Geologists were awarded to Kyle Gorynski and partially funded a two-year research assistantship, field work, and laboratory

research. Our work, although significant alone, is a part of a number of larger-scale and ongoing research projects at the University of Kansas involving the Cenozoic thermal and structural evolution of the Walker Lane and the Eastern California Shear-Zone (e.g., Walker and Coleman, 1991; Dunne and Walker, 1993; Glazner et al., 1994; Walker et al., 1995; Fillmore and Walker, 1996; Stockli et al., 2002; Stockli et al., 2003; Stockli, 2005; Tincher and Stockli, 2009) and the application of (U-Th)/He thermochronology in geothermal exploration (Sabin et al., 2005; Walker et al., 2005; Gorynski et al., 2010).

CHAPTER 1: REFERENCES

Atwater, T., and Stock, J., 1998, Pacific-North America plate tectonics of the Neogene southwestern United States: an update: International Geology Review, v. 40, p. 375-402.

Bell, J., and Ramelli, A., 2007, Active Faults and Neotectonics at Geothermal Sites in the Western Basin and Range: Preliminary Results: Geothermal Resources Council Transactions, v. 31, p. 375-378.

Bell, J., and Ramelli, A., 2009, Active Fault Controls at High-Temperature Geothermal Sites: Prospecting for New Faults: Geothermal Resources Council Transactions, p. 425-429.

Blewitt, G., Coolbaugh, M., Holt, W., Kreemer, C., Davis, J., and Bennett, R., 2002, Targeting of potential geothermal resources in the Great Basin from regional relationships between geodetic strain and geological structures: Geothermal Resources Council Transactions, v. 26, p. 523-526.

Blewitt, G., Coolbaugh, M., Sawatzky, D., Holt, W., Davis, J., and Bennett, R., 2003, Targeting of potential geothermal resources in the Great Basin from regional to basin-scale relationships between geodetic strain and geological structures: Geothermal Resources Council Transactions, p. 3-8.

Blewitt, G., Hammond, W., and Kreemer, C., 2005, Relating geothermal resources to Great Basin tectonics using GPS: Geothermal Resources Council Transactions, v. 29, p. 331–335.

Burchfiel, B., Cowan, D., and Davis, G., 1992, Tectonic overview of the Cordilleran orogen in the western United States: The Cordilleran orogen: Conterminous US: Boulder, Colorado, Geological Society of America, Geology of North America, v. 3, p. 407–479.

Cashman, P., Trexler Jr, J., Muntean, T., Faulds, J., Louie, J., and Oppliger, G., 2009, Neogene tectonic evolution of the Sierra Nevada–Basin and Range transition zone at the latitude of Carson City,

Nevada: Late Cenozoic structure and evolution of the Great Basin-Sierra Nevada transition, p. 171-188.

Caskey, S., and Wesnousky, S., 2000, Active faulting and stress redistributions in the Dixie Valley, Beowawe, and Brady's geothermal fields: implications for geothermal exploration in the Basin and Range: Proceedings, Twenty-fifth workshop on geothermal reservoir engineering, p. 24-26.

Christiansen, R., Yeats, R., Graham, S., Niem, W., and Niem, A., 1992, Post-Laramide geology of the US Cordilleran region: in Burchfiel, B.C., Lipman, P.W., and Zoback, M.L., eds., The Cordilleran orogen: Conterminous US: Boulder, Colorado, Geological Society of America, Geology of North America, v. 3, p. 261–406.

Coney, P.J., and Reynolds, S.J., 1977, Cordilleran Benioff zones: Nature, v. 270, p. 403-406.

Coolbaugh, M., and Shevenell, L., 2004, A method for estimating undiscovered geothermal resources in Nevada and the Great Basin: Geothermal Resources Council Transactions, v. 28, p. 13-18.

Coolbaugh, M., Taranik, J., Rains, G., Shevenell, L., Sawatzky, D., Bedell, R., and Minor, T., 2002, A geothermal GIS for Nevada: defining regional controls and favorable exploration terrains for extensional geothermal systems: TRANSACTIONS-GEOTHERMAL RESOURCES COUNCIL, p. 485-490.

Dilles, J., 1993, Cenozoic strike-slip faults in the northern Wassuk Range, Walker Lane: Geological Society of America, Abstracts with Programs;(United States), v. 25.

Dilles, J., and Gans, P., 1995, The chronology of Cenozoic volcanism and deformation in the Yerington area, western Basin and Range and Walker Lane: Geological Society of America Bulletin, v. 107, p. 474-486.

Duebendorfer, E., and Simpson, D., 1994, Kinematics and timing of Tertiary extension in the western Lake Mead region: Nevada: Geological Society of America Bulletin, v. 106, p. 1057-1073.

Dunne, G.C., and Walker, J.D., 1993, Age of Jurassic volcanism and tectonism, southern Owens Valley region, east-central California: Bulletin of the Geological Society of America, v. 105, p. 1223-1230.

Faulds, J., Coolbaugh, M., Vice, G., and Edwards, M., 2006, Characterizing structural controls of geothermal fields in the northwestern Great Basin: A progress report: Geothermal Resources Council Transactions, v. 30, p. 69-76.

Faulds, J., and Henry, C., 2008, Tectonic influences on the spatial and temporal evolution of the Walker Lane: An incipient transform fault along the evolving Pacific–North American plate boundary: Ores and orogenesis: Circum-Pacific tectonics, geologic evolution, and ore deposits, Arizona Geological Society Digest, v. 22, p. 437-470.

Fillmore, R.P., and Walker, J.D., 1996, Evolution of a supradetachment extensional basin: The lower Miocene Pickhandle basin, central Mojave Desert, California: Geological Society of America Special Papers, v. 303, p. 107-126.

Foster, D.A., Howard, K.A., and John, B.E., 1994, Thermochronological constraints on the development of metamorphic core complexes in the lower Colorado River area: in Eighth International Conference on Geochronology, Cosmochronology, and Isotope Geology edited by M.A. Lanphere, G.B. Dalrymple, and B.D. Turrin, U.S. Geol. Surv. Circ., 1107, p. 103.

Foster, D.A., and John, B.E., 1999, Quantifying tectonic exhumation in an extensional orogen with thermochronology: examples from the southern Basin and Range Province: Geological Society London Special Publications, v. 154, p. 343-364.

Foster, D.A., Miller, D.S., and Miller, C.F., 1991, Tertiary extension in the Old Woman Mountains area, California: evidence from apatite fission track analysis: Tectonics, v. 10, p. 875-886.

Glazner, A., Walker, J., Bartley, J., Coleman, D., and Taylor, W., 1994, Igneous activity at releasing bends and transfer zones in extensional systems: Implications for site and mode of geothermal activity: Geothermal Resources Council Transactions, p. 7-7.

Hammond, W., Kreemer, C., and Blewitt, G., 2007, Exploring the Relationship between Geothermal Resources and Geodetically Inferred Faults Slip Rates in the Great Basin: Geothermal Resource Council Transactions, v. 31, p. 391-395.

Hardyman, R., and Oldow, J., 1991, Tertiary tectonic framework and Cenozoic history of the central Walker Lane, Nevada, Volume 1, p. 279-301.

Hickman, S., Barton, C., Zoback, M., Morin, R., Sass, J., and Benoit, R., 2009, In situ stress and fracture permeability along the Stillwater fault zone, Dixie Valley, Nevada: International Journal of Rock Mechanics and Mining Sciences, v. 34, p. 414.

John, D.A., Thomason, R.E., and McKee, E.H., 1989, Geology and K-Ar geochronology of the Paradise Peak Mine and the relationship of pre-Basin and Range extension to early Miocene precious metal mineralization in west-central Nevada: Economic Geology, v. 84, p. 631-649.

Kistler, R.W., and Peterman, Z.E., 1973, Variations in Sr, Rb, K, Na, and initial Sr87/Sr86 in Mesozoic granitic rocks and intruded wall rocks in central California: Geological Society of America Bulletin, v. 84, p. 3489-3512.

Koenig, J., and McNitt, J., 1983, Controls on the location and intensity of magmatic and non-magmatic geothermal systems in the Basin and Range province: Geothermal Resources Council, Special Report No. 13, pp. 93.

Kreemer, C., Blewitt, G., and Hammond, W., 2006, Using geodesy to explore correlations between crustal deformation characteristics and geothermal resources: Geothermal Resources Council Transactions, v. 30, p. 441–446.

Miller, E., Dumitru, T., Brown, R., and Gans, P., 1999, Rapid Miocene slip on the Snake Range–Deep Creek Range fault system, east-central Nevada: Geological Society of America Bulletin, v. 111, p. 886-905.

Oldow, J., 1992, Late Cenozoic displacement partitioning in the northwestern Great Basin, p. 17–52.

Oldow, J., Geissman, J., and Stockli, D., 2008, Evolution and strain reorganization within late Neogene structural stepovers linking the central Walker Lane and northern Eastern California shear zone, western Great Basin: International Geology Review, v. 50, p. 270-290.

Oldow, J., Kohler, G., and Donelick, R., 1994, Late Cenozoic extensional transfer in the Walker Lane strike-slip belt, Nevada: Geology, v. 22, p. 637-640.

Oldow, J.S., Bally, A.W., Avé Lallemant, H., and Leeman, W.P., 1989, Phanerozoic evolution of the North American Cordillera; United States and Canada: The geology of North America: An overview: Boulder, Colorado, Geological Society of America, Geology of North America, v. A, p. 139–232.

Proffett, J., 1977, Cenozoic geology of the Yerington district, Nevada, and implications for the nature and origin of Basin and Range faulting: Geological Society of America Bulletin, v. 88, p. 247-266.

Reheis, M.C., and Sawyer, T.L., 1997, Late Cenozoic history and slip rates of the Fish Lake Valley, Emigrant Peak, and Deep Springs fault zones, Nevada and California: Geological Society of America Bulletin, v. 109, p. 280-299.

Reiners, P.W., Brady, R., Farley, K.A., Fryxell, J.E., Wernicke, B., and Lux, D., 2000, Helium and argon thermochronometry of the Gold Butte block, south Virgin Mountains, Nevada: Earth and Planetary Science Letters, v. 178, p. 315-326.

Roberts, B.J., 2009, Geothermal Resources of the United States: National Renewable Energy Laboratory for the US Department of Energy.

Ryall, A., and Priestley, K., 1975, Seismicity, secular strain, and maximum magnitude in the Excelsior Mountains area, western Nevada and eastern California: Bulletin of the Geological Society of America, v. 86, p. 1585-1592.

Sabin, A., Walker, J.D., Unruh, J., and Combs, J., 2005, Kinematic and dynamic studies: genetic occurrence models for geothermal prospecting: Report for Contract No. N68936-04-C-0057 (US Navy).

Sass, J., Lachenbruch, A., Munroe, R., Greene, G., and Moses Jr, T., 1971, Heat flow in the western United States: Journal of Geophysical Research, v. 76, p. 6376-6413.

Seedorff, E., 1991, Magmatism, extension, and ore deposits of Eocene to Holocene age in the Great Basin—Mutual effects and preliminary proposed genetic relationships, p. 133–178.

Stewart, J., 1980, Regional tilt patterns of late Cenozoic basin-range fault blocks, western United States: Bulletin of the Geological Society of America, v. 91, p. 460-464.

Stewart, 1998, Regional characteristics, tilt domains, and extensional history of the later Cenozoic Basin and Range province, western North America: Geological Society of America Special Papers, v. 323, p. 47-74.

Stewart, J.H., Carlson, J.E., Tingley, S.L., Survey, G., Mines, N.B.o., and Geology, 1977, Geologic map of Nevada, Nevada Bureau of Mines and Geology, University of Nevada.

Stockli, D., 2005, Application of low-temperature thermochronometry to extensional tectonic settings: Reviews in Mineralogy and Geochemistry, v. 58, p. 411-448.

Stockli, D., Dumitru, T., McWilliams, M., and Farley, K., 2003, Cenozoic tectonic evolution of the White Mountains, California and Nevada: Geological Society of America Bulletin, v. 115, p. 788-816.

Stockli, D., Farley, K., and Dumitru, T., 2000, Calibration of the apatite (U-Th)/He thermochronometer on an exhumed fault block, White Mountains, California: Geology, v. 28, p. 983-986.

Stockli, D., Surpless, B., Dumitru, T., and Farley, K., 2002, Thermochronological constraints on the timing and magnitude of Miocene and Pliocene extension in the central Wassuk Range, western Nevada: Tectonics, v. 21, p. 1028-1047.

Surpless, B., Stockli, D., Dumitru, T., and Miller, E., 2002, Two-phase westward encroachment of Basin and Range extension into the northern Sierra Nevada: Tectonics, v. 21, p. 1002-1015.

Tincher, C.R., and Stockli, D.F., 2009, Cenozoic volcanism and tectonics in the Queen Valley area, Esmeralda County, western Nevada: Late Cenozoic structure and evolution of the Great Basin-Sierra Nevada transition, p. 255-274.

Walker, J.D., and Coleman, D.S., 1991, Geochemical constraints on mode of extension in the Death Valley region: Geology, v. 19, p. 971-974.

Walker, J.D., Fletcher, J.M., Fillmore, R.P., Martin, M.W., Taylor, W.J., Glazner, A.F., and Bartley, J.M., 1995, Connection between igneous activity and extension in the central Mojave metamorphic core complex, California: Journal of Geophysical Research, v. 100, p. 10477-10494.

Walker, J.D., Sabin, A., Unruh, J., Combs, J., and Monastero, F., 2005, Development of genetic occurrence models for geothermal prospecting: Transactions-Geothermal Resources Council, v. 29, p. 309-314.

Wernicke, B., AXEN, G.J., and Snow, J., 1988, Basin and Range extensional tectonics at the latitude of Las Vegas, Nevada: Bulletin of the Geological Society of America, v. 100, p. 1738-1757.

Wesnousky, S., 2005a, Active faulting in the Walker Lane: Tectonics, v. 24, p. 3009 – 3044.

Wesnousky, S., 2005b, The San Andreas and Walker Lane fault systems, western North America: Transpression, transtension, cumulative slip and the structural evolution of a major transform plate boundary: Journal of Structural Geology, v. 27, p. 1505-1512.

CHAPTER 1: FIGURES AND CAPTIONS

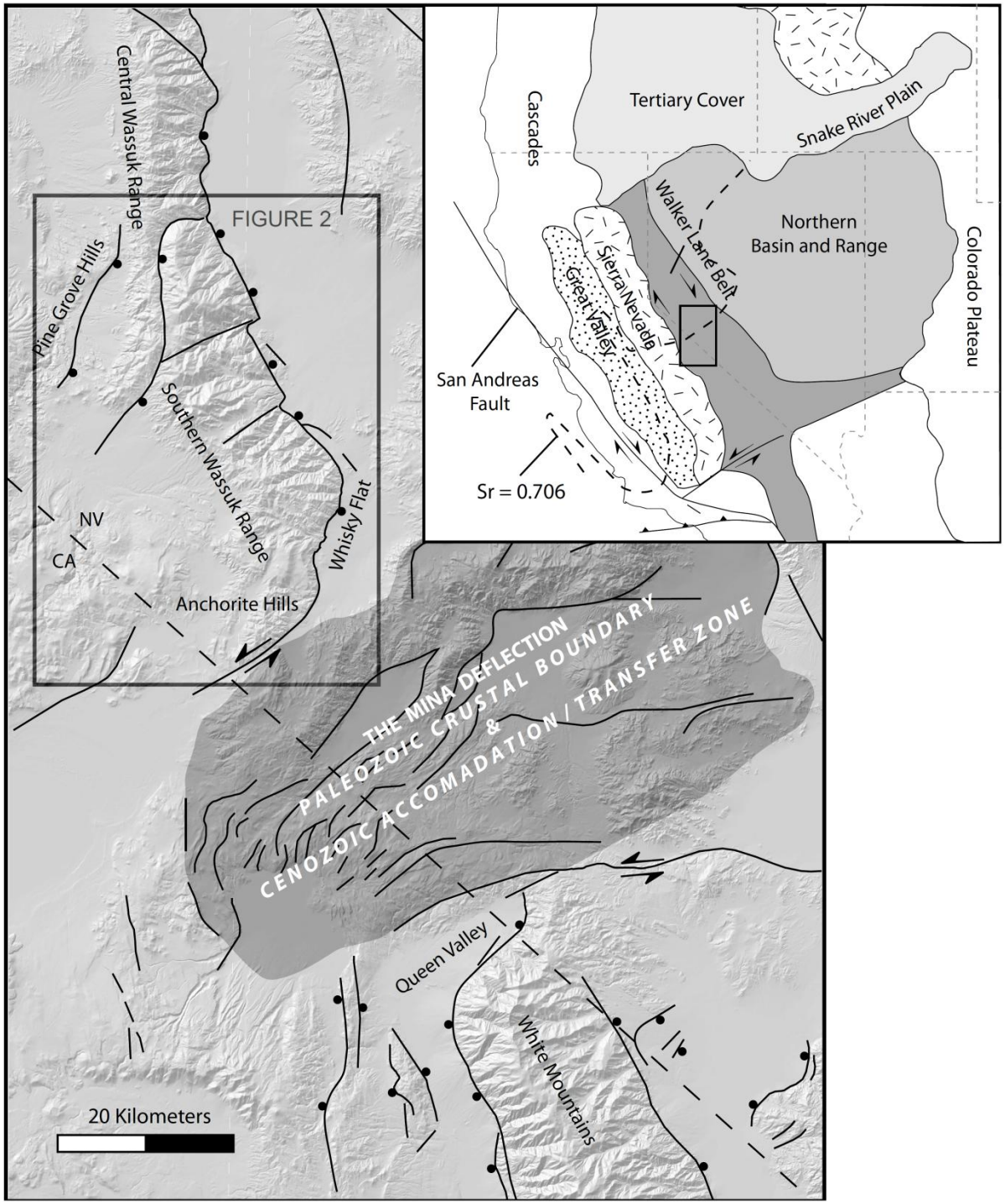
Central Wassuk Range
FIGURE 2
Pine Grove Hills
Southern Wassuk Range
Whisky Flat
NV
CA
Anchorite Hills
THE MINA DEFLECTION
PALEOZOIC CRUSTAL BOUNDARY
&
CENOZOIC ACCOMADATION / TRANSFER ZONE
Queen Valley
White Mountains
20 Kilometers
Cascades
Tertiary Cover
Snake River Plain
Walker Lane Belt
Northern
Basin and Range
Colorado Plateau
Sierra Nevada
Great Valley
San Andreas
Fault
Sr = 0.706

Figure 1. Digital elevation model of the central Wassuk Range with major late Cenozoic faults (modified after Stewart, et al., 1977; Oldow, 1992; Rehis and Sawyer, 1997; Stockli et al., 2003). The west-tilted Wassuk Range footwall and east-tilted White Mountains footwall are separated by the east-west-trending faults of the Mina Deflection. Insert map shows the location of the study area with respect to the western margin of the North American craton, as defined by the $^{87}Sr/^{86}Sr$ 0.706 line (Kistler and Peterman, 1973; Oldow et al., 2008).

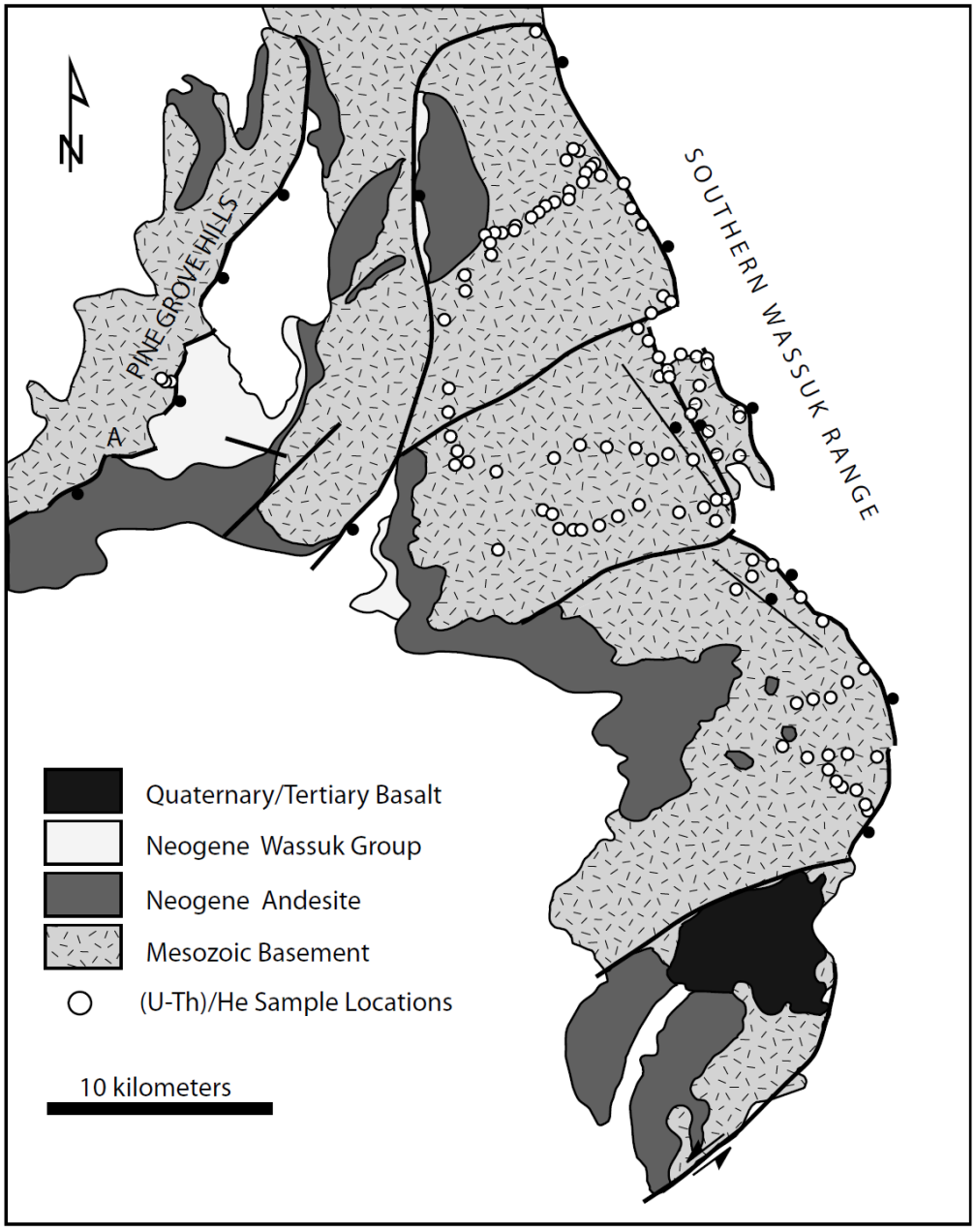
N
PINE GROVE HILLS
SOUTHERN WASSUK RANGE
A
Quaternary/Tertiary Basalt
Neogene Wassuk Group
Neogene Andesite
Mesozoic Basement
(U-Th)/He Sample Locations
10 kilometers

Figure 2. Generalized geologic map of the southern Wassuk Range footwall. (U-Th)/He samples were taken from theseveral footwall blocks, each which has a different tilt, and sample the entire exposed upper-crustal sections below the Paleogene nonconformity.

CHAPTER 2: (U-Th)/He Thermochronometrically Constrained Evolution and Anatomy of a Miocene Extensional Transfer Zone and Tilt Domain Boundary: The Southern Wassuk Range, Nevada

ABSTRACT

Apatite (AHe) and Zircon (ZHe) (U-Th)/He thermochronometric data from the southern Wassuk Range (WR) and Pine Grove Hills (PGH) footwalls, coupled with $^{40}Ar/^{39}Ar$ age data from the overlying tilted Neogene section, are used to constrain the thermal and tectonic evolution of an extensional accommodation zone and tilt-domain boundary. AHe and ZHe data record two episodes of fast-paced cooling related to the tectonic exhumation of the WR footwall beginning at ~12 – 15 Ma and ~3 – 5 Ma, and agree with the timing of tilting documented in the overlying Neogene section. Exhumation and extension were accommodated primarily through fault-block rotation along a horizontal north-northeast-trending axis and variably tilted the southern WR to the west from ~60° -70° in the central WR to ~15° - 35° in the southernmost WR and PGH, and blocks are not tilted with respect to WR extension in the Mina Deflection (MD) to its south. Estimates of the pre-extensional geothermal gradient from the southern WR record a heating event immediately prior to large-magnitude extension. Heating was likely coeval with the extrusion of the Lincoln Flat andesite at ~14.8 – 15.1 Ma. Estimates of middle Miocene geothermal gradients from the southern WR increase from ~19° ± 4° C/km to ≥ 65° ± 20° C/km towards the middle Miocene MD accommodation zone. Our data suggest that the MD was the upper-crustal focus of Miocene arc magmatism and drastically perturbed the thermal structure of the southern WR. Due to the inferred shallow depth of the brittle/ductile transition zone in the southernmost WR and MD, extension and footwall advection in the middle Miocene was predominantly focused in the northern and central WR and coincidentally mollified the large lateral thermal gradient. We propose a cyclic model of heating of accommodation zones in the upper crust beginning with magmatic advection focused along structurally predisposed tilt-domain boundaries followed by footwall advection focused along the more distal segments of extensional systems.

INTRODUCTION

The onset of large-magnitude extension in the Basin and Range province was intimately associated with Cenozoic magmatism. Major igneous activity often immediately precedes major extension (Gans et al., 1989; Gans and Bohrson, 1998) and is spatially and temporally related to the formation of tilt-domain boundaries and accommodation zones between extended terrains (Aldrich, 1986; Axen, 1998; Faulds and Varga, 1998; Rowley, 1998; Stewart, 1998). This relationship is also realized throughout Walker Lane where Miocene arc volcanism (e.g., Christiansen et al., 1992) and heating peak immediately prior to middle Miocene extension (e.g., Dilles and Gans, 1995; Stockli et al., 2002; Surpless et al., 2002), and spatially overlap with strike- and oblique-slip transfer zones (Stewart, 1998). The uninterrupted progression of volcanism and extension suggests that upper-crustal deformation is partly a response to its thermal weakening during magmatic advection (Kusznir and Park, 1987; Stockli et al., 2002; Surpless et al., 2002). However, the thermal evolution of accommodation zones in Walker Lane has received little attention. As preexisting weaknesses in the crust, accommodation zones play a major role in the localization of magmatism, volcanism and heating prior to extension and subsequently influence the degree of syn-extensional footwall advection by controlling the architecture and structural evolution of extended terrains.

GEOLOGY AND TECTONIC HISTORY

The Central Walker Lane

The Walker Lane belt (Stewart, 1980; 1988) is a northwest-trending belt of like-striking, Cenozoic age strike-slip, transtensional and extensional structures that lies between the highly extended Basin and Range Province and the stable Sierra Nevada block. The Walker Lane belt is underlain by Triassic – Lower Jurassic metasedimentary and metavolcanic rocks that were intruded by Middle Jurassic – Cretaceous granitic plutons and silicic volcanic rocks (Dilles and Wright, 1988; Dilles and Gans, 1995).

Late Cenozoic –Paleogene erosion resulted in the formation of a prominent, laterally continuous nonconformity (ca. 40 Ma) across Mesozoic intrusive and associated wall rocks throughout western Nevada and eastern California (Van Buer et al., 2009). Throughout the Walker Lane, Mesozoic basement is nonconformably overlain by a sequence of Cenozoic volcanic, tuffaceous and siliciclastic rocks. The basal Paleogene nonconformity is overlain by Oligocene rhyolite ignimbrites (e.g. Mickey Pass Tuff and Singatse Tuff) and Miocene andesites (e.g. Lincoln Flat, Kate Peak and Alta lithologies) (Thompson, 1956; Proffett and Proffett, 1976; Dilles and Gans, 1995). Oligocene ignimbrites show large variations in thickness and are generally confined to paleovalleys (Henry, 2008). Miocene andesites commonly overlie the Oligocene ignimbrites, except where the ignimbrites are absent, Miocene andesites nonconformably overlie the Mesozoic basement. Syntectonic, Miocene, siliciclastic rocks (e.g., Wassuk Group) were deposited within fault-bounded basins and overlie Miocene andesites (Axelrod, 1956; Gilbert and Reynolds, 1973). Finally, gently tilted late Miocene basaltic andesites overlie, often in slight angular unconformity, middle – upper Miocene sedimentary rocks of the Wassuk Group (Gilbert and Reynolds, 1976; Dilles and Gans, 1995).

The central Walker Lane is characterized by a spectrum of coeval and kinematically linked northerly striking normal, northeast-striking sinistral and northwest-striking dextral-slip faults (Stewart, 1988; Hardman and Oldow, 1991, Oldow, 1992; Stewart, 1998; Wesnousky, 2005a). Two distinct phases of Cenozoic deformation are recognized throughout the central Walker Lane belt and involve the episodic occupation and reactivation of Cenozoic structures (e.g., Dilles and Gans, 1995; Stockli et al., 2002; Surpless et al., 2002; Stockli et al., 2003). Faulting in the central Walker lane began between 15 and 10 Ma (Hardyman and Oldow, 1991) and resulted from east-west directed, back-arc extension (Stewart, 1998). In the Basin and Range province, moderate- to large-magnitude extension during the middle – late Miocene was mostly accommodated through slip on low-angle detachments, but in the central Walker Lane, deformation was accommodated by large degrees of footwall rotation (40-70°)

along high-angle normal faults (e.g., Proffett, 1977; Dilles and Gans, 1995; Surpless et al., 2002). Strike-slip faults that initiated during this time are interpreted as transfer and accommodation structures partly because of their orientation, running orthogonal to the regional structural grain and roughly parallel to the middle-late Miocene extension direction (Liggett and Childs, 1977; Guth, 1981; Wernicke et al., 1984; Stewart, 1998). A second episode of deformation began in the late Miocene – Pliocene and was the result of far-field stresses along the Pacific plate margin (Atwater and Stock, 1998; Faulds and Henry, 2008). A prominent right step in the northwest structural grain of the central Walker Lane occurs at the latitude of Mono Lake (Figure 1). This right step is marked by a number of east-northeast-trending sinistral-slip faults throughout the Excelsior region and is known as the Mina Deflection (Ryall and Priestly, 1975). The Mina Deflection is an active structural step over that transfers displacement from misaligned northwest-striking transcurrent faults to its north and south (Oldow, 1992; Oldow, 1994; Stockli et al., 2003; Oldow et al., 2008). Like many of the structures in Walker Lane, the Mina Deflection has been reactivated throughout the Neogene and is the successor to the middle - late Miocene Silver Peak – Lone Mountain extensional step-over system (Oldow, 1992; Oldow et al., 1994; Stockli et al., 2003; Tincher and Stockli, 2009); collectively these structures are referred to as the Central Walker Lane displacement transfer system (CWLDTS) (Oldow et al., 2008). During the middle Miocene, the CWLDTS acted as a right-lateral accommodation zone, transferring displacement on its eastern end between northwest-striking transcurrent faults of the central Walker Lane and the northern Furnace Creek fault system (Oldow, 1992; Oldow et al., 1994; Oldow et al., 2009); on its western end it was a dextral antithetic accommodation zone (Stockli et al., 2003; Tincher and Stockli, 2009) between oppositely dipping footwalls of the Wassuk Range and White Mountains to its north and south, respectively (Figure 1). The present-day configuration of the Mina Deflection was established by the middle Pliocene and now accommodates displacement transfer between the transcurrent faults of the central Walker Lane and those of the northern Owens Valley and Furnace Creek fault systems (Oldow et al., 2008).

Wassuk Range and Pine Grove Hills

The Wassuk Range is ~90 km long and is in the footwall of a north-south trending, east-dipping normal fault on the western margin of the Great Basin (Figure 1, 2). Extension throughout the Cenozoic in the Wassuk Range area has exhumed kilometers-thick sections (≤ 10 km) of granitic crust and overlying Neogene cover. In the southern Wassuk Range and Pine Grove Hills, granitic basement rocks are nonconformably overlain by the Miocene Lincoln Flat andesite and sedimentary and volcanic rocks of the Wassuk Group, deposited in fault-bounded basins (Dilles and Gans, 1995; Surpless et al., 2002). The extrusion of the Lincoln Flat andesite at 14.8 – 15.1 Ma immediately precedes extension in the northern and central Wassuk Range, and the attitude of the Lincoln Flat andesite reflects the cumulative Neogene tilting of the Wassuk Range footwall (e.g., Stockli et al., 2002; Surpless et al., 2002).

The Wassuk Range underwent two episodes of extension and rapid footwall exhumation throughout the Neogene that are recorded by apatite fission track (AFT) and apatite (AHe) and zircon (ZHe) (U-Th)/He thermochronologic data from its eastern flank (i.e., Stockli et al., 2002; Surpless et al., 2002; Stockli, 2005; Krugh, 2008). Extension and footwall exhumation at ~12 – 15 Ma was accommodated by westward footwall rotation (< 60°) along east-dipping, high-angle normal faults (Dilles and Gans, 1995; Surpless, 1999; Stockli et al., 2002; Surpless et al., 2002). Miocene geothermal gradient estimates of 27° ± 5° C/km from the central Wassuk Range are higher than those of the Sierra Nevada (< 15° – 20° C/km) (Stockli, 1999), to which the Wassuk Range belonged, and indicates an increase in the geothermal gradient immediately prior to middle Miocene extension and likely facilitated extension by thermally destabilizing the upper crust (Stockli et al., 2002; Surpless et al., 2002). A second episode of exhumation initiated at ~4 Ma and is related to active, high-angle faulting along the present-day range front in the central Wassuk Range (Stockli et al., 2002; Surpless et al., 2002), and transtensional deformation at the southernmost Wassuk Range at the Whisky Flat pull-apart structure

(Stockli et al., 2003; Krugh, 2008). Mio-Pliocene deformation in the Wassuk Range is synchronous with the development of pull-apart structures at the northern end of the White Mountains (Stockli et al., 2003; Tincher and Stockli, 2009) and normal and transcurrent faults in the Mina Deflection (Stewart, 1988; Hardyman and Oldow, 1992; Oldow, 1992; Oldow et al., 2001), and correlate with a period of structural reorganization throughout the central Walker Lane (Oldow et al., 2008).

METHODOLOGY

Structural Mapping Derived Tilting Histories

Mapping of the pre- and syn-extensional Neogene cover sequence of the Wassuk Range has proved useful in determining its Neogene history of deformation and tilting (e.g., Gilbert and Reynolds, 1976; Proffett, 1977; McIntyre, 1990; Dilles and Gans, 1995; Surpless et al., 2002). The most complete history of extension and footwall rotation is recorded by differentially tilted Miocene andesites and younger sedimentary and volcanic rocks of the Wassuk Group, preserved in fault-bounded basins west of the Wassuk Range. Two basins are defined by the present-day Coal and Fletcher valleys and lie immediately west of the southern Wassuk Range. These basins are bounded to their west by east-dipping, high-angle normal faults along the range front of the Pine Grove Hills (Figure 2). Although Quaternary sediments cover much of the Neogene section in Fletcher Valley, a rather continuous and folded Miocene section is preserved in Coal Valley. This area was previously mapped by Gilbert and Reynolds (1976), who focused on the distribution of Miocene andesites, as well as the Aldrich Station, Coal Valley and Morgan Ranch Formations of the Wassuk Group. In order to better constrain the temporal and lateral variability of tilting, our mapping further divided the Wassuk Group into smaller, continuous and more easily recognizable packages of sedimentary and volcanic rocks, and their distributions were mapped along the western flank of the southern Wassuk Range.

(U-Th)/He Thermochronology

(U-Th)/He thermochronometry is a widely applied thermochronometric technique and has been utilized in a number of extensional studies (e.g., Stockli, 2005 and references therein) in order to determine the onset of rapid footwall exhumation related to large-magnitude extension and to evaluate the thermal state of the crust immediately prior to extension (e.g., Fitzgerald et al., 1990; Howard and Foster, 1996; Miller et al., 1999; Foster and John, 1999; Stockli et al., 2002; Surpless et al., 2002). (U-Th)/He dating is based on the radioactive decay of ^{235}U, ^{238}U, ^{232}Th, and ^{147}Sm to radiogenic ^{4}He, and the subsequent loss of ^{4}He during thermally controlled diffusion. Since the diffusion domain is the crystal itself, the temperature at which ^{4}He is lost is controlled primarily by mineralogy. In this study we utilize the AHe and ZHe thermochronometers because together they cover the thermal evolution of individual samples through a temperature range of ~40° - 200° C. Assuming a geothermal gradient of ~25° C/km and a surface temperature of 10° ± 5° C/km, the AHe and ZHe thermochronometers together record thermal processes in the upper ~1 – 7.5 km of the crust (e.g., Stockli, 2005).

AHe thermochronometry is the most utilized (U-Th)/He thermochronometer because of its well-defined diffusion kinetics (e.g., Farley, 2000) and applicability to the study of low-magnitude thermal events in the uppermost crust (e.g., Stockli et al., 2000). Diffusion of ^{4}He out of the apatite crystal is variable over a range of temperatures from 40° to 80° C, termed the helium partial retention zone (PRZ), but is completely lost by diffusion above temperatures of 80° C and completely retained at temperatures below 40° C. The onset of exhumation is recorded by the rapid cooling of fault blocks through the AHe PRZ resulting in invariant AHe ages for samples that resided below the 80° C isotherm prior to extension, and above the 40° C isotherm after extension. Fossil AHe PRZs are recognized in exhumed fault blocks as a spectrum of ages that decrease with increasing paleodepth and are bounded by inflection points in an AHe age vs. paleodepth plot.

The ZHe thermochronometer, although less utilized, has been applied to a number of extensional studies (e.g., Reiners, 2000; Stockli, 2005) and is important in constraining the thermal evolution of footwall blocks at temperatures between ~140° and 200° C. The ZHe PRZ is somewhat poorly defined because of its less well-behaved diffusion kinetics (Reiners et al., 2002, 2004), and its infrequent preservation that requires exhumation on the order of ~5 -8 km. Although the closure temperature of the ZHe thermochronometer at ~175 – 193° C has been known for some time (Dodson, 1979; Reiners et al., 2004), only recently have works constrained the ZHe PRZ to a temperature range of ~140° - 200° C, based on studies of exhumed and modern ZHe PRZs (e.g, Reiners et al., 2000; 2002; Wolfe and Stockli, 2010).

Pre-extensional Paleodepth Estimates

Placing thermochronological samples in an accurate paleodepth reference frame is imperative to our interpretation of the pre-extensional thermal state of the crust. A sample's paleodepth consists of both its structural depth, measured orthogonal to a paleohorizontal reference, and any sedimentary or volcanic overburden. Structural depth is measured here by flattening the Paleogene nonconformity and then measuring downward from the overlying, westward-dipping, Lincoln Flat andesite (e.g., Stockli, et al., 2002; Surpless et al., 2002; Stockli et al., 2003). This method generates obvious uncertainties by assuming a lack of topography on the Paleogene nonconformity, and neglects tilting or folding resulting from deformation other than fault-block rotation. Nevertheless, topographic relief on the Paleogene nonconformity was likely minor as evident from its planar nature and observed small wavelength (Mancktelow and Grasemann, 1977), and would only affect paleodepth estimates for samples at the shallowest structural levels (e.g., Stockli et al., 2002). Finally, errors of ± 5° were added to westward tilted footwall blocks in order to account for the most heavily-weighted uncertainties of measuring fault-block rotation.

The pre-extensional overburden above the Paleogene nonconformity must also be calculated in order to determine a sample's paleodepth. The simplest way to determine overburden is by measuring the pre-extensional stratigraphic thickness above the nonconformity, and in the Wassuk Range is the thickness of Oligocene conglomerates and ignimbrites, and the overlying Miocene Lincoln Flat andesite. Overburden can also be thermally estimated by projecting model-derived, geothermal gradient estimates up through the crustal section, and then calculating the vertical distance between a thermally defined surface at 10 ± 5° C and the Paleogene nonconformity (e.g., Stockli et al., 2002; Stockli, 2005).

Pre-extensional Geothermal Gradient Estimates

Coupling of a geochronometrically constrained tilting history with thermochronologic data provides a unique opportunity to study the structural and thermal evolution of the upper crust prior to and during extension (e.g., Howard and Foster, 1996; Foster and John, 1999; Stockli et al., 2002; Stockli, 2005). This study applies the methods utilized by Stockli and others (2002) and outlined by Stockli (2005), to estimate geothermal gradients prior to episodic, large-magnitude extension beginning in the middle Miocene and Mio-Pliocene. Two methods for determining geothermal gradients are outlined below and both heavily rely on the palinspastic restoration of tilted footwall blocks (discussed in the previous section) in order to put thermochronologic data collected at the surface into a paleodepth reference frame.

The apatite and zircon (U-Th)/He PRZs are important in the formation of thermal markers in the crust, where their upper and lower boundaries are defined by isotherms and are recognized by inflections in AHe and ZHe vs. paleodepth plots. Estimates of the geothermal gradient immediately prior to extension are acquired by determining the temperature difference between the paleosurface and the observed inflection points for the ZHe (~140° C and 200° C) and AHe (~40° C and 80° C) PRZs. Similarly, the distance between the top and the bottom of the PRZs can be used to estimate the

geothermal gradient, but errors are usually large due to the small change in temperature and thinness of the PRZs. A second method for estimating the geothermal gradient uses inverse-model-derived time-temperature histories for individual samples to estimate the temperature of a sample immediately prior to extension. The distribution of sample temperatures with depth show a linear relationship, and the slope of a best-fit line through these points defines the geothermal gradient. Additionally, the overburden can also be estimated, where its thickness is comparable to the distance between the paleohorizontal surface (i.e., Paleogene nonconformity) and the intersection of the geothermal gradient linear regression with the thermally-defined surface.

STRUCTURAL RESULTS

The southern portion of the Wassuk Range (Figures 1, 2) is particularly important in our understanding of the structural and thermal characteristics of a terminating normal fault and tilt-domain boundary. In map view, the width of the southern Wassuk Range shortens from ~20 km in the area south of Walker Lake to ~9 km in the Anchorite Hills, and is associated with a similar southward decrease in fault-block tilting, from > 60° to < 10°, and exposed paleodepths. Abrupt tilt discontinuities are accommodated by northeast-striking scissor faults that gradually lessen tilting and topography of the southern Wassuk Range, which terminates at a northeast-striking sinistral-slip fault along the northern Mina Deflection (Figures 1, 2). Four tilt blocks are recognized in the southern Wassuk Range and are defined by regions of consistent dip and are separated by northeast-striking scissor or sinistral-slip faults expressed as en-echelon right steps along the modern range-front system. Each of the tilt blocks is described in detail below and are (from north to south) the Mount Grant, Coryville, Lucky Boy and Anchorite Hills blocks (Figure 2).

Mount Grant Block

The Mt. Grant block exposes a ~9.5 km crustal section comprised primarily of Mesozoic quartz monzonite and Triassic – Jurassic metavolcanic rocks and is structurally similar to the central Wassuk Range (i.e., Stockli et al., 2002; Surpless et al., 2002). North-northwest-striking, high-angle, east-dipping normal faults run along the entire eastern flank of the Mt. Grant block (Figure 2, 3). Mt. Grant is the highest point in the Wassuk Range at almost 3.5 km in elevation and is topped by steeply, northwest-dipping (60° – 70°), Miocene andesites, presumably the Lincoln Flat andesite, and calcareous lacustrine and fluvial deposits of the Wassuk Group's Aldrich Station Formation (Figure 3). The overlying Neogene units (Table 1) strike to the northeast and are oriented oblique to the north-northwest-trending range front, therefore, exposed paleodepths increase towards the southeast corner of the Mt. Grant block. A low-angle, scoop-shaped normal fault dips to the east and dissects the Mt. Grant block repeating the Mesozoic and Neogene section to the west (Figure 3). In the Coal Valley, west of the Mt. Grant block, the entire Mesozoic through Neogene section is preserved between the Wassuk Range and Pine Grove Hills to the west (Figure 4) and has been mapped previously by Gilbert and Reynolds (1976).

In Coal Valley, the entire Neogene section has been folded into a gentle, west-northwest-trending syncline (Figure 4). Miocene andesites and Miocene Wassuk Group rocks young towards the west and their dips shallow up section. Hornblende andesites of Lincoln Flat nonconformably overlie Mesozoic crystalline rocks of the southern Wassuk Range and dip 60 - 75° to the west, except where in faulted contact, dip as little as 17 - 35°. The Wassuk Group overlies the Lincoln Flat andesite and has dips ranging from ~5 - 60° to the west. $^{40}Ar/^{39}Ar$-dated interbedded tuffs from the Wassuk Group bracket much of the middle Miocene Wassuk Range tilting history (Table 1, Figures 5, 6). A tuff dipping ~10° to the west yielded a $^{40}Ar/^{39}Ar$ plateau age of 11.33 ± 0.07 Ma and overlies slightly older tuffs with $^{40}Ar/^{39}Ar$ plateau ages of 11.74 ± 0.07 Ma and 11.59 ± 0.09 Ma that dip ~35° to the west (Figures 4, 6),

thereby constraining much of the Miocene tilting. An abrupt increase in dip occurs up section where 30-50° dipping andesitic and tuffaceous sandstones from the Morgan Ranch Formation appear to be obliquely thrusted over units of the younger Coal Valley Formation. Further to the west a north-south-trending, east-dipping normal fault juxtaposes the uppermost Wassuk Group against Mesozoic granites of the Pine Grove Hills.

Coryville Block

Miocene tilting and extension in the Coryville block exposed a ~8 km-thick crustal section. The block is bounded to the north and south by northeast-striking scissor faults and to its east by north-northwest-striking, east-dipping normal faults (Figure 2, 3, 6). The range front of the Coryville block is structurally more complicated than that of the Mt. Grant block and is defined by a complex network of normal and transtensional faults (e.g., Heinz et al., 2010). Many of the range-front structures developed within a pull-apart zone (Bell and Hinz, 2010; Heinz et al., 2010; Moeck et al., 2010) at the northeastern corner of the Coryville block, marked by a ~1 – 2 km right step in the range front (Figure 3). Quaternary fault scarps along the range front penetrate into basement and gradually step down basement topography into the present-day Walker Lake basin (Figure 6) and is evident in ~1.2 km deep geothermal test holes near the range front that penetrated basement at depths of 300 – 500 m (Lazaro et al., 2010; Schoffner, personal communication 2010) and gravity data imaging basement at depths of ~1 – 1.5 km in the center of the Walker Lake basin (Schoffner et al., 2010).

In Fletcher Valley, immediately west of the Coryville block, the Miocene Lincoln Flat andesite nonconformably overlies Mesozoic basement of the Wassuk Range (Figures 2, 3). The Lincoln Flat andesite dips consistently along the western flank of the Coryville block at ~35° to the west. Although Quaternary alluvium covers most of the Neogene section in Fletcher Valley, calcareous siltstones from the lowermost Aldrich Station Formation (9.3 – 13 Ma) of the Wassuk Group (Axelrod, 1956; Gilbert and

Reynolds, 1976) are exposed where they dip ~30 - 35° to the west and overlie the Lincoln Flat andesite. An east-dipping normal fault that dissects the Mt. Grant block to the north is projected into Fletcher Valley and likely offsets the Neogene section.

Lucky Boy Block

The Lucky Boy block sits at the southernmost Wassuk Range and is bounded to the north by a northeast-striking scissor fault and to east by high-angle, east-dipping normal faults. The Lucky Boy block is primarily composed of Cretaceous granite and Miocene andesite, and exposes a < 4 km thick crustal section. The gently dipping (≤ 15°) Lincoln Flat andesite is found on top of a few peaks throughout the Lucky Boy block where it nonconformably overlies Mesozoic basement and also forms a ~3 - 9 km-long dip slope along its northwestern flank (Figure 6) . Aside from the Lincoln Flat andesite and a few flat-lying Neogene–Quaternary basalt plugs and lava fields, the remaining Neogene section is covered by Quaternary alluvium. In contrast to the Mt. Grant and Coryville blocks to the north, the strike of the range front of the Lucky Boy block varies by almost 90°. The strike of the northernmost Lucky Boy block range front matches that of the entire southern Wassuk Range and is oriented north-northwest, but in the south turns ~90° clockwise over a distance of ~3 – 5 km (Figure 1, 2). This smooth curvilinear fault trace forms the Pliocene age Whisky Flat pull-apart structure, and demarks the northern extent of the Mina Deflection (Stockli et al., 2003); it is the structural equivalent to the Queen Valley pull-apart structure (Figure 1) at the northern terminus of the White Mountains (e.g., Stockli et al., 2003; Tincher and Stockli, 2009).

Anchorite Hills Block

The Anchorite Hills are composed of Mesozoic granite nonconformably overlain by Neogene andesites, ignimbrites and siliciclastic rocks and are further overlain in areas by Neogene – Quaternary basalts (Stewart et al., 1981, 1984). Neogene volcanic and sedimentary rocks are variably inclined, and

although predominantly dipping towards the west, their attitude appears to be primarily controlled by local structures that are unrelated to Wassuk Range tilting. The Anchorite Hills are bound to the south by the left-lateral Anchorite fault zone. The Anchorite fault zone strikes to the northeast and extends from along the eastern flank of the southern Wassuk Range, through Anchorite Pass and into a diffuse zone of fault splays and lineaments in the northern Mono Lake Basin (Wesnousky, 2005). The deepest structural levels are recognized as areas of exposed Mesozoic basement and are only present at the southeastern corner of the Anchorite Hills block. Thermochronometric data from Mesozoic intrusive rocks exposed along the Anchorite Hills range front record the Late Cretaceous – middle Eocene denudation of Sierran intrusive and associated wall rocks, but contain no signal of middle Miocene exhumation (Krugh, 2008).

Pine Grove Hills

The Pine Grove Hills are a ~30 km-long, northeast-striking range that lies immediately west of the Mt. Grant block. An east-dipping, high-angle normal fault along its eastern extent has exhumed a ~2.5 km-thick crustal section of Mesozoic basement and overlying Neogene cover. Oligocene silicic Ignimbrites and Miocene andesites dip ~5° - 30° to the west (Gilbert and Reynolds, 1976), and appear to have been tilted prior to the deposition of the 12 – 8 Ma Wassuk Group (Dilles and Gans, 1995). Tilting dissimilarities between the Mt. Grant block and Pine Grove Hills suggests that middle Miocene deformation was not kinematically linked between the two blocks, despite their latitudinal contiguity. Tilting of the Pine Grove Hills footwall more closely resembles that of the Coryville block, which both experienced a slightly later onset and therefore shorter duration of tilting than seen in the Mt. Grant block, and central Wassuk Range.

THERMOCHRONOMETRIC RESULTS

Approximately 85 samples were collected from the southern Wassuk Range and Pine Grove Hills, and were taken from outcrops of unaltered and unweathered Mesozoic granite and metavolcanic rocks (Figure 2).

Mt. Grant Block

ZHe ages from the Mt. Grant block range between ~70 and 12.6 Ma and show an overall younging toward the southeast. An apparent Miocene ZHe PRZ in the ZHe vs. Miocene paleodepth profile is evident by the presence of two inflection points at ~34 Ma and ~15 Ma and 6.1 ± 0.5 km and 7.7 ± 0.7 km, respectively (Figure 7). ZHe ages above the PRZ decrease with increasing depth from ~70 Ma to ~35 Ma at a rate of ~5 Myr/km and record Paleogene cooling at a rate of ~2° – 2.5° C/Ma related to the cessation of Sierran arc magmatism and subsequent denudation (Figure 8). Apparent ZHe ages below the PRZ are invariant and record the onset of rapid cooling related to footwall exhumation at ~12 – 15 Ma. Assuming a mean annual surface temperature of 10° ± 5° C, the depth of the upper and lower isotherms defining the ZHe PRZ together, yield an average Miocene geothermal gradient of ~21.5° ± 2° C/km.

AHe ages from the Mt. Grant block also young towards the southeast where Mio-Pliocene paleodepths are greatest at ~3.4 km. A few exceptions to this overall younging trend are from samples that were collected directly beneath the Lincoln Flat andesite, and a few along the present-day range front; both sets of ages experienced reheating either by overlying volcanic rocks or migrating hydrothermal fluids along range-front structures. Two inflection points in the AHe vs. Mio-Pliocene paleodepth profile are recognized (Figure 9) and occur at ~15 Ma and ~1.2 km and ~4 Ma and ~2.6 km. These inflection points define the location of the upper and lower limits of the Mio-Pliocene AHe PRZ defined by the 40° C and 80° C isotherms, respectively. An AHe age of 15.6 ± 1.2 Ma above the Mio-

Pliocene PRZ and invariant AHe ages of ~4 Ma below the Mio-Pliocene PRZ record the onset of rapid cooling related to the exhumation of the southern Wassuk Range. The measured depth of the upper and lower limits of the Mio-Pliocene AHe PRZ below the Paleogene nonconformity provides a mean, Mio-Pliocene geothermal gradient estimate of ~32° ± 9° C/km.

Coryville Block

Both ZHe and AHe ages from the structurally intact Coryville block young with increasing paleodepth towards the east. However, samples to the east along the range front were collected from structurally detached fault blocks and yielded older ages analogous to those from the uppermost crustal levels on the western side of the Coryville block. The southernmost transect is the most complete and has the smallest sample spacing of the two transects and will be the primary dataset for the Coryville block. Two inflection points are recognized in the ZHe age vs. Miocene paleodepth profile at ~35 – 40 Ma and ~3.5 km, and ~12 – 14 Ma and ~5.8 km, and define the upper and lower limits of the Miocene ZHe PRZ (Figure 7). In the entire Coryville block, ZHe ages above the PRZ are Cretaceous to late Eocene in age and young towards the southeast and likely record cooling related to the cessation of the Sierran Magmatic arc and erosional denudation associated with the formation of the Paleogene nonconformity. Below the PRZ, ZHe ages are invariant at ~12 – 14 Ma and record the onset of rapid cooling. The depth of the 140° and 200° C isotherms yields an average Miocene geothermal gradient estimate of ~36° ± 2° C /km.

A ~3 km-thick Mio-Pliocene section is exposed in the Coryville block. AHe ages from the Coryville block young towards the southeast and record the entire Cenozoic cooling history of the southern Wassuk Range. AHe ages from the northwestern corner of the Coryville block are Paleocene to Oligocene in age, and are the result of heating and cooling throughout the Paleogene. Three inflection points are recognized in the AHe age vs. Mio-Pliocene paleodepth profile from the

northernmost transect and occur at ~15 Ma and ~0.7 km, ~15 Ma and ~1 km, and at ~3.5 – 5 Ma and ~2.4 km. Only two of the inflection points are recognized in the southernmost transect (Figure 9) and are well defined at ~15 Ma and ~0.7 km, and ~3 -4 Ma and ~2 km. These two inflection points define the upper and lower limits of the Mio-Pliocene AHe PRZ (Figure 9) and are further defined by the 40° C and 80° C isotherms thereby yielding a mean geothermal gradient estimate of ~39° ± 7° C/km.

Lucky Boy Block

Sample transects were only collected between ~1.5 and ~4 km Miocene paleodepth, and did not reach the Paleogene nonconformity. In general, both ZHe and AHe ages from the structurally intact Lucky Boy block young towards Whisky Flat in the southeast, where the southern Wassuk Range -front fault trace becomes curvilinear and strikes towards the northeast. A small population of Paleogene ZHe cooling ages is present along the range front and is not represented anywhere else in the Lucky Boy block, even on its westernmost margins, and therefore likely sampled structurally detached slivers of the southern Wassuk Range. ZHe ages from the structurally intact Lucky Boy block show little variation, and all range between ~20 and 12 Ma and define the lowermost portion of the ZHe vs. Miocene paleodepth profile described in the Mt. Grant and Coryville blocks to the north, and likely resided directly below the Miocene ZHe PRZ. The middle transect, which sampled Miocene paleodepths of ~1.5 – 3.5 km, may arguably have preserved the lowermost portion of the PRZ at a depth of ~2.2 km where the shallowest ZHe ages approach 20 Ma (Figure 7). These transects provide us with a lowermost constraint on the depth of the Miocene 200° C isotherm, and therefore estimates for a geothermal gradient of ≥ 76° ± 5° C/km; these estimates are significantly higher than those for the Coryville and Mt. Grant blocks to the north.

AHe ages from the structurally intact Lucky Boy block are similarly invariant with respect to the ZHe dataset and range between ~2.8 and ~6.4 Ma at Mio-Pliocene paleodepths of ~0.6 - 2.3 km. These

samples represent the deepest portion of the AHe vs. Mio-Pliocene paleodepth profile, as seen in the Mt. Grant and Coryville blocks, and likely resided below the Mio-Pliocene AHe PRZ and therefore below 80° C. A very slight inflection point in the middle vertical transect occurs at ~3 Ma and 0.7 km, and may mark the depth of the Mio-Pliocene 80° C isotherm (Figure 9). Although poorly constrained, these data provide Mio-Pliocene geothermal gradient estimates of ≥ 80° ± 26° C/km, despite the absence of a complete, preserved, Mio-Pliocene AHe PRZ.

Pine Grove Hills

Only three samples were collected from Mesozoic granites from the eastern flank of the Pine Grove Hills (Figure 2). In the sample area, Miocene andesites are not in depositional contact with Mesozoic basement and therefore paleodepth estimates are difficult. However, 35° west-dipping Miocene andesites, approximately 8 km north of the study area, provide some constraints on the degree of tilting where east-dipping normal faults exposed a ~2.5 km-thick crustal section. (U-Th)/He samples were only collected from the deepest structural paleodepths and do not sample the entire section. The three ZHe cooling ages from the Pine Grove Hills are Paleocene and Eocene in age (Figure 10) and their cooling was therefore unaffected by Miocene and younger extension. AHe ages, however, are invariant at ~12.5 – 13 Ma and likely represent the structurally lowest portion of the Miocene AHe PRZ and are associated with rapid cooling during exhumation of the Pine Grove Hills footwall (Figure 10). Even though AHe samples resided below the PRZ, no geothermal gradient estimates can be made for the Pine Grove Hills since Neogene tilting and therefore paleodepths are poorly constrained.

Inverse Modeled Time-Temperature Histories

The *He*lium *M*odeling *P*rogram (HeMP) (Hager and Stockli, 2009) was used to model individual sample datasets with ZHe and AHe age data from the southern Wassuk Range and Pine Grove Hills. Inverse modeling through HeMP is practically identical to Ketcham's (2005) HeFTy software, in that it

solves the ^{4}He production and diffusion equations using a series of user-constrained, but random, Monte Carlo-type simulated time-temperature (T-t) paths. Model (U-Th)/He ages for each sample are then statistically compared to laboratory-derived ages in order to evaluate the compatibility of the associated model-generated T-t path. The advantage to HeMP is its ability to simultaneously model AHe and ZHe age data from an individual sample, thereby expanding its thermochronometrically constrainable thermal history. Inverse models were used to constrain the Cretaceous and younger cooling history of individual samples from a range of structural paleodepths in the southern Wassuk Range (Figure 11). Additionally, paleotemperatures derived from modeled T-t histories in collaboration with paleodepth calculations were used to estimate both the pre-extensional geothermal gradient and volcanic overburden (e.g., Stockli et al., 2002; Stockli, 2005).

Structurally shallow samples from the southern Wassuk Range were modeled to constrain the earliest thermal evolution of the upper crust. Inverse T-t histories show two phases of cooling starting with a period of slow cooling from ~85 to ~40 Ma, and followed by a rapid-cooling event between ~12 – 15 Ma. Protracted cooling throughout the Late Cretaceous and Paleogene are recorded in the modeling data and are consistent with the development of the Paleogene unconformity during erosional unroofing of the Sierra Nevada over the same time span (e.g., Christiansen et al., 1992, Van Buer et al., 2009). Modeling results from all three tilt blocks show a southward progressive absence or overprinting of early pre-Cenozoic cooling, and modeled samples from even the shallowest structural levels only record middle Miocene and younger cooling.

Inverse T-t histories from samples along the range front represent the deepest structural levels of the Wassuk Range and record an episodic three-stage thermal history characterized by rapid cooling at ~12 – 15 Ma, followed by a period of isothermal holding, and finally renewed cooling at ~3 - 5 Ma. These events are consistent with the faulting history derived from the tilting of Miocene and younger

units west of the southern Wassuk Range, and inflections in the AHe and ZHe vs. paleodepth plots. T-t histories from the Pine Grove Hills to the west record an earlier three-stage thermal history starting with protracted cooling throughout the Paleogene associated with the erosional unroofing of the Wassuk Range region, followed by rapid cooling at ~12 Ma and isothermal holding till the present day. The similar T-t histories shared by the Pine Grove Hills and the shallowest structural levels in the southern Wassuk Range suggest that the area immediately west of the Wassuk Range was devoid of any Mio-Pliocene and younger exhumation and extension.

Model-derived middle Miocene geothermal gradients increase towards the south and are ~19° ± 4° C/km in the Mt. Grant block, ~29° ± 4° C/km in the Coryville block, and ≥ 65° ± 20° C/km in the Lucky Boy block (Figures 12, 13) and are in agreement with geothermal gradient estimates gleaned from the positions of the middle Miocene ZHe PRZ (Figure 7). The geothermal gradient estimates are used to determine overburden and when projected upward, intersects the thermally defined surface at ~0.8 km above the Paleogene nonconformity. Overburden estimates of ~0.8 km agree with other mapped (e.g., Surpless, 1999) and thermally determined (Stockli et al., 2002) regional thickness estimates for the Lincoln Flat andesite.

Mio-Pliocene geothermal gradients also show a similar increase towards the southernmost Wassuk Range and are ~27° ± 4° C/km in the Mt. Grant block, ~28° ± 2° C/km in the Coryville block, and ≥ 65° ± 8° C/km in the Lucky Boy block. Temperature estimates from the Mt. Grant and Coryville blocks are within error of the present-day Basin and Range geothermal gradient (35° ± 5° C/km). The Mio-Pliocene geothermal gradient in the Mt. Grant block exhibits a significant increase (8° ± 7° C/km) since the middle Miocene and follows a period of large-magnitude extension, exhumation and tilting. Indiscernible middle Miocene to Mio-Pliocene footwall advection in the southernmost Wassuk Range correlates with decreasing amounts of middle Miocene extension, exhumation and tilting (Figure 13).

DISCUSSION

Faulting and Tilting History of the Southern Wassuk Range

Integrated structural and (U-Th)/He thermochronological data constrain the thermal and structural evolution of the southern Wassuk Range and Pine Grove Hills prior to and during break away from the eastern Sierra Nevada magmatic arc. AHe and ZHe age data indicate that the southern Wassuk Range underwent three episodes of cooling since the Late Cretaceous, associated first with the formation of the Paleogene nonconformity, followed by two episodes of Neogene extension and footwall exhumation. This thermal history is in good agreement with the $^{40}Ar/^{39}Ar$-constrained tilting history of overlying Neogene cover in the Coal and Fletcher Valleys, and Neogene extension documented in the central Wassuk Range (McInyre, 1990; Dilles and Gans, 1995; Surpless et al., 2002; Stockli et al., 2002; Stockli, 2005).

Late Cretaceous through Paleogene cooling was related to the erosional unroofing of the Sierra Nevada block and is recorded in AHe and ZHe ages from the shallowest structural levels in the Mt. Grant and Coryville blocks in the southern Wassuk Range (Figures 7- 9), and in ZHe data at all structural levels from the Pine Grove Hills (Figure 10). The most complete record of Cenozoic cooling is preserved in the Mt. Grant block, where ZHe ages from the upper ~6 km of section, cover most of the Paleogene and record a cooling rate of < 2° – 2.5° C/Myr (Figure 8), which is consistent with a period of deep erosion following the cessation of Sierran magmatism ca. 85 Ma and prior to the development of the Paleogene unconformity surface ca. 40 Ma (Van Buer et al., 2009).

Miocene and younger cooling ages result from the tectonic exhumation of the southern Wassuk Range and Pine Grove Hills. An episode of middle Miocene east – west extension is recorded across the entire Wassuk Range (e.g., Surpless et al., 2002; Stockli et al., 2002) and to the west in the northern Singatse Range (Proffett, 1977; Proffett and Dilles, 1984; Dilles and Gans, 1995), Grey Hills (Surpless et

al., 2002), and Pine Grove Hills. AHe and ZHe data indicate the onset of rapid footwall exhumation at ~12 – 15 Ma in the southern Wassuk Range and ~12.5 – 13 Ma in the Pine Grove Hills to the west (Figure 7, 9, 10). Middle Miocene large-magnitude extension was accommodated primarily by footwall rotation along a north-northwest-trending axis and variably tilted the southern Wassuk Range and Pine Grove Hills, as documented by the tilting of the overlying Neogene cover. Tilting was greatest in the Mt. Grant block to the north and matched the tilting history of the central Wassuk Range (e.g., Stockli et al., 2002; Surpless et al., 2002), where Miocene extension resulted in ~60° of westward footwall rotation. Degree of footwall rotation decreases dramatically towards the south to ~35° in the Coryville block and Pine Grove Hills, and ~15 - 20° in the Lucky Boy block. East-northeast-striking scissor faults in the southern Wassuk Range formed the boundaries between tilt blocks and accommodated large tilt discontinuities, and are expressed in map view as en-echelon right steps in the modern range front. Despite their similarities in tilting, exhumation of the southern Wassuk Range was much greater than that of the Pine Grove Hills and is evident by the presence of young (≤ 15 Ma) ZHe ages along the entire Wassuk Range front, and non-reset (≥ 35 Ma) ZHe ages in the Pine Grove Hills.

The westernmost Mina Deflection likely developed in response to the onset of east-west extension in the White Mountains at ~12 Ma (Stockli et al., 2003), since extension in the White Mountains is synchronous or slightly younger than that of the southernmost Wassuk Range. Interestingly, a number of right en-echelon steps in the southern Wassuk Range front developed in response to differential tilting, but also appear to gradually mitigate misalignment between the strike of the Wassuk Range and White Mountain range-front faults. Nevertheless, the southern Wassuk Range is a terminating normal-fault system in the sense that it dies into transverse-strike and oblique-slip fault zone (e.g., Faulds and Varga, 1998), which like many throughout the Basin and Range are characterized by the absence of major tilted blocks, disrupted structural and topographic grain, and changes in the faulting and fracture density (Slemmons, 1967; Stewart, 1980).

As evident from AHe thermochronologic data, a second episode of rapid exhumation began at ~3 – 5 Ma in the southern Wassuk Range and developed in response to right-lateral transtensional deformation in the Walker Lane belt. Mio-Pliocene transtension was accommodated primarily by dextral-oblique slip along the southern Wassuk Range front. A number of Mio-Pliocene pull-apart structures also developed at this time and are highlighted by the distribution of young (< 5 Ma) AHe ages at en-echelon steps in the range front and at Whisky Flat, and are analogous to the development of pull-apart structures along the northern White Mountains (Stockli et al., 2003; Tincher and Stockli, 2009), normal and transcurrent faults in the Mina Deflection (Stewart, 1988; Hardyman and Oldow, 1991; Oldow, 1992; Oldow et al., 2001), and structural reorganization throughout the central Walker Lane (Oldow et al., 2008). Unlike the central and southern Wassuk Range (e.g., Stockli et al., 2002; Surpless et al., 2002), the Pine Grove Hills did not experience any Mio-Pliocene deformation, as evident from the absence of Mio-Pliocene and younger cooling ages, and suggests that the Wassuk Range defines the western limit of Mio-Pliocene right-lateral, Walker Lane transtension.

Upper-Crustal Thermal Structure of the Southern Wassuk Range

The Wassuk Range and Pine Grove Hills were part of the Sierra Nevada magmatic arc prior to middle Miocene extension and therefore experienced a similar pre-extensional thermal history and post-Cretaceous geothermal gradient of < 15° - 20° C/km (e.g., Stockli, 1999; Stockli et al., 2002; Surpless et al., 2002). ZHe data from the shallowest structural levels show that Sierran plutonic rocks and associated wall rocks cooled at a rate of < 2 – 2.5° C/Myr during their denudation until ~40 Ma and are in agreement with other age estimates for the development of the Paleogene nonconformity (e.g., Van Buer et al., 2009). Thermochronologic data from the southern Wassuk Range indicate an increase in the middle Miocene geothermal gradient (> ~22° C/km) immediately prior to extension and agree with

similar results from the central Wassuk Range (Stockli et al., 2002; Surpless et al., 2002) and the Anchorite Hills (Krugh, 2008) that document a post-20 Ma heating event.

Model-derived middle Miocene geothermal gradient estimates increase dramatically towards the south from ~19° ± 4° C/km in the Mt. Grant block, ~29° ± 4° C/km in the Coryville block, and ≥ 65° ± 20° C/km in the Lucky Boy block, and agree with estimates derived from the position of the fossil middle Miocene ZHe PRZ in the three northern tilt blocks (Figure 13). Middle Miocene heating was focused towards the south, and overprinted much of the Paleogene ZHe cooling record. Therefore, in addition to geothermal gradient estimates, the thermal structure of the southern Wassuk Range can be viewed qualitatively by analyzing the distribution of Paleogene ZHe ages (Figure 14) where the Paleogene nonconformity does not parallel ZHe isopleths, but is instead intersected by progressively younger isopleths towards the south where Paleogene ZHe ages are absent from the structurally intact southern Wassuk Range. When the southern Wassuk Range is palinspastically restored to its pre-extensional configuration, Paleogene ZHe age isopleths cut up section and again are absent at all structural levels in the Lucky Boy block, corroborating a thermally elevated southern Wassuk Range (Figure 15). The hot middle Miocene southern Wassuk Range likely resulted from localized arc magmatism (e.g., Christiansen et al., 1992; Stewart, 1998) that occupied the structurally weak crustal boundary along the Mina Deflection (e.g., Aldrich, 1986; Rowley, 1998; Faulds and Varga, 1998).

Mio-Pliocene geothermal gradient estimates for the southern Wassuk Range also increase toward the south and substantiate that the southernmost Wassuk Range remained hot until at least ~3 Ma. Subsequent footwall advection during middle Miocene exhumation of the Wassuk Range raised the geothermal gradient to its Mio-Pliocene levels by as much as 8° ± 7° C/km (Figure 12), values which are on par with the present-day geothermal gradient of 35° ± 5° C/km in the Basin and Range province. Middle Miocene geothermal gradients in the southern Wassuk Range show an inverse correlation with

Miocene and younger tilting, exhumation, and footwall advection (Figure 13) and consequently placate upper-crustal thermal variations between tilt blocks.

A final episode of extension associated with the onset of right-lateral transtension in the Walker Lane belt initiated at ~3 -5 Ma in the southern Wassuk Range, and continues today (e.g., Stockli et al., 2002; Surpless et al., 2002; Krugh, 2008; Hinz et al., 2010; Moeck et al., 2010). Footwall advection is concentrated along en-echelon right steps at the range front and at Whisky Flat where the range front is oriented roughly orthogonal to the regional northwest-southeast extension direction. These pull-apart zones are characterized by increased footwall advection and range-front faulting. Geothermal exploration along the southern Wassuk Range front and Walker Lake basin (e.g., Gorynski et al., 2010; Kratt et al., 2010: Lazaro et al., 2010; Penfield et al., 2010; Gorynski, Chapter 3) reveals a number of thermal perturbations related to the thermal redistribution of heat by hydrothermal fluids from the hot Wassuk Range footwall to the hanging-wall basin also concentrated at range-front pull-apart structures (e.g., 2010; Hinz et al., 2010; Moeck et al., 2010; Gorynski, Chapter 3).

CONCLUSIONS

Structural and thermochronometric data from the southern Wassuk Range and Pine Grove Hills are used here to describe the Cenozoic thermal anatomy and evolution of an accommodation zone and tilt-domain boundary. The Wassuk Range and Pine Grove Hills areas were once part of the Sierran magmatic arc, and experienced the same slow (< 2 – 2.5° C/Ma), Paleogene cooling history associated with its erosional denudation and culmination as a relatively cool (< 15° - 20° C/km) (Stockli, 1999) crustal block. Model-derived middle Miocene geothermal gradient estimates for the southern Wassuk Range increase towards the south from ~19° ± 4° C/km in the Mt. Grant block, to ~29° ± 4° C/km in the Coryville block and to ≥ 65° ± 20° C/km in the Lucky Boy block, and represent the thermal state of the crust immediately prior to large-magnitude extension. Geothermal gradient estimates are further

supported by the spatially concordant shallowing of the Miocene ZHe PRZ and progressive overprinting of Paleogene ZHe cooling ages that are synchronous with the extrusion of the Lincoln Flat andesite at 14.8 – 15.1 Ma, which itself becomes immensely hydrothermally altered towards the south (Gilbert and Reynolds, 1976). We propose that the southernmost Wassuk Range and Mina Deflection were the focus of middle Miocene magmatism and volcanism of the Miocene magmatic arc that occupied the structurally predisposed crustal boundary demarked by the $^{87}Sr/^{86}Sr$ 0.706 line. An episode of heating immediately prior to middle Miocene extension is also documented throughout the Wassuk Range and Anchorite Hills (i.e., Stockli et al., 2002; Surpless et al., 2002; Krugh, 2008) and likely resulted from the associated magmatism and shallow dike emplacement.

AHe and ZHe thermochronologic data from the Wassuk Range footwall in combination with $^{40}Ar/^{39}Ar$-constrained, westward-tilted Miocene andesites and Wassuk Group rocks show two episodes of extension and exhumation beginning at ~12 – 15 Ma and ~3 – 5 Ma. Middle Miocene east-west extension immediately follows regional magmatic advection during extrusion of the Lincoln Flat andesite and thermally destabilized the crust (e.g., Kuznir and Park, 1987; Stockli et al., 2002; Surpless et al., 2002). Middle Miocene extension variably tilted the Wassuk Range footwall to ≥ 60° in the central Wassuk Range (Stockli et al., 2002; Surpless et al., 2002) and Mt. Grant block, ~35° in the Coryville block and Pine Grove Hills, ~15 – 20° in the Lucky Boy block, with little to no associated tilting or exhumation in the Anchorite Hills or Mina Deflection. The southward decreasing size of footwall tilt blocks in the southern Wassuk Range is a direct result of the elevated geothermal gradient and a shallowing of the brittle/ductile transition zone. Therefore, E-W extension at the Mina Deflection was instead accommodated along east-striking dextral-slip faults which further accommodated differential tilting between the west-dipping Wassuk Range and east-dipping White Mountains.

As shown by Mio-Pliocene geothermal gradient estimates, footwall advection accompanied middle Miocene extension and in the Mt. Grant block raised the geothermal gradient by ~8° ± 7° C/km (Figure 12). Miocene footwall rotation and advection for the Mt. Grant, Coryville and Lucky Boy tilt blocks are inversely proportional to their pre-extensional geothermal gradients, meaning that the focus of advection shifted from magmatic advection in the southern Wassuk Range prior to middle Miocene tilting, to footwall advection in the central and northern Wassuk Range during middle Miocene tilting and consequently damped large lateral thermal variations. A second episode of rapid footwall exhumation began at ~3- 5 Ma and resulted from transtension along the southern Wassuk Range associated with the onset of right-lateral, Walker Lane deformation. Exhumation and footwall advection was focused at pull-apart structures located at right en-echelon steps along the range front and at Whisky Flat. Mio-Pliocene transtension is mirrored in the White Mountains by the formation of the Queen Valley pull apart at ~3 Ma on its northern terminus (Stockli et al., 2003; Tincher and Stockli, 2009), and transtension along transcurrent faults in the Mina Deflection (Stewart, 1988; Hardyman and Oldow, 1992; Oldow, 1992; Oldow et al., 2001).

The southern Wassuk Range and Mina Deflection were thermally and kinematically linked and worked in tandem to raise the geothermal gradient throughout the Neogene. This detailed thermochronologic study provides a model for the thermal evolution of an accommodation zone and associated extensional system that involves cycles of magmatic and footwall advection that mimic successions of volcanism and amagmatic extension recorded throughout the Basin and Range (e.g., Gans and Bohrson, 1998). Pre-extensional magmatism and volcanism focus along structurally permeable accommodation zones in the upper crust. These events thermally elevate the entire area at depth, but show large lateral thermal variations at the upper-crustal levels, where heating is greatest near volcanic and magmatic centers. This model predicts an elevated brittle/ductile transition zone near these volcanic centers which restricts the thickness and geometry of extending footwall tilt-blocks.

Subsequent extension and footwall advection are therefore greatest at the distal portions of extensional systems and consequently abate upper-crustal thermal disparities.

Chapter 2: REFERENCES

Aldrich Jr, M., 1986, Tectonics of the Jemez lineament in the Jemez Mountains and Rio Grande rift: Journal of Geophysical Research, v. 91, p. 1753-1762.

Al-Rawi, Y., 1969, Cenozoic history of the northern part of Mono Basin, California and Nevada: Ph.D. Thesis; University of California, Berkley California.

Atwater, T., and Stock, J., 1998, Pacific-North America plate tectonics of the Neogene southwestern United States: an update: International Geology Review, v. 40, p. 375-402.

Axelrod, D., 1956, Mio-Pliocene floras from west-central Nevada: California University Publications Geological Society, v. 33, p. 1-322.

Axen, G.J., 1998, The Caliente-Enterprise zone, southeastern Nevada and southwestern Utah: Geological Society of America Special Papers, v. 323, p. 181-194.

Bell, J.W., and Hinz, N., 2010, Young Walker Basin faults provide new insights into structural relations controlling geothermal potential at the Hawthorne army weapons depot, central Nevada: Transactions-Geothermal Resources Council, v. 34, p. 751-754.

Bonham Jr, H., and Garside, L., 1979, Geology of the Tonopah: Lone Mountain, Klondike, and northern Mud Lake quadrangles, Nevada: Nevada Bureau of Mines and Geology Bulletin, v. 92, p. 1-142.

Burchfiel, B., Cowan, D., and Davis, G., 1992, Tectonic overview of the Cordilleran orogen in the western United States: The Cordilleran orogen: Conterminous US: Boulder, Colorado, Geological Society of America, Geology of North America, v. 3, p. 407–479.

Christiansen, R., Yeats, R., Graham, S., Niem, W., and Niem, A., 1992, Post-Laramide geology of the US Cordilleran region: in Burchfiel, B.C., Lipman, P.W., and Zoback, M.L., eds., The Cordilleran orogen: Conterminous US: Boulder, Colorado, Geological Society of America, Geology of North America, v. 3, p. 261–406.

Coney, P.J., and Harms, T.A., 1984, Cordilleran metamorphic core complexes: Cenozoic extensional relics of Mesozoic compression: Geology, v. 12, p. 550-554.

Crone, A.J., and Haller, K.M., 1991, Segmentation and the coseismic behavior of Basin and Range normal faults: examples from east-central Idaho and southwestern Montana, USA: Journal of Structural Geology, v. 13, p. 151-164.

DePolo, C.M., Clark, D.G., Slemmons, D.B., and Ramelli, A.R., 1991, Historical surface faulting in the Basin and Range province, western North America: implications for fault segmentation: Journal of Structural Geology, v. 13, p. 123-136.

Dilles, J., and Wright, J., 1988, The chronology of early Mesozoic arc magmatism in the Yerington district of western Nevada and its regional implications: Bulletin of the Geological Society of America, v. 100, p. 644-653.

Dilles, J., and Gans, P., 1995, The chronology of Cenozoic volcanism and deformation in the Yerington area, western Basin and Range and Walker Lane: Geological Society of America Bulletin, v. 107, p. 474-486.

Dodson, M., 1979, Theory of cooling ages: Lectures in isotope geology, p. 194–202.

Duebendorfer, E., and Black, R., 1992, Kinematic role of transverse structures in continental extension: An example from the Las Vegas Valley shear zone: Nevada: Geology, v. 20, p. 1107–1110.

Farley, K., 2000, Helium diffusion from apatite: General behavior as illustrated by Durango fluorapatite: Journal of Geophysical Research, v. 105, p. 2903-2914.

Faulds, J., and Varga, R., 1998, The role of accommodation zones and transfer zones in the regional segmentation of extended terranes: Geological Society of America Special Papers, v. 323, p. 1-45.

Faulds, J., and Henry, C., 2008, Tectonic influences on the spatial and temporal evolution of the Walker Lane: An incipient transform fault along the evolving Pacific–North American plate boundary: Ores and orogenesis: Circum-Pacific tectonics, geologic evolution, and ore deposits, Arizona Geological Society Digest, v. 22, p. 437-470.

Fitzgerald, P.G., and Gleadow, A.J.W., 1990, New approaches in fission track geochronology as a tectonic tool: examples from the Transantarctic Mountains: International Journal of Radiation Applications and Instrumentation. Part D. Nuclear Tracks and Radiation Measurements, v. 17, p. 351-357.

Foster, D.A., and John, B.E., 1999, Quantifying tectonic exhumation in an extensional orogen with thermochronology: examples from the southern Basin and Range Province: Geological Society London Special Publications, v. 154, p. 343-364.

Gans, P.B., Mahood, G.A., and Schermer, E., 1989, Synextensional magmatism in the Basin and Range province: A case study from the eastern Great Basin: Geological Society of America, 1-53.

Gans, P., and Bohrson, W., 1998, Suppression of volcanism during rapid extension in the Basin and Range Province, United States: Science, v. 279, p. 66-68.

Gilbert, C.M., and Reynolds, M.W., 1973, Character and chronology of basin development, western margin of the Basin and Range province: Geological Society of America Bulletin, v. 84, p. 2489-2510.

Gorynski, K.E., Stockli, D.F., Walker, J.D., and Sabin, A., 2010, Application of (U-Th)/He thermochronometry as a geothermal exploration tool in extensional tectonic settings: the Wassuk Range, Hawthorne, Nevada: Transactions-Geothermal Resources Council, v. 34, p. 685-688.

Guth, P.L., 1981, Tertiary extension north of the Las Vegas Valley shear zone, Sheep and Desert Ranges, Clark County, Nevada: Geological Society of America Bulletin, v. 92, part I,, p. 763-771.

Hager, C., 2009, A new Matlab©-based helium modeling package ("HeMP") for thermal history recovery from single and multi-thermochronometer (U-Th)/He data and data arrays.

Hardyman, R., and Oldow, J., 1991, Tertiary tectonic framework and Cenozoic history of the central Walker Lane, Nevada, Volume 1, p. 279-301.

Henry, C., 2008, Ash-flow tuffs and paleovalleys in northeastern Nevada: Implications for Eocene paleogeography and extension in the Sevier hinterland, northern Great Basin: Geosphere, v. 4, p. 1-35.

Hinz, N.H., Faulds, J.E., Moeck, I., Bell, J.W., and Oldow, J.S., 2010, Structural controls of three blind geothermal resources at the Hawthorne ammunition depot, west-central Nevada: Transactions-Geothermal Resources Council, v. 34, p. 785-790.

Howard, K.A., and Foster, D.A., 1996, Thermal and unroofing history of a thick, tilted Basin-and-Range crustal section in the Tortilla Mountains, Arizona: Journal of Geophysical Research, v. 101, p. 511-522.

Johnson, R.F., 1951, Geology of the Masonic Mining District, Mono County, California, University of California, Berkeley.

Ketcham, R., 2005, Forward and inverse modeling of low-temperature thermochronometry data: Reviews in Mineralogy and Geochemistry, v. 58, p. 275-314.

Kistler, R.W., and Peterman, Z.E., 1973, Variations in Sr, Rb, K, Na, and initial Sr87/Sr86 in Mesozoic granitic rocks and intruded wall rocks in central California: Geological Society of America Bulletin, v. 84, p. 3489-3512.

Kratt, C., Sladek, C., and Coolbaugh, M., 2010, Boom and bust with the latest 2m temperature surveys: dead horse wells, Hawthorne army depot, terraced hills, and other areas in Nevada: Transactions-Geothermal Resources Council, v. 34, p. 567-574.

Kuiper, K., Deino, A., Hilgen, F., Krijgsman, W., Renne, P., and Wijbrans, J., 2008, Synchronizing rock clocks of Earth history: Science, v. 320, p. 500-504.

Kusznir, N., and Park, R., 1987, The extensional strength of the continental lithosphere: its dependence on geothermal gradient, and crustal composition and thickness: Geological Society London Special Publications, v. 28, p. 35-52.

Lazaro, M., Page, C., Tiedeman, A., Sabin, A., Bjornstad, S., Alm, S., Meade, D., Shoffner, J., Mitchell, K., and Crowder, B., 2010, United States department of the Navy geothermal exploration leading to shallow and intermediate/deep drilling at Hawthorne ammunition depot, Hawthorne, NV: Transactions-Geothermal Resources Council, v. 34, p. 595-598.

Liggett, M.A., and Childs, J.F., 1977, An application of satellite imagery to mineral exploration: in, Woll, P.W., and Fischer, W.A., eds., Proceedings of the first annual William T. Pecora Memorial Symposium, October 1975, Sioux Falls, South Dakota: U.S. Geological Survey Professional Paper 1015, p. 253-270.

Mancktelow, N.S., and Grasemann, B., 1997, Time-dependent effects of heat advection and topography on cooling histories during erosion: Tectonophysics, v. 270, p. 167-195.

McIntyre, J., 1990, Late Cenozoic structure of the central Wassuk Range, Mineral County, Nevada, p. 1-120.

Miller, E.L., Dumitru, T.A., Brown, R.W., and Gans, P.B., 1999, Rapid Miocene slip on the Snake Range–Deep Creek Range fault system, east-central Nevada: Geological Society of America Bulletin, v. 111, p. 886-905.

Min, K., Mundil, R., Renne, P.R., and Ludwig, K.R., 2000, A test for systematic errors in 40Ar/39Ar geochronology through comparison with U/Pb analysis of a 1.1-Ga rhyolite: Geochimica et Cosmochimica Acta, v. 64, p. 73-98.

Moeck, I., Hinz, N.H., Faulds, J.E., Bell, J.W., Kell-Hills, A., and Louie, J.N., 2010, 3D Geological mapping as a new method in geothermal exploration: a case study from central Nevada: Transactions-Geothermal Resources Council, v. 34, p. 807-811.

Oldow, J., 1992, Late Cenozoic displacement partitioning in the northwestern Great Basin, p. 17–52.

Oldow, J., 2003, Active transtensional boundary zone between the western Great Basin and Sierra Nevada block, western US Cordillera: Geology, v. 31, p. 1033-1036.

Oldow, J.S., Bally, A.W., Avé Lallemant, H., and Leeman, W.P., 1989, Phanerozoic evolution of the North American Cordillera; United States and Canada: The geology of North America: An overview: Boulder, Colorado, Geological Society of America, Geology of North America, v. A, p. 139–232.

Oldow, J., Kohler, G., and Donelick, R., 1994, Late Cenozoic extensional transfer in the Walker Lane strike-slip belt, Nevada: Geology, v. 22, p. 637-640.

Oldow, J., Aiken, C., Hare, J., Ferguson, J., and Hardyman, R., 2001, Active displacement transfer and differential block motion within the central Walker Lane, western Great Basin: Geology, v. 29, p. 19-22.

Oldow, J., Geissman, J., and Stockli, D., 2008, Evolution and strain reorganization within late Neogene structural stepovers linking the central Walker Lane and northern Eastern California shear zone, western Great Basin: International Geology Review, v. 50, p. 270-290.

Oldow, J.S., Elias, E.A., Ferranti, L., McClelland, W.C., and McIntosh, W.C., 2009, Late Miocene to Pliocene synextensional deposition in fault-bounded basins within the upper plate of the western Silver Peak–Lone Mountain extensional complex, west-central Nevada: Late Cenozoic structure and evolution of the Great Basin-Sierra Nevada transition, p. 275-312.

Penfield, R., Zehner, R., Coolbaugh, M., Shevenell, L., Hastings, J., Johnson, G., Snyder, W., Morgos, D., Kurz, K., Sabin, A., Lazaro, M., Bjornstad, S., and Halsey, G., 2010, Geothermal site assessment using the national geothermal data system (NGDS), with examples from the Hawthorne ammunition depot area: Transactions-Geothermal Resources Council, p. 709-714.

Proffett, J., 1977, Cenozoic geology of the Yerington district, Nevada, and implications for the nature and origin of Basin and Range faulting: Geological Society of America Bulletin, v. 88, p. 247-266.

Proffett, J.M., Dilles, J., Mines, M.S.o., and Company, A., 1984, Geologic map of the Yerington district, Nevada, Nevada Bureau of Mines and Geology.

Proffett Jr, J.M., and Proffett, B.H., 1976, Stratigraphy of the Tertiary Ash-flow Tuffs in the Yerington District, Nevada, NV Bureau of Mines & Geology.

Reheis, M.C., and Sawyer, T.L., 1997, Late Cenozoic history and slip rates of the Fish Lake Valley, Emigrant Peak, and Deep Springs fault zones, Nevada and California: Geological Society of America Bulletin, v. 109, p. 280-299.

Reiners, P.W., Brady, R., Farley, K.A., Fryxell, J.E., Wernicke, B., and Lux, D., 2000, Helium and argon thermochronometry of the Gold Butte block, south Virgin Mountains, Nevada: Earth and Planetary Science Letters, v. 178, p. 315-326.

Reiners, P.W., Farley, K.A., and Hickes, H.J., 2002, He diffusion and (U-Th)/He thermochronometry of zircon: initial results from Fish Canyon Tuff and Gold Butte: Tectonophysics, v. 349, p. 297-308.

Reiners, P.W., Spell, T.L., Nicolescu, S., and Zanetti, K.A., 2004, Zircon (U-Th)/He thermochronometry: He diffusion and comparisons with 40Ar/39Ar dating: Geochimica et Cosmochimica Acta, v. 68, p. 1857-1887.

Rowley, P., 1998, Cenozoic transverse zones and igneous belts in the Great Basin, western United States: Their tectonic and economic implications: Geological Society of America Special Papers, v. 323, p. 195-228.

Ryall, A., and Priestley, K., 1975, Seismicity, secular strain, and maximum magnitude in the Excelsior Mountains area, western Nevada and eastern California: Bulletin of the Geological Society of America, v. 86, p. 1585-1592.

Shoffner, J.D., Li, Y., Hinz, N., Sabin, A., Lazaro, M., and Alm, S., 2010, Understanding fault characteristics and sediment depth for geothermal exploration using 3d gravity inversion in Walker Valley, Nevada: Transactions-Geothermal Resources Council, v. 34, p. 633-636.

Slemmons, D., 1967, Pliocene and Quaternary crustal movements of the Basin and Range Province, USA: J. Geosci., Osaka City Univ, v. 10, p. 91-103.

Smith, D.L., Gans, P.B., and Miller, E.L., 1991, Palinspastic Restoration of Cenozoic Extension in the Central and Eastern Basin and Range Province at Latitude 39-40 N, *in* Raines, G.L., Lisle, R.E., Schafer, R.W., and Wilkinson, W.H.e, eds., Geology and ore deposits of the Great Basin: Reno, Geological Society of Nevada, p. 75-86.

Stewart, J., 1980, Regional tilt patterns of late Cenozoic basin-range fault blocks, western United States: Bulletin of the Geological Society of America, v. 91, p. 460-464.

Stewart, 1988, Tectonics of the Walker Lane belt, western Great Basin: Mesozoic and Cenozoic deformation in a zone of shear: Metamorphism and crustal evolution of the western United States, v. 7, p. 683–713.

Stewart, J., 1992, Walker Lane Belt, Nevada and California–An overview, p. 1–16.

Stewart, 1998, Regional characteristics, tilt domains, and extensional history of the later Cenozoic Basin and Range province, western North America: Geological Society of America Special Papers, v. 323, p. 47-74.

Stewart, J.H., Carlson, J.E., Tingley, S.L., Survey, G., Mines, N.B.o., and Geology, 1977, Geologic map of Nevada, Nevada Bureau of Mines and Geology, University of Nevada.

Stewart, J., Kleinhampl, F., Johannesen, D., Speed, R., and Dohrenwend, J., 1981, Geologic map of the Huntoon valley quadrangle, Mineral County, Nevada and Mono County, California: U.S. Geological Survey, Open-File Report OF-81-274.

Stewart, J., Kleinhampl, F., Speed, R., and Johannesen, D., 1984, Geologic map of the Little Huntoon Valley quadrangle, Mineral County, Nevada: U.S. Geological Survey, Open-File Report OF-84-503.

Stockli, D.F., 1999, Regional timing and spatial distribution of Miocene extension in the northern Basin and Range Province: Ph.D. Thesis; Stanford University; Stanford, California, p. 1-239.

Stockli, D., 2005, Application of low-temperature thermochronometry to extensional tectonic settings: Reviews in Mineralogy and Geochemistry, v. 58, p. 411-448.

Stockli, D., Farley, K., and Dumitru, T., 2000, Calibration of the apatite (U-Th)/He thermochronometer on an exhumed fault block, White Mountains, California: Geology, v. 28, p. 983-986.

Stockli, D., Surpless, B., Dumitru, T., and Farley, K., 2002, Thermochronological constraints on the timing and magnitude of Miocene and Pliocene extension in the central Wassuk Range, western Nevada: Tectonics, v. 21, p. 1028-1047.

Stockli, D., Dumitru, T., McWilliams, M., and Farley, K., 2003, Cenozoic tectonic evolution of the White Mountains, California and Nevada: Geological Society of America Bulletin, v. 115, p. 788-816.

Surpless, B.E., 1999, Tectonic evolution of the northern Sierra Nevada-Basin and Range transition zone; a study of crustal evolution in extensional provinces: Ph.D. Thesis; Stanford University; Stanford, California, p. 1-340.

Surpless, B., 2008, Modern strain localization in the central Walker Lane, western United States: Implications for the evolution of intraplate deformation in transtensional settings: Tectonophysics, v. 457, p. 239-253.

Surpless, B., Stockli, D., Dumitru, T., and Miller, E., 2002, Two-phase westward encroachment of Basin and Range extension into the northern Sierra Nevada: Tectonics, v. 21, p. 1002-1015.

Thompson, G.A., 1956, Geology of the Virginia City Quadrangle, Nevada: Geology of the Johnson Creek quadrangle, Caribou County, Idaho, in Gulbrandsen, R.A., Contributions to Economic Geology, Geological Survey Bulletin, v. 1042, p. 45-78.

Tincher, C.R., and Stockli, D.F., 2009, Cenozoic volcanism and tectonics in the Queen Valley area, Esmeralda County, western Nevada: Late Cenozoic structure and evolution of the Great Basin-Sierra Nevada transition, p. 255-274.

Unruh, J., Humphrey, J., and Barron, A., 2003, Transtensional model for the Sierra Nevada frontal fault system, eastern California: Geology, v. 31, p. 327-330.

Van Buer, N., Miller, E., and Dumitru, T., 2009, Early Tertiary paleogeologic map of the northern Sierra Nevada batholith and the northwestern Basin and Range: Geology, v. 37, p. 371-374.

Wernicke, B.P., Guth, P.L., and Axen, G.J., 1984, Tertiary extensional tectonics in the Sevier thrust belt of southern Nevada: in Lintz, J., Jr., Western geological excursions; Reno, Nevada, Mackay School of Mines, v. 4, p. 473-495.

Wesnousky, S., 2005a, The San Andreas and Walker Lane fault systems, western North America: Transpression, transtension, cumulative slip and the structural evolution of a major transform plate boundary: Journal of Structural Geology, v. 27, p. 1505-1512.

Wesnousky, S., 2005b, Active faulting in the Walker Lane: Tectonics, v. 24. p. 3009-3044.

Wolfe, M.R., and Stockli, D.F., 2010, Zircon (U-Th)/He thermochronometry in the KTB drill hole, Germany, and its implications for bulk He diffusion kinetics in zircon: Earth and Planetary Science Letters. v. 295, p. 69-82.

Zoback, M.L., Anderson, R., and Thompson, G., 1981, Cainozoic evolution of the state of stress and style of tectonism of the Basin and Range province of the western United States: Philosophical Transactions of the Royal Society of London. Series A, Mathematical and Physical Sciences, v. 300, p. 407-434.

Zoback, M., 1989, State of stress and modern deformation of the northern Basin and Range province: Journal of Geophysical Research, v. 94, p. 7105-7128.

CHAPTER 2: FIGURES AND TABLES

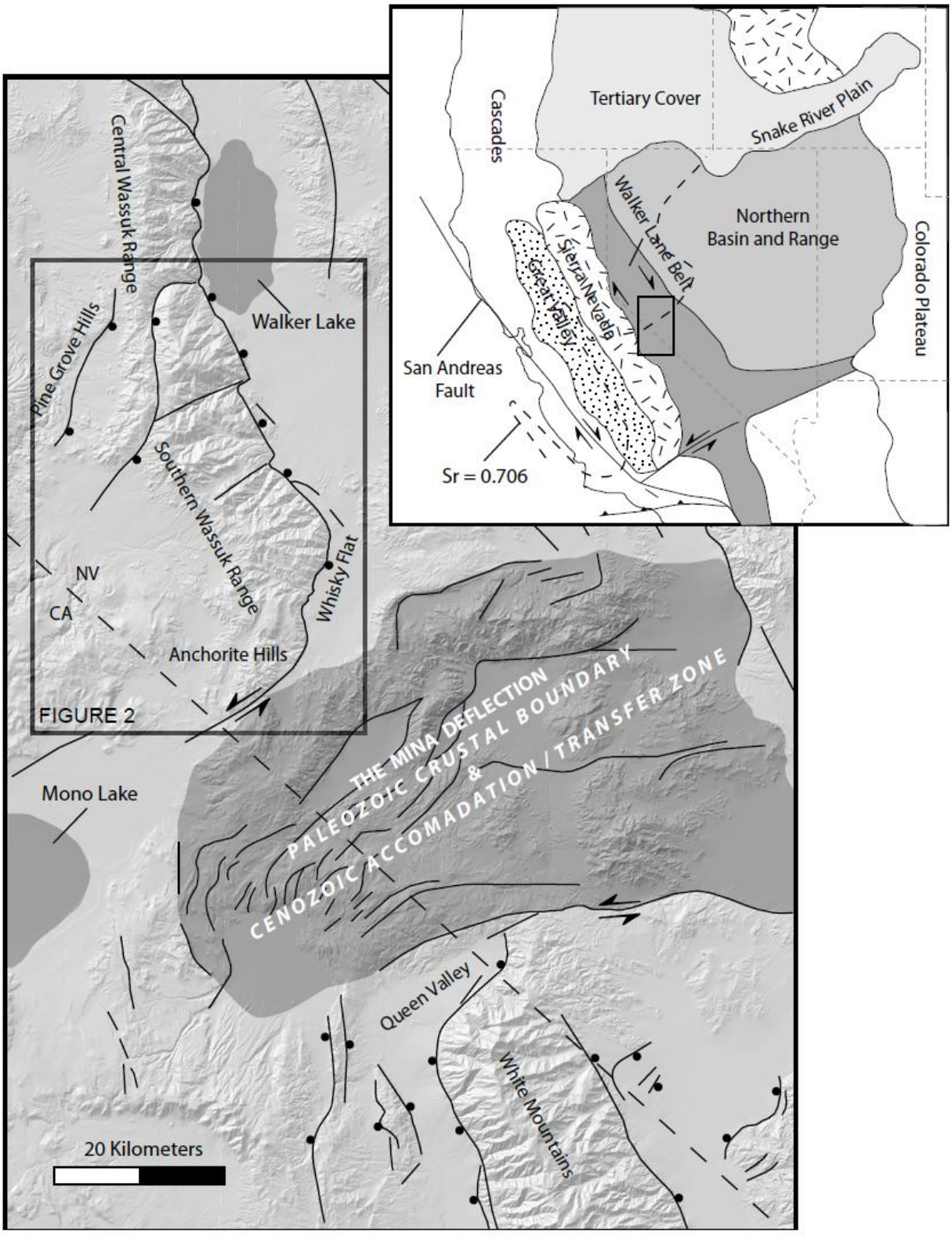
Cascades
Tertiary Cover
Snake River Plain
Walker Lane Belt
Northern
Basin and Range
Colorado Plateau
Sierra Nevada
Great Valley
San Andreas
Fault
Sr = 0.706
Central Wassuk Range
Walker Lake
Pine Grove Hills
Southern Wassuk Range
Whisky Flat
NV
CA
Anchorite Hills
FIGURE 2
THE MINA DEFLECTION
PALEOZOIC CRUSTAL BOUNDARY
&
CENOZOIC ACCOMADATION / TRANSFER ZONE
Mono Lake
Queen Valley
White Mountains
20 Kilometers

Figure 1. Major late Cenozoic faults (modified after Stewart et al., 1977; Oldow, 1992; Reheis and Sawyer, 1997; Stockli et al., 2003) for the central Walker Lane belt. The west-tilted Wassuk Range footwall and the east-tilted White Mountains footwall are separated by the east-west trending faults of the Mina Deflection. Insert map shows the location of the study area with respect to the ancient crustal boundary defined by the $^{87}Sr/^{86}Sr$ 0.706 line.

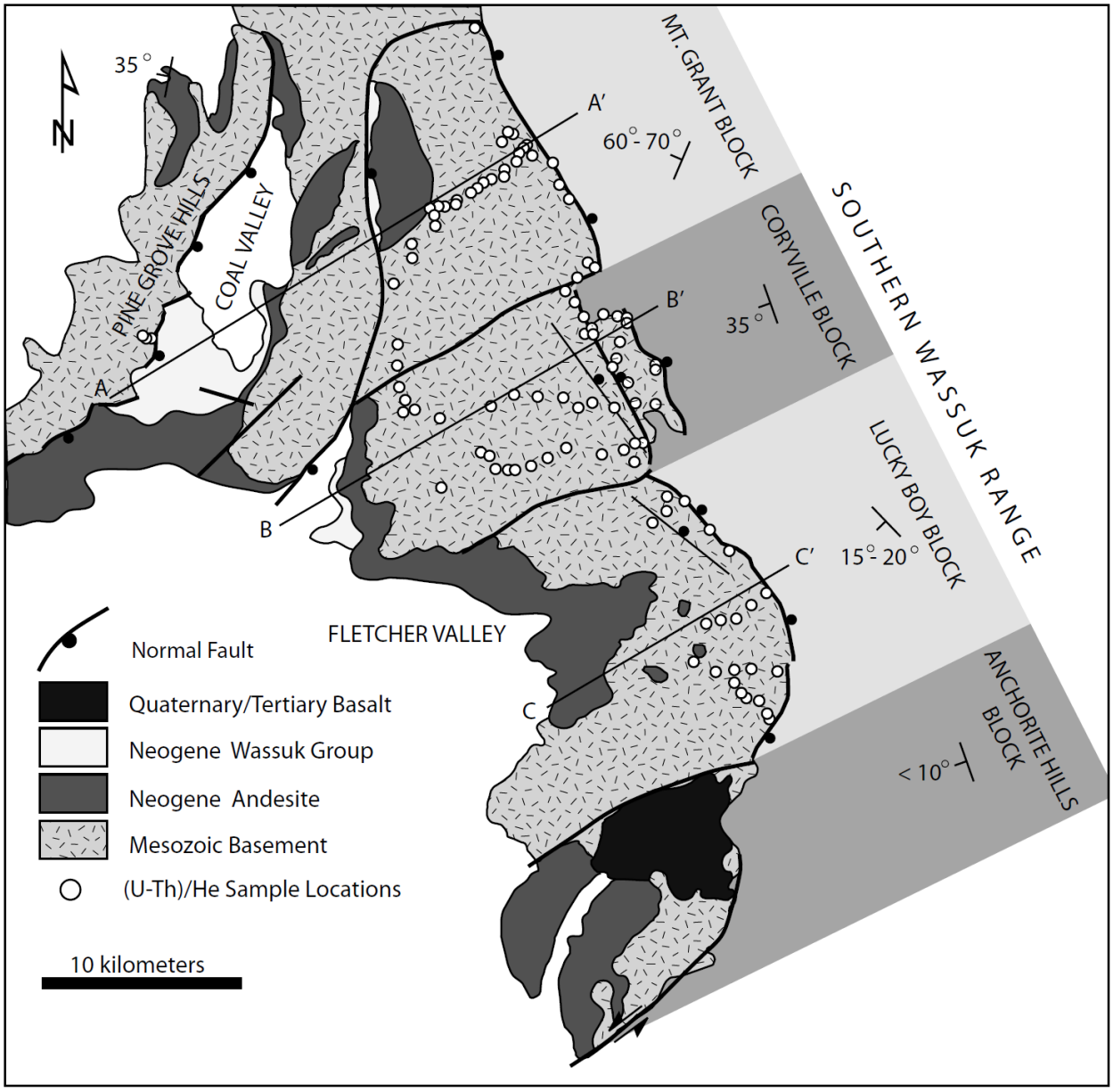
N
35°
A
A'
B
B'
C
C'
60°-70°
35°
15°-20°
< 10°
PINE GROVE HILLS
COAL VALLEY
FLETCHER VALLEY
MT. GRANT BLOCK
CORYVILLE BLOCK
LUCKY BOY BLOCK
ANCHORITE HILLS BLOCK
SOUTHERN WASSUK RANGE
Normal Fault
Quaternary/Tertiary Basalt
Neogene Wassuk Group
Neogene Andesite
Mesozoic Basement
(U-Th)/He Sample Locations
10 kilometers

Figure 2. Simplified geologic map of the southern Wassuk Range and Anchorite Hills, showing west tilted blocks of Mesozoic basement overlying Neogene cover. Four tilt blocks are recognized in the southern block and are defined as regions of consistent dip along strike. (U-Th)/He sample locations are shown above, and sampled the three northernmost tilt blocks, and the Pine Grove Hills to the west. Cross-section lines (A-A', B-B', C-C') are shown in figure 6.

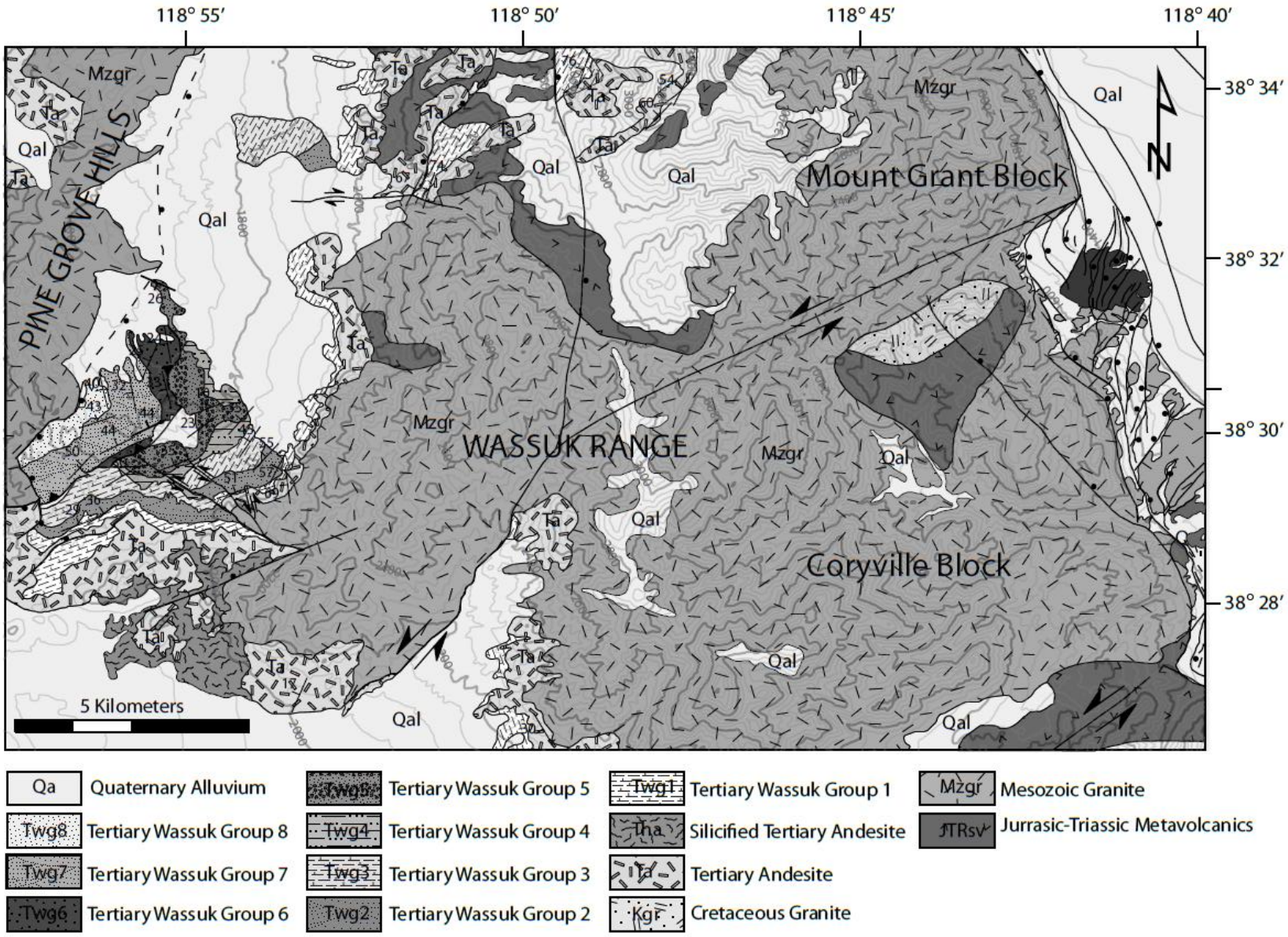
118° 55′
118° 50′
118° 45′
118° 40′
38° 34′
38° 32′
38° 30′
38° 28′
N
PINE GROVE HILLS
WASSUK RANGE
Mount Grant Block
Coryville Block
Mzgr
Qal
Ta
5 Kilometers
Qa Quaternary Alluvium
Twg8 Tertiary Wassuk Group 8
Twg7 Tertiary Wassuk Group 7
Twg6 Tertiary Wassuk Group 6
Twg5 Tertiary Wassuk Group 5
Twg4 Tertiary Wassuk Group 4
Twg3 Tertiary Wassuk Group 3
Twg2 Tertiary Wassuk Group 2
Twg1 Tertiary Wassuk Group 1
Tha Silicified Tertiary Andesite
Ta Tertiary Andesite
Kgr Cretaceous Granite
Mzgr Mesozoic Granite
JTRsv Jurrasic-Triassic Metavolcanics

Figure 3. Geologic map of the Mt. Grant and Coryville blocks from the southern Wassuk Range, and nonconformably overlying tilted Neogene section in the Coal and Fletcher Valleys to their west. The variably tilted Neogene section in Coal Valley, west of the Mt. Grant block, was used to constrain the timing and magnitude of Miocene tilting related to Wassuk Range footwall rotation. Range-front faults to the east of the Wassuk Range footwall were modified after Heinz et al., (2010) and illustrate a number of Pleistocene transtensional faults that occupy a prominent right en-echelon step in the range front, and tilt-block boundary. The tilt-block boundary is defined by a northeast-striking scissor fault that accommodated differential tilting between the Mt. Grant and Coryville blocks. An east-dipping, scoop-shaped normal fault on the western flank of the Mt. Grant block repeats the Mesozoic and Neogene section.

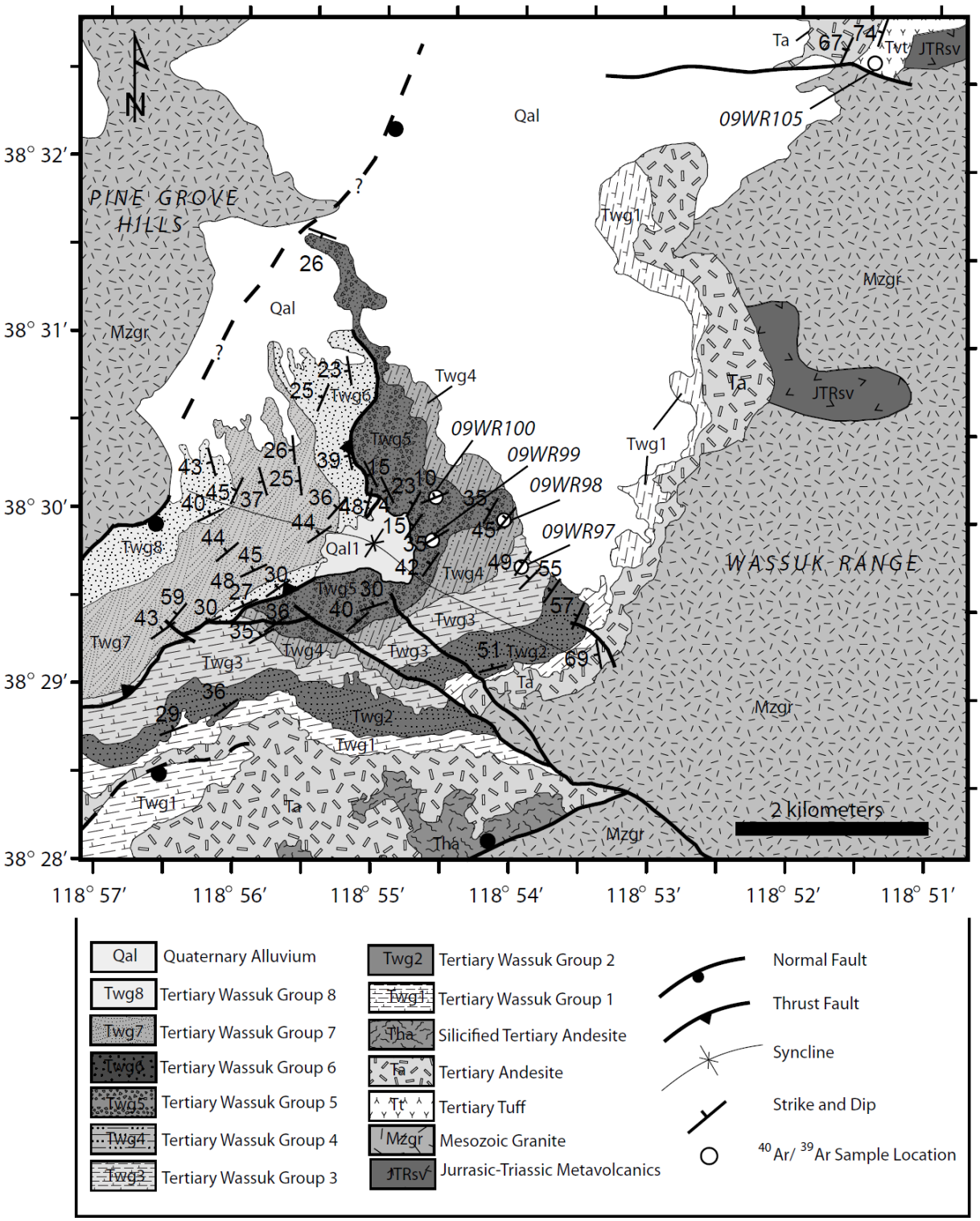
PINE GROVE HILLS
WASSUK RANGE
09WR105
09WR100
09WR99
09WR98
09WR97
Qal
Qal1
Twg1
Twg2
Twg3
Twg4
Twg5
Twg6
Twg7
Twg8
Ta
Tt
Tha
JTRsv
Mzgr
2 kilometers
38° 32′
38° 31′
38° 30′
38° 29′
38° 28′
118° 57′
118° 56′
118° 55′
118° 54′
118° 53′
118° 52′
118° 51′
Quaternary Alluvium
Tertiary Wassuk Group 8
Tertiary Wassuk Group 7
Tertiary Wassuk Group 6
Tertiary Wassuk Group 5
Tertiary Wassuk Group 4
Tertiary Wassuk Group 3
Tertiary Wassuk Group 2
Tertiary Wassuk Group 1
Silicified Tertiary Andesite
Tertiary Andesite
Tertiary Tuff
Mesozoic Granite
Jurrasic-Triassic Metavolcanics
Normal Fault
Thrust Fault
Syncline
Strike and Dip
40Ar/ 39Ar Sample Location

Figure 4. Geologic map of Neogene sedimentary and volcanic rocks in the Coal Valley between the southern Wassuk Range and Pine Grove Hills footwalls. Miocene units dip towards the west and record the progressive tilting of the southern Wassuk Range footwall and are used to calculate the pre-extensional paleodepths for footwall AHe and ZHe samples.

$^{40}Ar/^{39}Ar$ Age Spectra

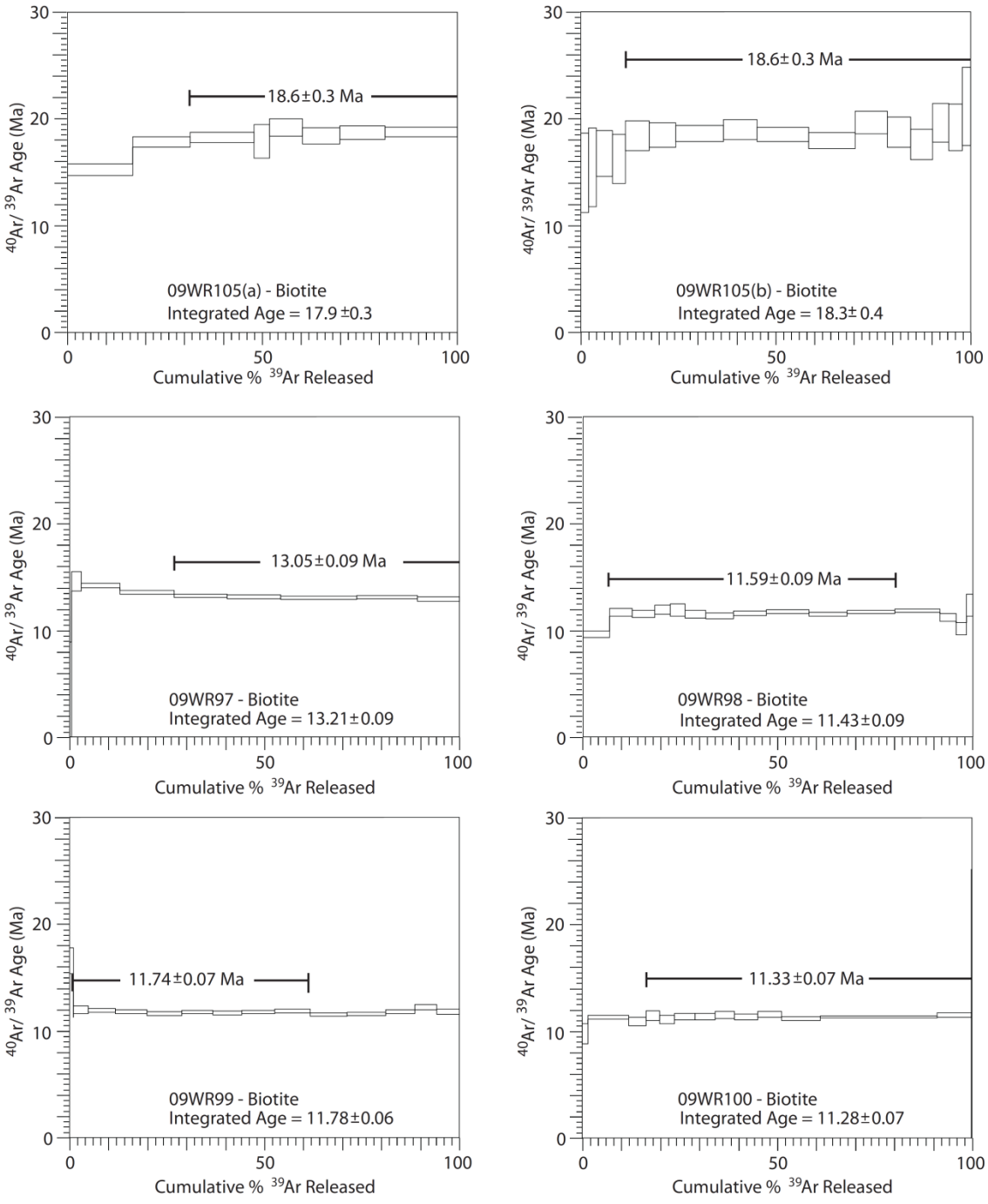

Figure 5. Biotite $^{40}Ar/^{39}Ar$ release spectra for interbedded tuffs in the variably tilted Neogene sections in Coal Valley west of the southern Wassuk Range. Sample Locations are shown in Figure 3. $^{40}Ar/^{39}Ar$ ages record and constrain the progressive tilting of the southern Wassuk Range footwall.

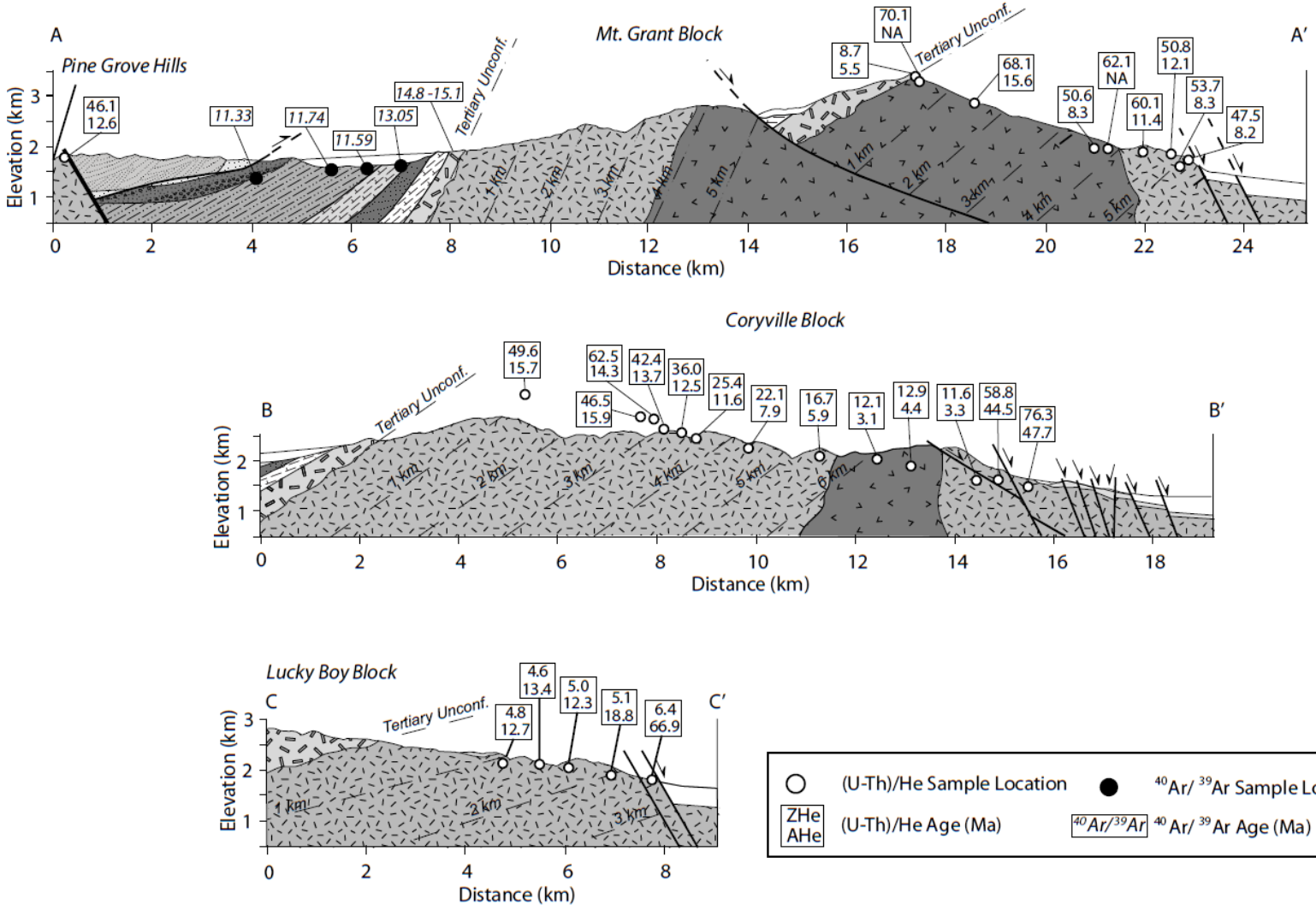
A
Pine Grove Hills
Mt. Grant Block
A'
Tertiary Unconf.
Elevation (km)
Distance (km)
46.1 12.6
11.33
11.74
11.59
13.05
14.8 -15.1
8.7 5.5
70.1 NA
68.1 15.6
50.6 8.3
62.1 NA
60.1 11.4
50.8 12.1
53.7 8.3
47.5 8.2
1 km
2 km
3 km
4 km
5 km
Coryville Block
B
B'
49.6 15.7
62.5 14.3
42.4 13.7
36.0 12.5
25.4 11.6
22.1 7.9
16.7 5.9
12.1 3.1
12.9 4.4
11.6 3.3
58.8 44.5
76.3 47.7
46.5 15.9
6 km
Lucky Boy Block
C
C'
4.6 13.4
5.0 12.3
5.1 18.8
6.4 66.9
4.8 12.7
(U-Th)/He Sample Location
40Ar/ 39Ar Sample Location
ZHe AHe
(U-Th)/He Age (Ma)
40Ar/39Ar
40Ar/ 39Ar Age (Ma)

Figure 6. Simplified cross sections through the Mt. Grant (A-A'), Coryville (B-B'), and Lucky Boy (C-C') blocks of the southern Wassuk Range (Figure 2). The Wassuk Range fault blocks are west tilted and bounded along their eastern flank by high-angle normal faults. ~60° - 70° of footwall rotation in the Mt. Grant block is represented by the similarly west-tilted Paleogene nonconformity and overlying 14.8 – 15.1 Ma Lincoln Flat andesite. Tilting of the Mt. Grant footwall is much greater than that of the Coryville (~35°) and Lucky Boy (<20°) blocks and therefore exhumed much greater Miocene pre-extensional paleodepths. Range-front faults in the Coryville block have been modified after Heinz et al., (2010).

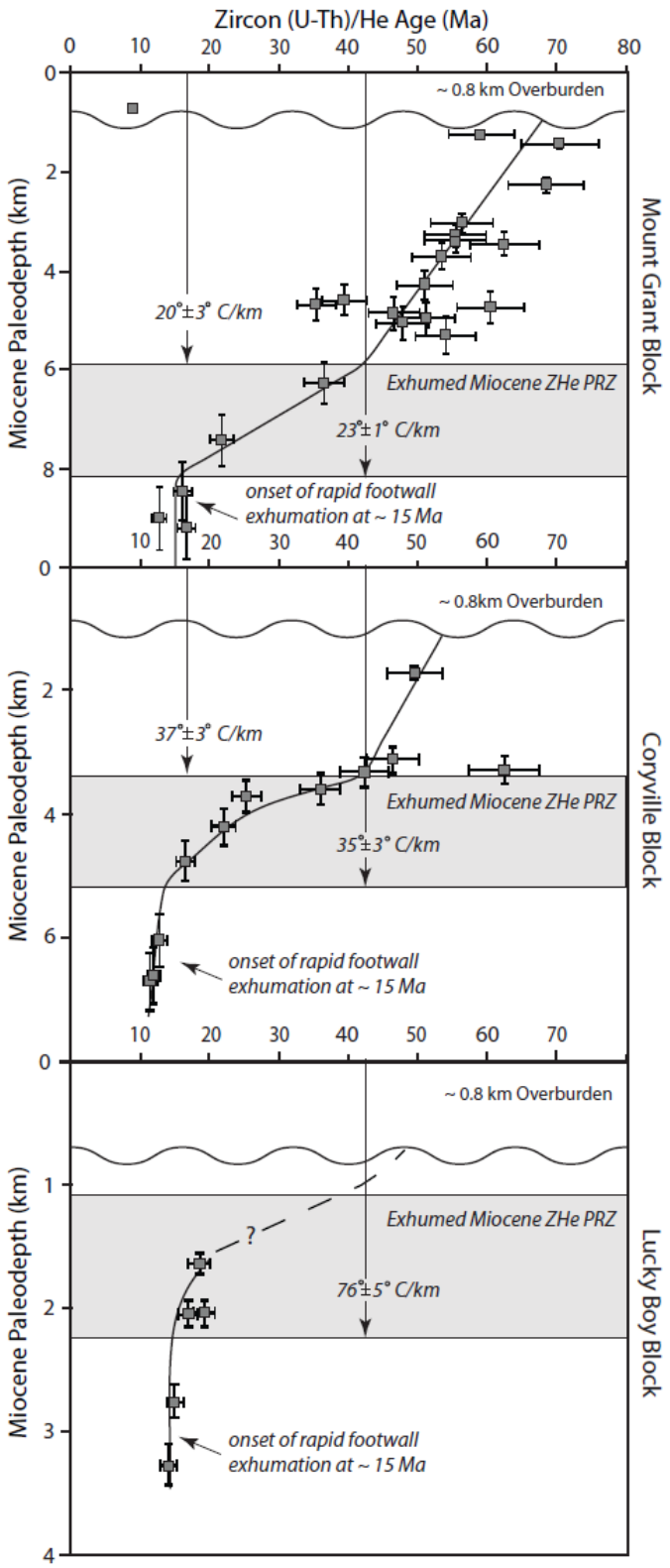
Zircon (U-Th)/He Age (Ma)
0 10 20 30 40 50 60 70 80
~ 0.8 km Overburden
Miocene Paleodepth (km)
20°±3° C/km
Exhumed Miocene ZHe PRZ
23°±1° C/km
onset of rapid footwall
exhumation at ~ 15 Ma
Mount Grant Block
~ 0.8km Overburden
37°±3° C/km
Exhumed Miocene ZHe PRZ
35°±3° C/km
onset of rapid footwall
exhumation at ~ 15 Ma
Coryville Block
~ 0.8 km Overburden
Exhumed Miocene ZHe PRZ
?
76°±5° C/km
onset of rapid footwall
exhumation at ~ 15 Ma
Lucky Boy Block

Figure 7. Plots of zircon (U-Th)/He age vs. pre-extensional paleodepth for the Mt. Grant, Coryville and Lucky Boy blocks of the southern Wassuk Range. The onset of fast-paced exhumation at ~12 – 15 Ma is evident throughout the Wassuk Range and is represented here by invariant ages at the deepest structural paleodepths. The location of the exhumed fossil Miocene ZHe PRZs are highlighted and yield middle Miocene pre-extensional geothermal gradient estimates that increase towards the Lucky Boy block at the southernmost Wassuk Range.

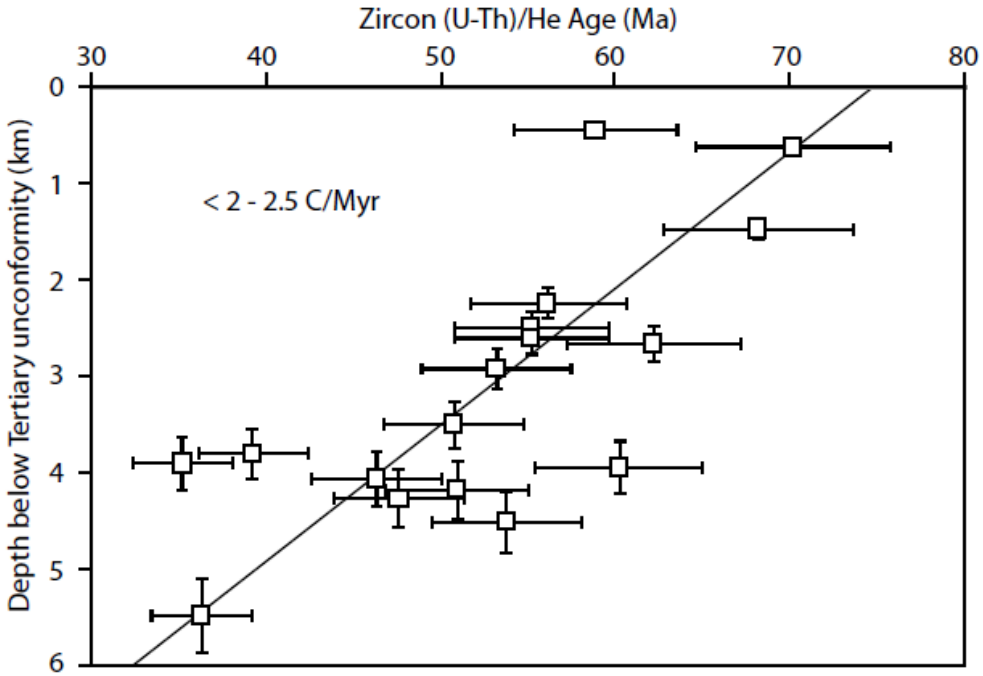
Zircon (U-Th)/He Age (Ma)
30
40
50
60
70
80
0
1
2
3
4
5
6
Depth below Tertiary unconformity (km)
< 2 - 2.5 C/Myr

Figure 8. Plot of zircon (U-Th)/He ages vs. depth below Paleogene nonconformity for samples in the Mt. Grant block that resided above the middle Miocene ZHe PRZ. Late – Cretaceous to Paleogene ZHe cooling ages record the erosional denudation of the Sierra Nevada batholiths after the end of Sierran arc magmatism at a rate of < 2° – 2.5° C/Ma.

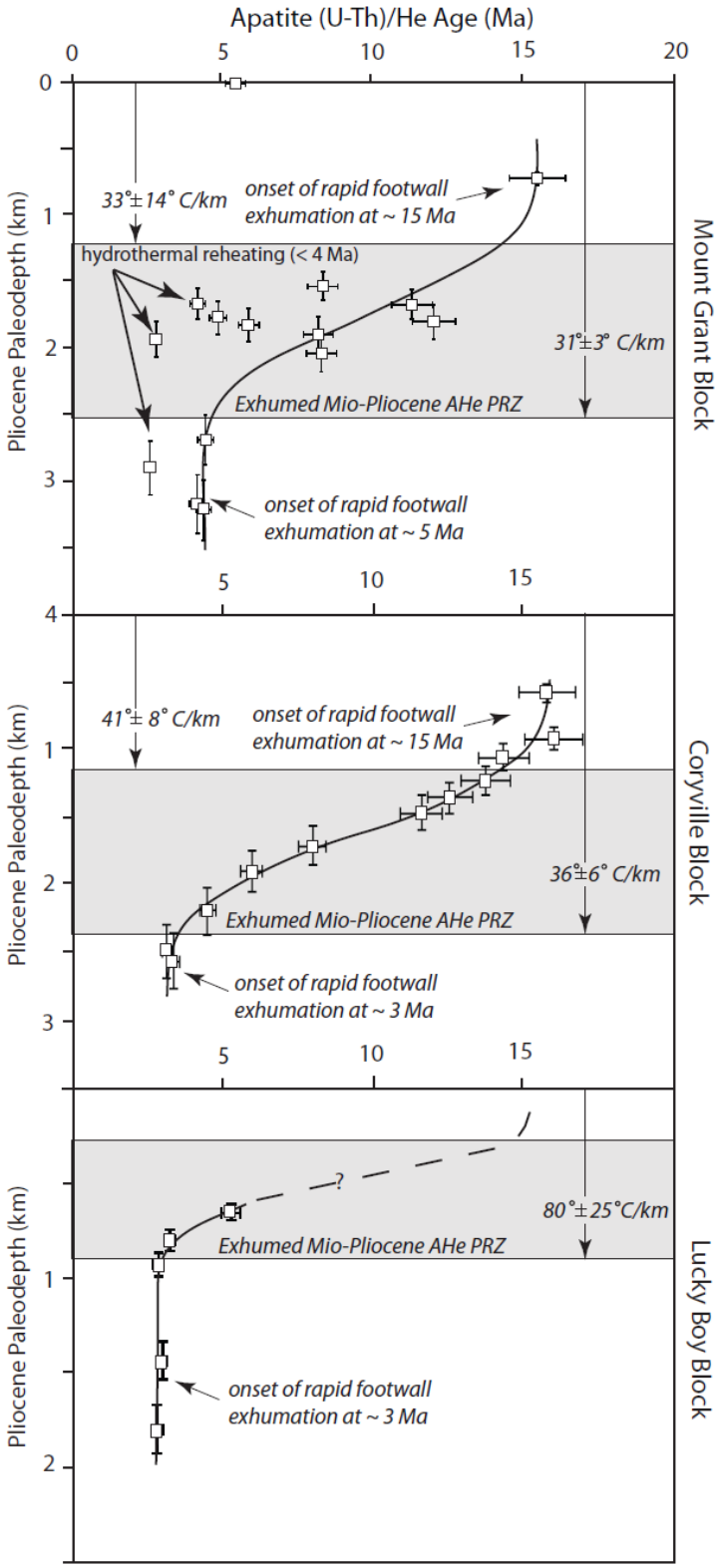
Apatite (U-Th)/He Age (Ma)
0
5
10
15
20
Pliocene Paleodepth (km)
33°±14° C/km
onset of rapid footwall exhumation at ~ 15 Ma
hydrothermal reheating (< 4 Ma)
31°±3° C/km
Exhumed Mio-Pliocene AHe PRZ
onset of rapid footwall exhumation at ~ 5 Ma
Mount Grant Block
41°± 8° C/km
onset of rapid footwall exhumation at ~ 15 Ma
36°±6° C/km
Exhumed Mio-Pliocene AHe PRZ
onset of rapid footwall exhumation at ~ 3 Ma
Coryville Block
?
80°±25°C/km
Exhumed Mio-Pliocene AHe PRZ
onset of rapid footwall exhumation at ~ 3 Ma
Lucky Boy Block

Figure 9. Plots of apatite (U-Th)/He age vs. pre-extensional paleodepth for the Mt. Grant, Coryville and Lucky Boy blocks of the southern Wassuk Range. Two episodes of fast-paced exhumation are recognized by invariant ages above and below the Mio-Pliocene AHe PRZs, and occurred at ~12 -15 Ma and ~3 – 5 Ma. The location of the exhumed fossil Mio-Pliocene AHe PRZs are highlighted and yield pre-extensional geothermal gradient estimates, which increase towards the Lucky Boy block at the southernmost Wassuk Range.

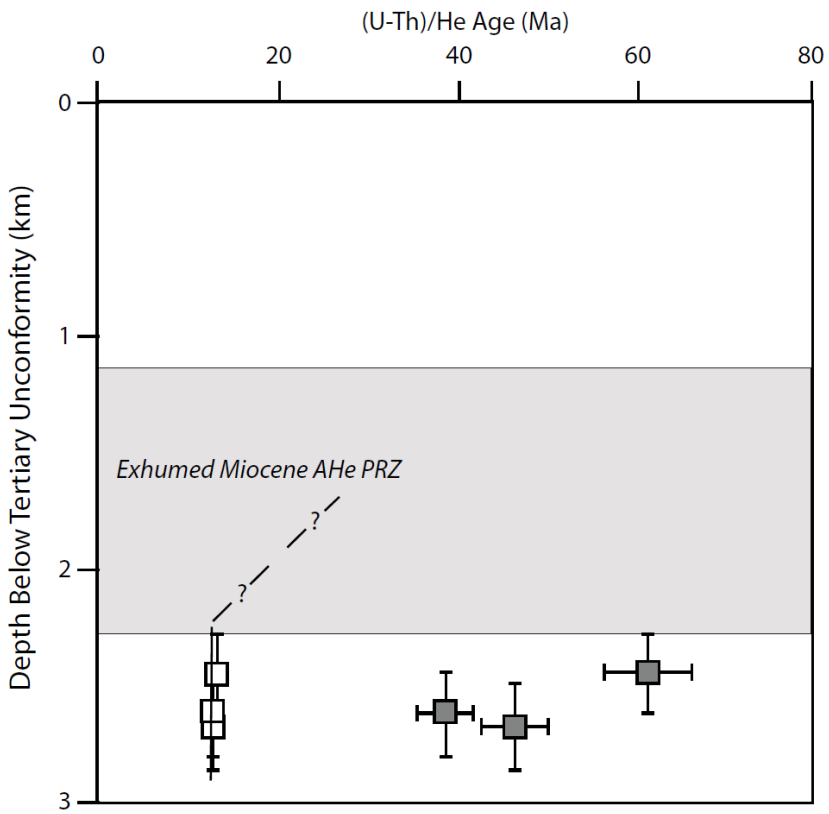
(U-Th)/He Age (Ma)
0
20
40
60
80
0
1
2
3
Depth Below Tertiary Unconformity (km)
Exhumed Miocene AHe PRZ
?
?

Figure 10. Plots of zircon and Apatite (U-Th)/He ages vs. depth below the Paleogene nonconformity for samples from the Pine Grove Hills. Only three samples were collected from the Pine Grove Hills block, and sampled the deepest exposed pre-extensional paleodepths. The onset of fast-paced footwall exhumation at ~12 Ma is recorded by the three invariant AHe ages that likely resided below a middle Miocene AHe PRZ.

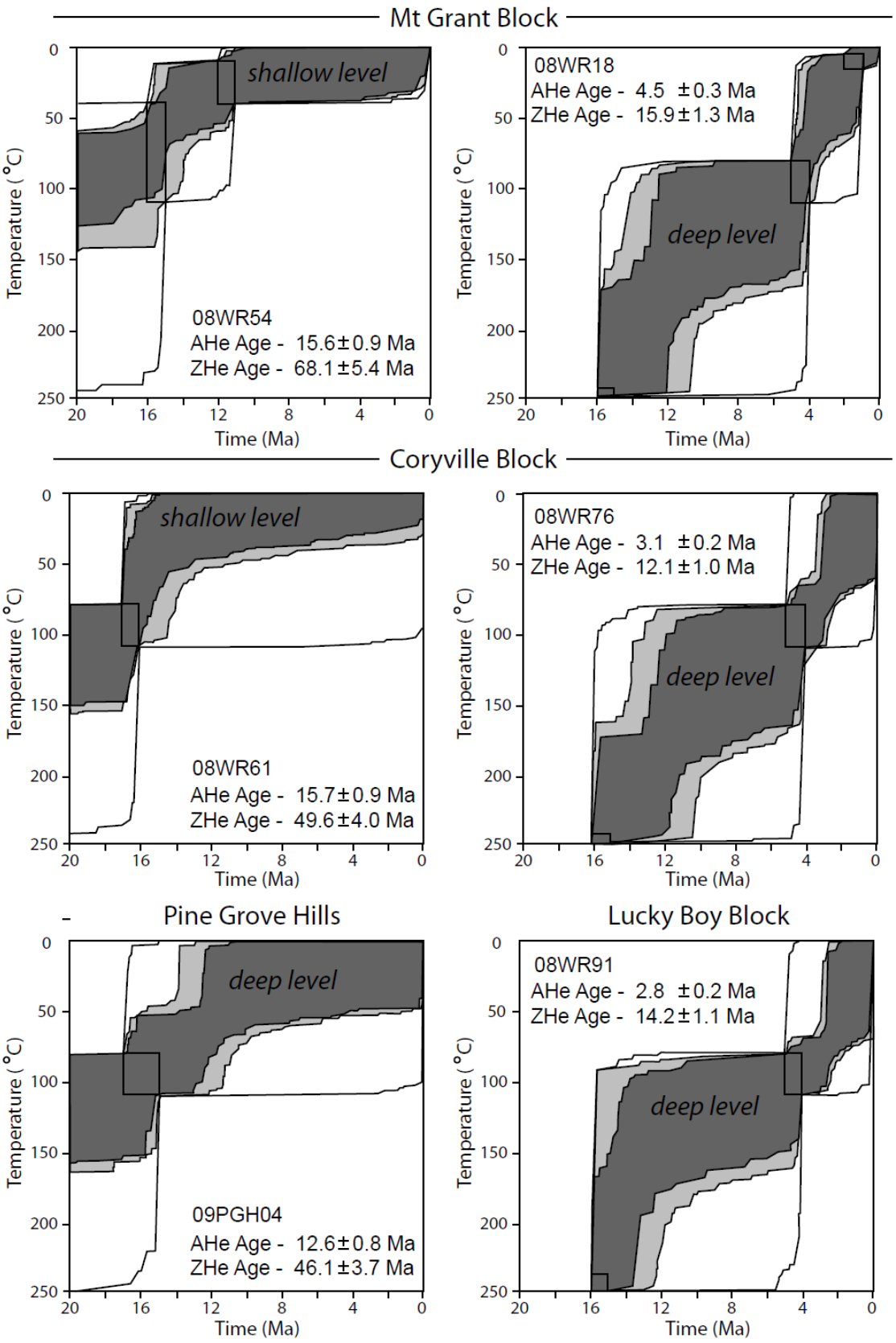
Mt Grant Block
shallow level
08WR54
AHe Age - 15.6±0.9 Ma
ZHe Age - 68.1±5.4 Ma
08WR18
AHe Age - 4.5 ±0.3 Ma
ZHe Age - 15.9±1.3 Ma
deep level
Coryville Block
shallow level
08WR61
AHe Age - 15.7±0.9 Ma
ZHe Age - 49.6±4.0 Ma
08WR76
AHe Age - 3.1 ±0.2 Ma
ZHe Age - 12.1±1.0 Ma
deep level
Pine Grove Hills
deep level
09PGH04
AHe Age - 12.6±0.8 Ma
ZHe Age - 46.1±3.7 Ma
Lucky Boy Block
08WR91
AHe Age - 2.8 ±0.2 Ma
ZHe Age - 14.2±1.1 Ma
deep level
Temperature (°C)
Time (Ma)
0
50
100
150
200
250
20
16
12
8
4
0

Figure 11. Apatite and zircon (U-Th)/He inverse time-temperature history modeling results for individual samples from the shallowest and deepest structural levels in the Mt. Grant and Coryville blocks, and from just the deepest levels in the Lucky Boy and Pine Grove Hills blocks. Modeling results from the shallow structural levels in the Mt. Grant and Coryville blocks record protracted cooling during the Paleogene related to the erosional denudation of the Sierra Nevada batholith, and associated Mesozoic wall rock; and a second fast-paced cooling event at ~12 – 15 Ma related to the exhumation of the Wassuk range footwall. Time-temperature history models for the deeper structural levels in the southern Wassuk Range record a three-stage thermal history with two episodes of fast-paced cooling starting at ~15 Ma and ~4 Ma, separated by a period of isothermal holding. Thermal modeling results for the Pine Grove Hills indicate that this fault block only experienced limited middle Miocene cooling starting at ~12 Ma, and is devoid of any Mio-Pliocene and younger cooling.

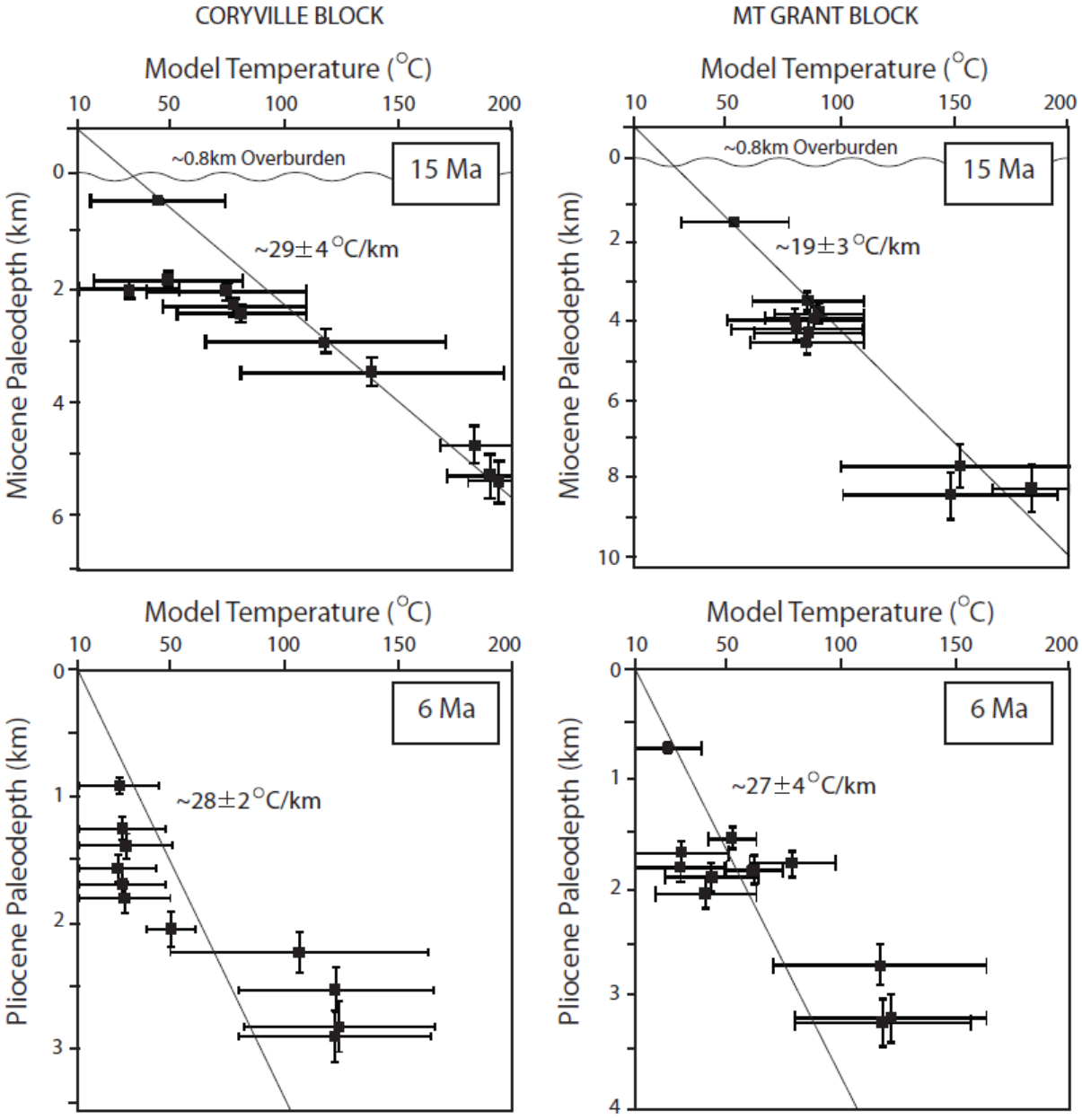
CORYVILLE BLOCK
MT GRANT BLOCK
Model Temperature (°C)
10
50
100
150
200
~0.8km Overburden
15 Ma
~29±4 °C/km
~19±3 °C/km
Miocene Paleodepth (km)
6 Ma
~28±2 °C/km
~27±4 °C/km
Pliocene Paleodepth (km)

Figure 12. Plots of model temperature vs. pre-extensional paleodepth for both the Mt. Grant and Coryville blocks immediately prior to middle Miocene and Mio-Pliocene extension. The geothermal gradient can be estimated by the slope of a best-fit line through the datasets, and can further be projected to a thermally defined surface at 10° ± 5° C to estimate middle Miocene pre-extensional overburden. Model-derived geothermal gradient estimates corroborate geothermal gradient estimates calculated from the depth of the ZHe and AHe PRZs (Figure 6, 8) and similarly illustrate an elevated geothermal gradient in the southernmost Wassuk Range. In the Mt. Grant block, an increase in the geothermal gradient of ~8° ± 7° C/km is attributed to footwall advection during middle Miocene large-magnitude extension.

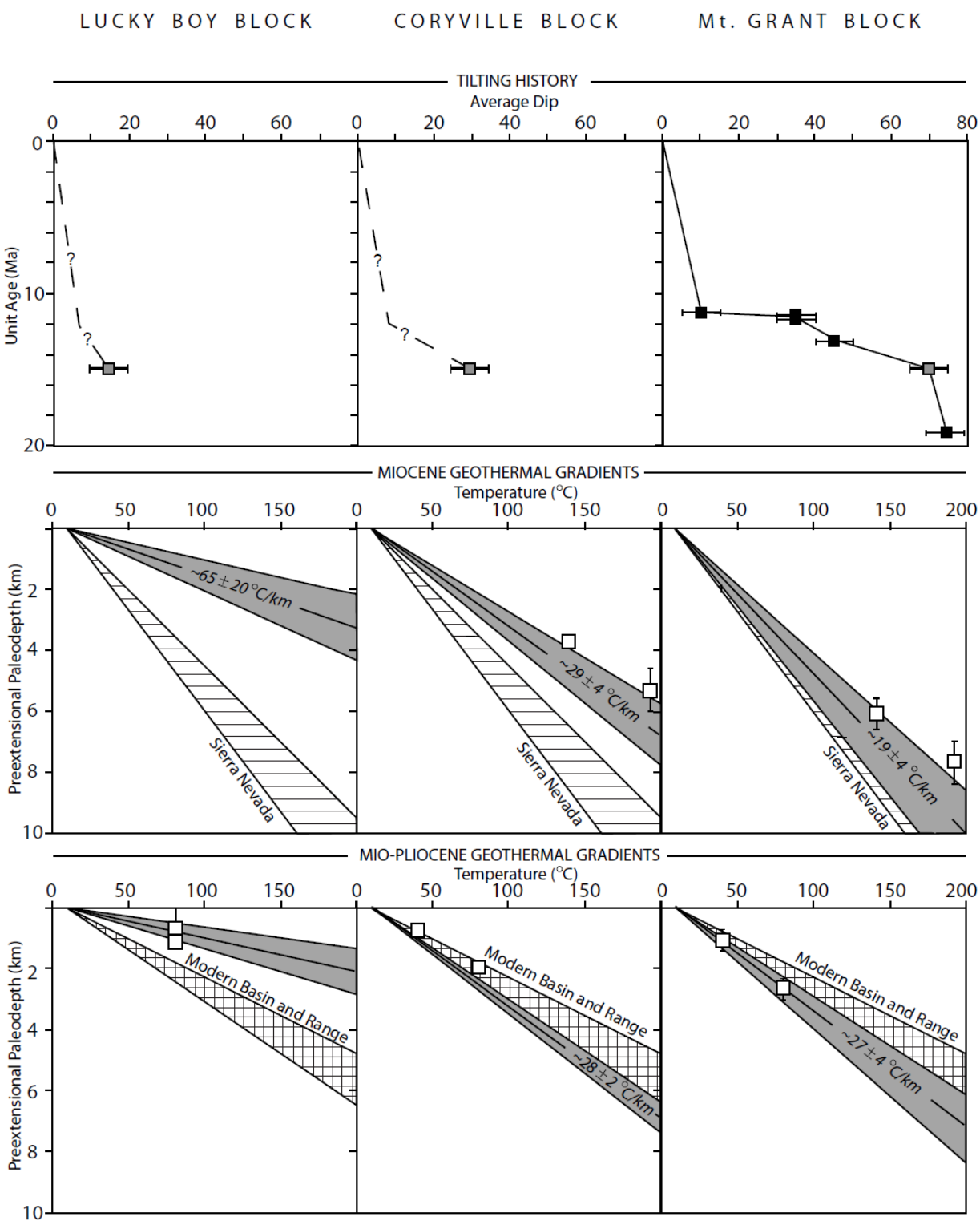
LUCKY BOY BLOCK
CORYVILLE BLOCK
Mt. GRANT BLOCK
TILTING HISTORY
Average Dip
Unit Age (Ma)
MIOCENE GEOTHERMAL GRADIENTS
Temperature (°C)
Preextensional Paleodepth (km)
~65±20 °C/km
~29±4 °C/km
~19±4 °C/km
Sierra Nevada
MIO-PLIOCENE GEOTHERMAL GRADIENTS
Modern Basin and Range
~28±2 °C/km
~27±4 °C/km

Figure 13. Summary figure showing the tilting and geothermal gradient histories for the southern Wassuk Range. Tilting history is illustrated by plots of a stratigraphic unit's $^{40}Ar/^{39}Ar$ age vs. dip and shows a southward decrease in cumulative Miocene tilting and fault-block rotation. Model-derived geothermal gradient estimates are also plotted below against the position of preserved isotherms (white data points) defined by inflections in the AHe and ZHe Age vs. paleodepth plots (Figure 6, 8). Together the diagrams show an increased geothermal gradient in the southernmost Wassuk Range, which is inversely correlated with degree of footwall rotation.

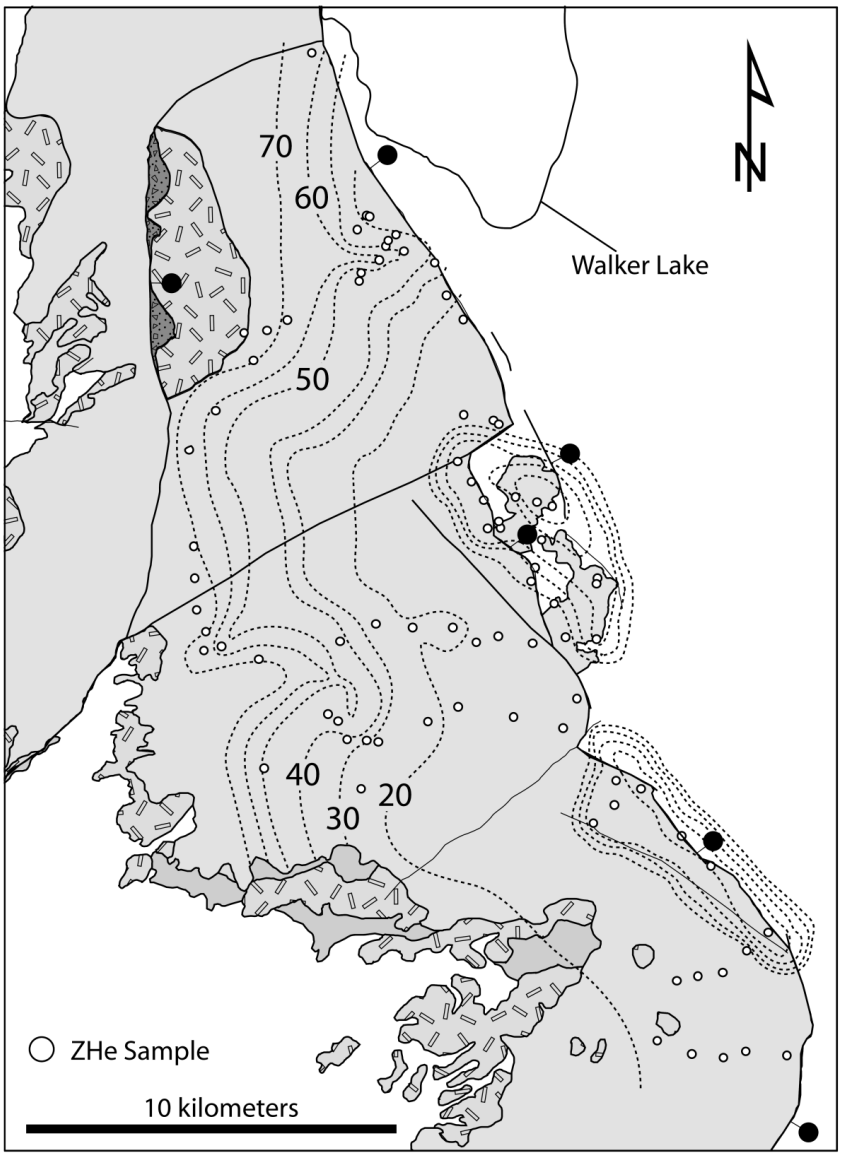
70
60
50
40
30
20
Walker Lake
N
ZHe Sample
10 kilometers

Figure 14. ZHe age map for samples from the southern Wassuk Range footwall. The Paleogene nonconformity is intersected by progressively younger ZHe age isopleths towards the south. Oligocene and older ZHe ages are absent from the structurally intact Lucky Boy block, even for samples adjacent to the Paleogene nonconformity. Anomalously old ages along the range front mark the location of range-front faults and structurally displaced slivers of Wassuk Range footwall.

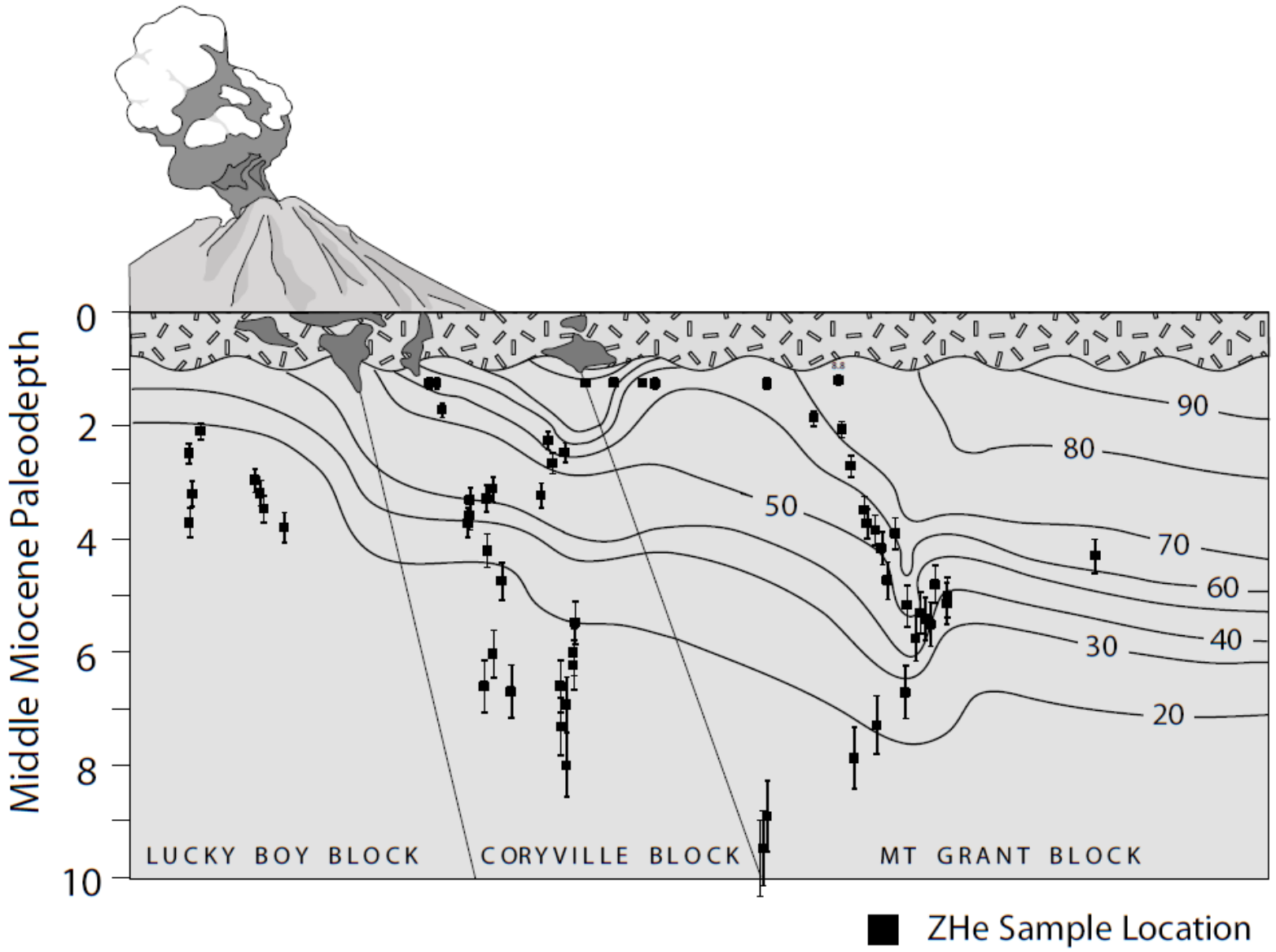
Middle Miocene Paleodepth
0
2
4
6
8
10
90
80
50
70
60
40
30
20
LUCKY BOY BLOCK
CORYVILLE BLOCK
MT GRANT BLOCK
ZHe Sample Location

Figure 15. Palinspastic restoration of the southern Wassuk Range footwall showing the distribution of footwall ZHe ages. ZHe age isopleths cut up section and mimic geothermal gradient trends that increase towards the south (Figure 14). ZHe age isopleths should roughly parallel the Paleogene nonconformity, under the assumption that the unconformity was a flat or slightly beveled surface and that Neogene volcanic overburden was uniform across the region. The absence of Oligocene and older ZHe ages from the shallowest structural levels in the southernmost Wassuk Range suggest that the oldest thermal record of post-Cretaceous erosion and denudation was overprinted by a Miocene heating event.

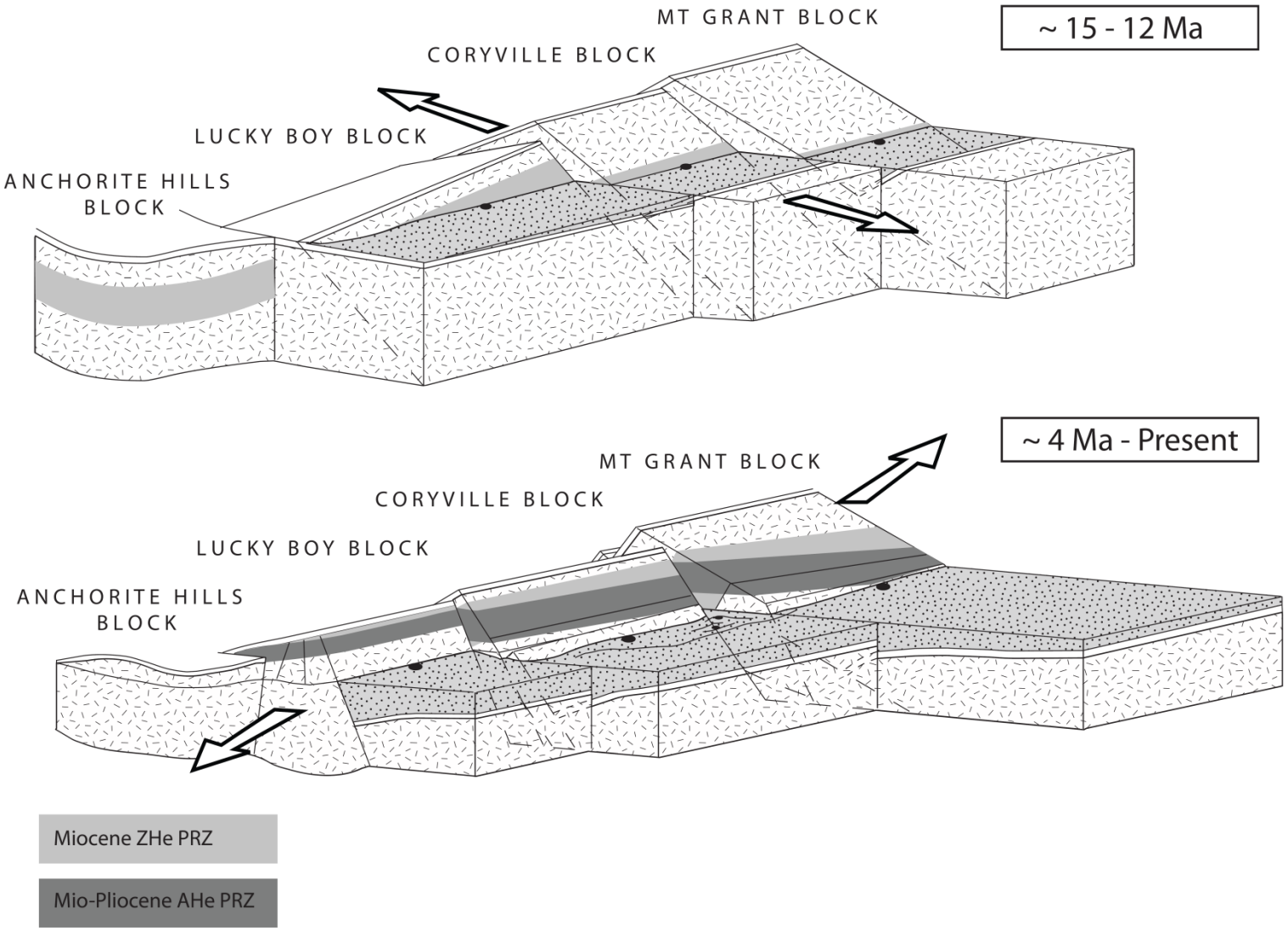
MT GRANT BLOCK
~ 15 - 12 Ma
CORYVILLE BLOCK
LUCKY BOY BLOCK
ANCHORITE HILLS BLOCK
~ 4 Ma - Present
MT GRANT BLOCK
CORYVILLE BLOCK
LUCKY BOY BLOCK
ANCHORITE HILLS BLOCK
Miocene ZHe PRZ
Mio-Pliocene AHe PRZ

Figure 16. Block evolution diagrams for the southern Wassuk Range footwall. The onset of extension in the southern Wassuk Range occurred at ~15Ma in the northern and central Wassuk Range and progressed towards the southwest, progressively tilting footwall blocks of the southern Wassuk Range and Pine Grove Hills. A second episode of extension initiated at ~4 Ma and resulted in range-front faulting across the entire central and southern Wassuk Range. Right en echelon steps along the range front are the product of middle Miocene tilting, and were the focus of Mio-Pliocene and younger transtensional deformation. The preserved Miocene ZHe and Mio-Pliocene AHe PRZs are shown on the tilted footwall blocks, and qualitatively illustrate the increased middle Miocene geothermal gradient towards the south (depth to the PRZ measured from the Paleogene nonconformity), and the focus of Mio-Pliocene exhumation at range-front pull aparts.

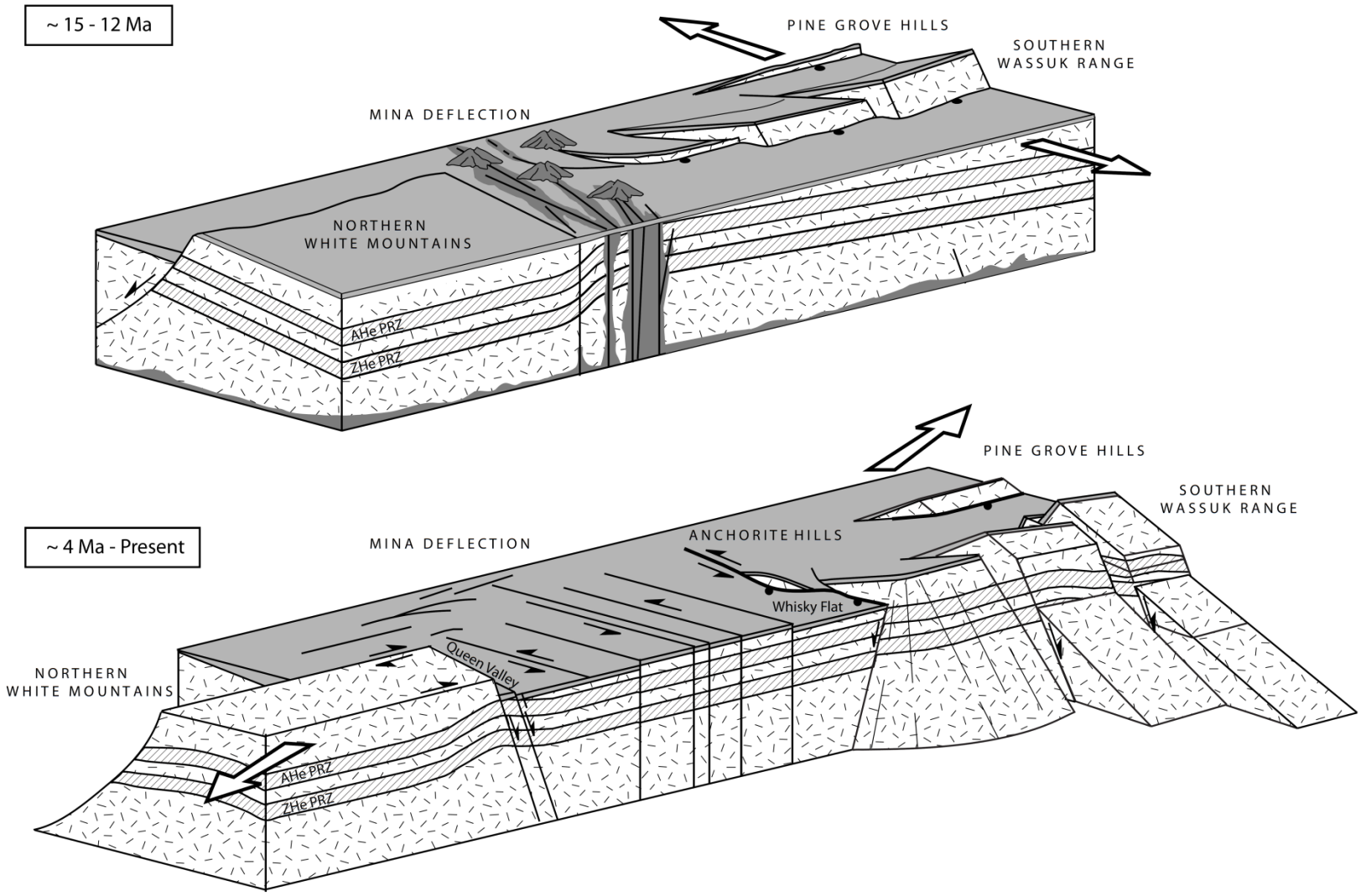
~ 15 - 12 Ma
PINE GROVE HILLS
SOUTHERN
WASSUK RANGE
MINA DEFLECTION
NORTHERN
WHITE MOUNTAINS
AHe PRZ
ZHe PRZ
~ 4 Ma - Present
PINE GROVE HILLS
SOUTHERN
WASSUK RANGE
MINA DEFLECTION
ANCHORITE HILLS
Whisky Flat
Queen Valley
NORTHERN
WHITE MOUNTAINS
AHe PRZ
ZHe PRZ

Figure 17. Block diagrams illustrating the structural and thermal evolution of the Mina Deflection accommodation zone, and Wassuk Range and White Mountains extensional systems to its north and south, respectively. The elevated middle Miocene geothermal gradient in the Mina Deflection area resulted from pre-extensional volcanism that was focused along its pre-existing structural weaknesses. Thermal, structural and rheological heterogeneities in the Mina Deflection impeded the southward propagation of the southern Wassuk Range extensional system, and instead accommodated a polarity switch between the west-tilted southern Wassuk Range and east-tilted White Mountains. The onset of "Walker Lane style" right-lateral shearing initiated at ~3 – 4 Ma throughout the central Wassuk Range, and resulted in transtension across the southern Wassuk Range front and the formation of pull-apart structures at right, en-echelon steps along the range front. Similarly, pull-apart structures also developed at ~3 Ma along the northern and southern margins of the Mina Deflection at Whisky Flat in the southern Wassuk Range, and at Queen Valley (Stockli et al., 2003; Tincher and Stockli, 2009) in the northern White Mountains (Figure 1).

ID	Laser Watts	^{40}Ar	^{39}Ar	^{38}Ar	^{37}Ar	^{36}Ar	Ca/K	% ^{39}Ar	% ^{40}Ar	Age (Ma)	±1σ
09WR97, Biotite, J (X 10-3) ± 1s = 4.385 ± 0.003											
A	0.10	27.56	0.87	0.04	0.08	0.09	0.179	0.5	1.4	3.39	2.73
B	0.30	16.26	4.50	0.08	0.14	0.03	0.059	2.6	51.1	14.54	0.44
C	0.50	37.34	16.99	0.27	0.27	0.02	0.031	9.9	81.7	14.15	0.12
D	0.70	42.39	23.74	0.36	0.12	0.01	0.010	13.8	96.1	13.53	0.08
E	0.90	41.28	23.32	0.36	0.07	0.01	0.006	13.6	94.5	13.18	0.08
F	1.10	41.14	23.65	0.36	0.03	0.01	0.003	13.8	95.4	13.08	0.09
G	1.30	58.34	33.45	0.52	0.04	0.01	0.002	19.5	94.6	13.00	0.06
H	1.50	46.74	26.85	0.41	0.01	0.01	0.000	15.6	95.2	13.06	0.08
I	1.70	31.88	18.24	0.28	0.01	0.01	0.001	10.6	93.4	12.86	0.11
Integrated Age = 13.21 ± 0.08 Ma **Plateau Age = 13.05 ± 0.09 Ma**											
09WR98, Biotite, J (X 10-3) ± 1s = 4.385 ± 0.003											
A	0.10	59.19	16.87	0.27	0.09	0.13	0.010	6.8	34.6	9.57	0.14
B	0.30	71.54	14.57	0.25	0.35	0.17	0.047	5.9	30.1	11.64	0.19
C	0.40	56.99	14.20	0.23	0.58	0.12	0.080	5.7	36.3	11.50	0.17
D	0.45	25.30	10.00	0.15	0.11	0.03	0.022	4.0	59.5	11.87	0.21
E	0.50	23.43	9.19	0.14	0.10	0.03	0.021	3.7	59.0	11.87	0.28
F	0.70	37.50	13.51	0.22	0.21	0.06	0.031	5.4	52.3	11.45	0.17
G	0.90	46.12	17.61	0.28	0.23	0.07	0.025	7.1	54.8	11.31	0.13
H	1.10	57.87	20.82	0.33	0.30	0.09	0.028	8.4	52.7	11.56	0.11
I	1.30	68.45	26.96	0.41	0.39	0.10	0.029	10.9	58.5	11.70	0.09
J	1.50	56.39	24.18	0.37	0.18	0.07	0.014	9.8	62.4	11.48	0.09
K	1.70	58.96	30.40	0.46	0.13	0.05	0.009	12.3	76.4	11.69	0.08
L	1.90	51.56	28.63	0.43	0.03	0.03	0.002	11.6	83.0	11.78	0.08
M	2.10	19.80	10.41	0.16	0.01	0.02	0.001	4.2	74.6	11.18	0.18
N	2.30	15.78	6.78	0.11	0.01	0.02	0.003	2.7	55.1	10.11	0.28
O	2.50	7.04	3.70	0.05	0.00	0.00	0.000	1.5	82.2	12.33	0.51
Integrated Age = 11.43±0.09 Ma **Plateau Age = 11.59 ± 0.09 Ma**											

NOTES:
Samples were irradiated for 20 hours using Cadmium shielding at the USGS TRIGA reactor in Denver, CO. Sanidine from the Fish Canyon Tuff was used as the neutrol fluence monitor with a reference age of 28.201 Ma (Kuiper et al., 1998).

Decay constants and isotopic abundances after Min et al., (2000)

ID	Laser Watts	^{40}Ar	^{39}Ar	^{38}Ar	^{37}Ar	^{36}Ar	Ca/K	% ^{39}Ar	% ^{40}Ar	Age (Ma)	1σ
09WR99, Biotite, J (X 10-3) ± 1s = 4.385 ± 0.003											
A	0.10	11.36	3.12	0.04	0.04	0.02	0.022	1.1	57.6	16.52	0.61
B	3.00	18.61	10.26	0.14	0.07	0.01	0.014	3.7	83.5	11.95	0.18
C	0.50	31.68	19.70	0.28	0.08	0.01	0.008	7.1	93.6	11.87	0.09
D	0.70	36.03	22.56	0.31	0.10	0.01	0.008	8.1	93.4	11.76	0.08
E	0.90	38.89	24.58	0.34	0.22	0.01	0.017	8.8	92.9	11.58	0.08
F	1.10	35.66	22.31	0.32	0.45	0.01	0.039	8.0	93.1	11.73	0.08
G	1.30	33.36	20.88	0.30	0.65	0.01	0.061	7.5	92.3	11.64	0.09
H	1.50	37.96	23.44	0.33	1.57	0.01	0.131	8.4	91.8	11.73	0.08
I	1.70	41.91	25.02	0.35	2.50	0.02	0.196	9.0	89.6	11.83	0.08
J	1.90	42.97	26.53	0.38	2.35	0.01	0.174	9.5	90.1	11.51	0.07
K	2.10	43.16	27.45	0.38	1.75	0.01	0.125	9.9	93.2	11.55	0.07
L	2.30	32.42	20.70	0.30	0.77	0.01	0.072	7.4	95.1	11.75	0.09
M	2.50	24.58	15.89	0.22	0.31	0.00	0.038	5.7	100.0	12.19	0.11
N	3.00	24.24	15.85	0.22	0.10	0.00	0.013	5.7	97.4	11.75	0.12
Integrated Age = 11.78 ± 0.07 Ma				**Plateau Age = 11.78 ± 0.06 Ma**							
09WR100, Biotite, J (X 10-3) ± 1s = 4.385 ± 0.003											
A	0.10	8.02	3.82	0.05	0.06	0.01	0.032	1.6	58.8	9.74	0.47
B	0.30	38.64	24.20	0.33	0.17	0.01	0.014	10.3	89.5	11.27	0.08
C	0.40	17.30	10.60	0.16	0.23	0.01	0.043	4.5	84.6	10.89	0.19
D	0.50	13.06	8.02	0.11	0.29	0.00	0.071	3.4	89.2	11.46	0.23
E	0.60	14.06	8.89	0.13	0.24	0.01	0.052	3.8	88.6	11.06	0.20
F	0.70	19.92	12.58	0.18	0.41	0.01	0.064	5.4	90.6	11.32	0.15
G	0.80	18.55	11.93	0.16	0.28	0.00	0.045	5.1	92.5	11.35	0.16
H	0.90	17.95	11.47	0.16	0.34	0.00	0.059	4.9	93.3	11.52	0.16
I	1.00	22.14	14.10	0.20	0.58	0.01	0.080	6.0	91.2	11.29	0.13
J	1.20	22.87	14.35	0.20	0.52	0.01	0.071	6.1	92.0	11.56	0.13
K	1.40	36.83	23.15	0.32	1.77	0.01	0.150	9.9	88.9	11.16	0.08
L	1.60	110.11	70.30	0.99	5.67	0.03	0.158	30.1	91.6	11.32	0.03
M	2.00	31.81	20.31	0.29	1.96	0.01	0.189	8.7	93.2	11.51	0.10
N	2.50	0.41	0.22	0.00	0.00	0.00	0.002	0.1	59.3	8.69	8.21
Integrated Age = 11.28±0.07 Ma				**Plateau Age = 11.33 ± 0.07 Ma**							

NOTES:
Samples were irradiated for 20 hours using Cadmium shielding at the USGS TRIGA reactor in Denver, CO. Sanidine from the Fish Canyon Tuff was used as the neutrol fluence monitor with a reference age of 28.201 Ma (Kuiper et al., 1998).

Decay constants and isotopic abundances after Min et al., (2000)

ID	Laser Watts	^{40}Ar	^{39}Ar	^{38}Ar	^{37}Ar	^{36}Ar	Ca/K	% ^{39}Ar	% ^{40}Ar	Age (Ma)	±1σ
09WR104, Biotite, J (X 10-3) ± 1s = 4.349 ± 0.002											
A	0.30	20.12	12.05	0.19	0.12	0.01	0.019	17.3	86.0	11.24	0.12
B	0.50	15.84	10.98	0.17	0.16	0.00	0.028	15.8	106.7	12.03	0.12
C	0.70	10.56	7.44	0.12	0.08	0.00	0.021	10.7	99.9	11.09	0.19
D	0.90	10.40	7.35	0.12	0.11	0.00	0.031	10.6	101.1	11.19	0.18
E	1.10	7.67	5.46	0.08	0.03	0.00	0.009	7.8	106.6	11.71	0.24
F	1.30	6.28	4.48	0.07	0.10	0.00	0.044	6.4	96.3	10.56	0.29
G	1.50	10.18	7.31	0.11	0.02	0.00	0.005	10.5	109.1	11.88	0.19
H	1.70	8.88	6.35	0.10	0.00	0.00	0.001	9.1	99.4	10.88	0.22
I	2.00	6.15	4.39	0.07	0.00	0.00	0.000	6.3	110.4	12.11	0.32
J	2.50	5.23	3.75	0.06	0.00	0.00	0.000	5.4	118.5	12.93	0.34
Integrated Age = 12.78 ± 0.07 Ma											

NOTES:
Samples were irradiated for 20 hours using Cadmium shielding at the USGS TRIGA reactor in Denver, CO. Sanidine from the Fish Canyon Tuff was used as the neutrol fluence monitor with a reference age of 28.201 Ma (Kuiper et al., 1998).

Decay constants and isotopic abundances after Min et al., (2000)

ID	Laser Watts	^{40}Ar	^{39}Ar	^{38}Ar	^{37}Ar	^{36}Ar	Ca/K	% ^{39}Ar	% ^{40}Ar	Age (Ma)	±1σ
09WR105B, Biotite, J (X 10-3) ± 1s = 4.349 ± 0.004											
A	0.10	102.16	11.46	0.22	0.08	0.27	0.014	16.8	21.7	15.22	0.28
B	0.30	64.91	10.11	0.17	0.07	0.14	0.013	14.8	35.2	17.80	0.24
C	0.50	61.67	11.26	0.18	0.05	0.12	0.009	16.5	42.3	18.24	0.23
D	0.00	17.96	2.63	0.05	0.03	0.04	0.026	3.8	33.3	17.89	0.78
E	0.90	43.96	5.87	0.10	0.08	0.10	0.028	8.6	32.6	19.19	0.41
F	1.10	50.28	6.53	0.11	0.18	0.12	0.055	9.5	30.3	18.37	0.38
G	1.30	60.83	7.97	0.15	0.31	0.14	0.077	11.6	31.1	18.70	0.33
H	1.50	93.09	12.59	0.23	3.03	0.21	0.472	18.4	32.2	18.74	0.23
Integrated Age = 17.90±0.03 Ma					**Plateau Age = 18.60 ± 0.03 Ma**						
09WR105B, Biotite, J (X 10-3) ± 1s = 4.349 ± 0.004											
A	0.01	10.24	0.77	0.02	0.00	0.03	0.000	2.1	14.1	14.85	1.86
B	0.10	8.25	0.74	0.02	0.00	0.02	0.000	2.0	17.5	15.40	1.83
C	0.20	13.24	1.47	0.03	0.00	0.03	0.000	4.0	23.6	16.68	1.07
D	0.30	9.72	1.24	0.02	0.02	0.02	0.032	3.4	26.3	16.18	1.16
E	0.50	13.97	2.21	0.04	0.01	0.03	0.008	6.1	36.9	18.35	0.70
F	0.75	13.85	2.48	0.04	0.03	0.03	0.027	6.8	42.0	18.44	0.58
G	1.00	23.34	4.43	0.07	0.00	0.04	0.002	12.1	44.8	18.59	0.37
H	1.25	16.58	3.19	0.05	0.00	0.03	0.003	8.7	46.3	18.94	0.46
I	1.60	22.85	4.78	0.08	0.02	0.04	0.008	13.1	49.1	18.47	0.33
J	2.00	26.58	4.40	0.07	0.09	0.06	0.038	12.1	37.6	17.90	0.38
K	2.30	18.00	3.01	0.05	0.05	0.04	0.030	8.3	41.7	19.59	0.52
L	2.60	11.50	2.14	0.04	0.11	0.02	0.102	5.9	44.1	18.67	0.71
M	3.00	9.79	2.05	0.03	0.15	0.02	0.143	5.6	46.6	17.54	0.70
N	3.50	6.54	1.54	0.02	0.14	0.01	0.173	4.2	58.7	19.57	0.92
O	4.00	5.25	1.27	0.02	0.08	0.01	0.131	3.5	58.9	19.17	1.09
P	4.50	3.15	0.74	0.01	0.02	0.00	0.061	2.0	63.2	21.09	1.83
Integrated Age = 18.30± 0.04 Ma					**Plateau Age = 18.60 ± 0.03 Ma**						

NOTES:
Samples were irradiated for 20 hours using Cadmium shielding at the USGS TRIGA reactor in Denver, CO. Sanidine from the Fish Canyon Tuff was used as the neutrol fluence monitor with a reference age of 28.201 Ma (Kuiper et al., 1998).

Decay constants and isotopic abundances after Min et al., (2000)

Table 1. Table of $^{40}Ar/^{39}Ar$ age data for biotites from interbedded tuffs in the tilted Wassuk Group.

Sample	Latitude	Longitude	Elevation	Age [Ma]	± (8%) [Ma]	U [ppm]	Th [ppm]	Sm [ppm]	He [ncc]	F_T	ESR
08WR01	38.4291	-118.6311	1770	65.3	5.2	497	233	2.06	53.9	0.83	85
08WR02	38.4208	-118.6204	1812	59.7	4.8	478	576	1.27	80.9	0.84	81
08WR03	38.3883	-118.6319	2056	12.7	1.0	470	213	0.61	2.3	0.73	44
08WR04	38.3898	-118.6243	2011	13.4	1.1	313	321	2.33	35.8	0.89	114
08WR05	38.3909	-118.6156	1946	12.3	1.0	688	175	1.03	5.7	0.78	52
08WR06	38.3971	-118.6071	1870	18.8	1.5	481	176	1.80	10.6	0.80	60
08WR07	38.4023	-118.5995	1787	66.9	5.4	428	160	1.17	39.8	0.82	67
08WR08	38.5982	-118.7513	1666	25.2	2.0	411	165	1.16	10.0	0.83	82
08WR09	38.6022	-118.7480	1597	39.1	3.1	453	195	1.74	9.7	0.76	50
08WR10	38.6019	-118.7469	1555	35.1	2.8	621	279	1.14	14.5	0.78	53
08WR11	38.5837	-118.7501	1948	50.7	4.1	965	380	0.93	19.9	0.74	44
08WR12	38.5897	-118.7432	1886	60.1	4.8	647	396	3.39	35.0	0.79	58
08WR13	38.5937	-118.7409	1881	46.2	3.7	551	290	2.89	19.8	0.78	54
08WR14	38.5952	-118.7400	1788	50.9	4.1	494	252	1.96	18.8	0.78	54
08WR15	38.5969	-118.7373	1703	47.5	3.8	525	283	1.12	61.7	0.84	78
08WR16	38.5923	-118.7344	1593	53.7	4.3	550	302	0.95	30.1	0.79	58
08WR17	38.5734	-118.7126	1408	21.6	1.7	1028	462	1.11	33.0	0.81	64
08WR18	38.5466	-118.7119	1500	15.9	1.3	662	223	2.30	6.0	0.77	50
08WR19	38.5452	-118.7012	1424	12.6	1.0	1027	269	1.39	7.0	0.76	50
08WR20	38.5441	-118.6993	1412	16.5	1.3	532	221	0.89	4.2	0.75	48
08WR22	38.5214	-118.6795	1414	76.3	6.1	479	225	1.51	23.7	0.78	53
08WR23	38.5147	-118.7025	1728	62.3	5.0	890	287	0.68	26.9	0.75	47
08WR24	38.5150	-118.6979	1743	58.3	4.7	955	326	0.98	84.4	0.83	72
08WR25	38.5167	-118.6986	1664	59.6	4.8	689	253	1.08	29.0	0.78	53
08WR26	38.5237	-118.6927	1534	68.5	5.5	1920	338	2.83	66.9	0.77	50

Sample	Latitude	Longitude	Elevation	Age [Ma]	± (8%) [Ma]	U [ppm]	Th [ppm]	Sm [ppm]	He [ncc]	F_T	ESR
08WR27	38.5223	-118.6850	1469	72.8	5.8	658	333	1.14	70.6	0.81	64
08WR29	38.4872	-118.7419	1949	27.0	2.2	351	114	0.75	16.2	0.81	70
08WR30	38.4865	-118.7287	1873	20.1	1.6	257	77	0.76	2.8	0.76	50
08WR31	38.4866	-118.7143	1818	29.7	2.4	1405	751	3.11	14.2	0.76	50
08WR32	38.4826	-118.7058	1744	14.2	1.1	269	67	0.79	6.0	0.81	65
08WR33	38.4844	-118.6980	1765	18.0	1.4	201	77	2.82	1.7	0.75	48
08WR34	38.4826	-118.6857	1656	14.8	1.2	685	305	0.90	7.6	0.78	54
08WR35	38.4845	-118.6739	1587	21.5	1.7	288	77	0.60	7.4	0.79	57
08WR36	38.4842	-118.6629	1525	52.0	4.2	359	157	2.32	21.8	0.81	62
08WR37	38.5685	-118.7911	3442	8.8	0.7	1431	5289	8.92	17.4	0.78	59
08WR38	38.5608	-118.7876	3310	70.1	5.6	241	99	1.36	18.2	0.79	58
08WR41	38.5464	-118.8007	2952	58.8	4.7	309	167	3.62	12.1	0.77	53
08WR43	38.5081	-118.8076	2836	69.9	5.6	912	542	3.72	53.5	0.77	53
08WR44	38.4992	-118.8070	2833	82.4	6.6	493	351	0.83	28.6	0.76	49
08WR45	38.4902	-118.8061	2908	89.4	7.2	1116	654	2.55	43.2	0.74	45
08WR46	38.4841	-118.8027	2936	70.3	5.6	803	418	2.80	71.5	0.81	66
08WR47	38.4788	-118.8033	2846	64.3	5.1	727	395	1.81	39.8	0.79	56
08WR48	38.4801	-118.7971	2728	54.8	4.4	1557	587	6.77	60.0	0.79	57
08WR49	38.4766	-118.7836	2417	68.1	5.4	878	338	2.32	33.6	0.77	51
08WR52	38.5693	-118.7830	3028	74.8	6.0	215	114	1.79	11.1	0.78	54
08WR54	38.5723	-118.7758	2797	68.1	5.4	120	55	0.57	10.3	0.82	66
08WR55	38.5764	-118.7671	2533	56.1	4.5	448	399	5.81	18.6	0.76	52
08WR56	38.5773	-118.7647	2450	55.1	4.4	471	334	2.75	12.1	0.75	47
08WR57	38.5799	-118.7611	2306	55.1	4.4	1704	730	5.38	50.2	0.75	47
08WR58	38.5818	-118.7567	2152	53.1	4.2	663	426	4.10	23.0	0.76	50

Sample	Latitude	Longitude	Elevation	Age [Ma]	± (8%) [Ma]	U [ppm]	Th [ppm]	Sm [ppm]	He [ncc]	F_T	ESR
08WR59	38.5860	-118.7496	1973	62.1	5.0	1146	460	6.60	64.7	0.78	54
08WR60	38.4407	-118.7461	2346	25.1	2.0	646	203	0.58	14.2	0.81	64
08WR61	38.4460	-118.7810	3117	49.6	4.0	1223	644	2.39	59.6	0.79	58
08WR62	38.4617	-118.7585	2976	46.5	3.7	1549	701	6.14	49.2	0.77	54
08WR63	38.4597	-118.7548	2847	62.5	5.0	895	332	0.67	51.7	0.83	70
08WR64	38.4545	-118.7514	2650	42.4	3.4	1135	323	0.85	28.3	0.77	50
08WR65	38.4544	-118.7445	2553	36.0	2.9	883	380	1.05	32.1	0.80	55
08WR66	38.4540	-118.7403	2449	25.4	2.0	693	269	0.63	28.7	0.80	62
08WR68	38.4600	-118.7226	2255	22.1	1.8	438	189	0.74	4.4	0.75	47
08WR69	38.4644	-118.7120	2136	16.7	1.3	924	333	0.53	16.7	0.80	59
08WR70	38.5334	-118.7138	1646	55.4	4.4	702	389	2.65	14.9	0.73	44
08WR71	38.5278	-118.7086	1662	58.8	4.7	355	182	0.79	21.3	0.79	57
08WR72	38.5226	-118.7041	1688	53.7	4.3	303	124	1.14	22.0	0.81	67
08WR73	38.5040	-118.6854	1703	46.0	3.7	544	165	0.68	25.4	0.81	62
08WR74	38.5000	-118.6866	1797	34.0	2.7	544	165	0.68	31.1	0.79	58
08WR75	38.4938	-118.6782	1646	28.2	2.3	298	80	0.26	5.8	0.78	53
08WR76	38.4589	-118.6742	1792	12.1	1.0	301	99	0.57	4.2	0.81	63
08WR77	38.4443	-118.6548	1786	57.3	4.6	1076	1288	2.86	28.6	0.74	45
08WR78	38.4422	-118.6459	1709	66.4	5.3	472	208	2.59	64.6	0.82	70
08WR79	38.5892	-118.7233	1442	36.2	2.9	916	488	0.97	17.8	0.76	50
08WR80	38.5802	-118.7189	1422	20.5	1.6	901	467	1.40	16.2	0.81	62
08WR81	38.5118	-118.6831	1526	58.1	4.6	1068	373	1.00	40.6	0.78	50
08WR82	38.4618	-118.6920	2034	12.9	1.0	838	233	0.52	9.7	0.80	58
08WR85	38.4673	-118.6694	1722	11.58	0.9	408	149	1.33	3.0	0.76	49
08WR87	38.4376	-118.6554	1752	57.43	4.6	567	249	2.21	40.3	0.81	65

Sample	Latitude	Longitude	Elevation	Age [Ma]	± (8%) [Ma]	U [ppm]	Th [ppm]	Sm [ppm]	He [ncc]	F_T	ESR
08WR88	38.4322	-118.6628	1818	57.89	4.6	442	229	1.57	42.3	0.82	71
09WR90	38.6477	-118.7687	1339	65.94	5.3	903	374	1.36	50.8	0.78	54
09WR91	38.3679	-118.5920	1885	14.18	1.1	1084	228	0.35	16.2	0.81	63
09WR92	38.3713	-118.6385	2332	18.60	1.5	745	216	0.85	9.2	0.78	52
09WR93	38.3678	-118.6262	2244	17.02	1.4	706	155	1.01	12.4	0.79	54
09WR94	38.3680	-118.6170	2547	19.33	1.5	548	178	0.18	8.7	0.79	57
09WR95	38.3688	-118.6068	2024	15.1	1.2	1071	277	0.97	15.2	0.79	58
09WR102	38.4996	-118.6633	1541	51.0	4.1	395	121	0.49	22.7	0.81	63
09PGH01	38.5039	-118.9472	1796	61.0	4.9	673	273	0.12	17.3	0.74	41
09PGH03	38.5047	-118.9452	1724	38.5	3.1	1323	338	0.28	23.6	0.75	46
09PGH04	38.5048	-118.9444	1704	46.1	3.7	682	224	0.27	36.5	0.79	58

Table 2. Zircon (U-Th)/He age data for the southern Wassuk Range and Pine Grove Hills footwalls.

Sample	Latitude	Longitude	Elevation	Age [Ma]	± (6%) [Ma]	U [ppm]	Th [ppm]	Sm [ppm]	He [ncc]	F_T	ESR
08WR01	38.4291	-118.6311	1770	9.9	0.6	32	79	46	0.137	0.64	44
08WR02	38.4208	-118.6204	1812	8.2	0.5	26	72	29	0.204	0.68	84
08WR03	38.3883	-118.6319	2056	4.8	0.3	34	53	20	0.072	0.64	72
08WR04	38.3898	-118.6243	2011	4.6	0.3	13	33	93	0.020	0.61	62
08WR05	38.3909	-118.6156	1946	5.0	0.3	26	39	24	0.073	0.67	77
08WR06	38.3971	-118.6071	1870	5.1	0.3	22	42	40	0.073	0.65	76
08WR07	38.4023	-118.5995	1787	6.4	0.4	22	57	28	0.117	0.67	81
08WR08	38.5982	-118.7513	1666	4.2	0.3	4	6	1	1.516	0.67	46
08WR09	38.6022	-118.7480	1597	4.9	0.3	12	12	8	0.032	0.72	43
08WR10	38.6019	-118.7469	1555	5.9	0.4	17	17	44	0.009	0.56	33
08WR11	38.5837	-118.7501	1948	8.4	0.5	19	29	524	0.014	0.58	55
08WR12	38.5897	-118.7432	1886	11.4	0.7	9	22	39	0.017	0.61	39
08WR13	38.5937	-118.7409	1881	13.1	0.8	9	22	45	0.021	0.61	39
08WR14	38.5952	-118.7400	1788	12.1	0.7	13	31	50	0.036	0.63	41
08WR15	38.5969	-118.7373	1703	8.2	0.5	5	25	42	0.005	0.55	56
08WR16	38.5923	-118.7344	1593	8.3	0.5	9	18	35	0.105	0.65	44
08WR17	38.5734	-118.7126	1408	2.6	0.2	17	26	22	0.026	0.70	68
08WR18	38.5466	-118.7119	1500	4.5	0.3	20	3	67	0.031	0.67	72
08WR19	38.5452	-118.7012	1424	4.2	0.3	15	10	59	0.025	0.67	72
08WR20	38.5441	-118.6993	1412	4.4	0.3	19	19	70	0.014	0.62	39
08WR22	38.5214	-118.6795	1414	47.7	2.9	8	18	47	0.132	0.62	39
08WR23	38.5147	-118.7025	1728	14.2	0.9	25	47	76	0.211	0.66	75
08WR24	38.5150	-118.6979	1743	10.4	0.6	20	40	74	0.105	0.66	75
08WR25	38.5167	-118.6986	1664	13.3	0.8	19	41	78	0.090	0.61	66
08WR26	38.5237	-118.6927	1534	44.1	2.6	30	25	73	0.454	0.64	69

Sample	Latitude	Longitude	Elevation	Age [Ma]	± (6%) [Ma]	U [ppm]	Th [ppm]	Sm [ppm]	He [ncc]	F_T	ESR
08WR27	38.5223	-118.6850	1469	76.6	4.6	26	17	35	0.721	0.67	45
08WR28	38.4821	-118.7547	2084	11.3	0.7	30	52	44	0.164	0.64	70
08WR29	38.4872	-118.7419	1949	8.8	0.5	18	26	26	0.086	0.66	75
08WR30	38.4865	-118.7287	1873	5.4	0.3	19	33	28	0.068	0.66	44
08WR31	38.4866	-118.7143	1818	9.2	0.6	23	31	35	0.192	0.71	88
08WR32	38.4826	-118.7058	1744	4.2	0.3	32	41	32	0.083	0.69	79
08WR33	38.4844	-118.6980	1765	4.3	0.3	23	40	18	0.051	0.65	73
08WR34	38.4826	-118.6857	1656	3.6	0.2	82	72	38	0.214	0.70	86
08WR35	38.4845	-118.6739	1587	4.7	0.3	17	27	26	0.050	0.66	76
08WR36	38.4842	-118.6629	1525	42.7	2.6	10	8	22	0.076	0.66	48
08WR37	38.5685	-118.7911	3442	5.5	0.3	9	83	109	0.033	0.67	48
08WR42	38.5352	-118.8101	2791	56.4	3.4	19	55	45	0.229	0.58	36
08WR43	38.5081	-118.8076	2836	58.1	3.5	36	82	106	0.334	0.60	38
08WR46	38.4841	-118.8027	2936	55.6	3.3	20	50	93	0.340	0.65	41
08WR47	38.4788	-118.8033	2846	25.2	1.5	3	6	21	0.022	0.68	50
08WR48	38.4801	-118.7971	2728	42.5	2.5	12	13	63	0.091	0.65	42
08WR49	38.4766	-118.7836	2417	15.6	0.9	21	15	85	0.106	0.70	49
08WR54	38.5723	-118.7758	2797	15.6	0.9	25	27	8	0.057	0.63	42
08WR60	38.4407	-118.7461	2346	11.6	0.7	14	17	65	0.152	0.71	53
08WR61	38.4460	-118.7810	3117	15.7	0.9	25	29	47	0.065	0.59	36
08WR62	38.4617	-118.7585	2976	16.0	1.0	14	25	89	0.194	0.67	46
08WR63	38.4597	-118.7548	2847	14.3	0.9	27	48	33	0.422	0.69	48
08WR64	38.4545	-118.7514	2650	13.7	0.8	22	24	87	0.070	0.66	45
08WR65	38.4544	-118.7445	2553	12.5	0.8	23	37	74	0.205	0.69	50
08WR66	38.4540	-118.7403	2449	11.6	0.7	25	47	61	0.107	0.63	41

Sample	Latitude	Longitude	Elevation	Age [Ma]	± (6%) [Ma]	U [ppm]	Th [ppm]	Sm [ppm]	He [ncc]	F_T	ESR
08WR68	38.4600	-118.7226	2255	7.9	0.5	32	36	58	0.122	0.68	49
08WR69	38.4644	-118.7120	2136	5.9	0.4	85	71	45	0.294	0.68	47
08WR70	38.5334	-118.7138	1646	66.2	4.0	11	21	36	0.697	0.62	40
08WR71	38.5278	-118.7086	1662	44.5	2.7	14	28	36	0.438	0.64	42
08WR73	38.5040	-118.6854	1703	8.9	0.5	18	26	58	0.150	0.71	53
08WR74	38.5000	-118.6866	1797	7.8	0.5	35	41	47	0.149	0.68	47
08WR75	38.4938	-118.6782	1646	6.9	0.4	6	13	16	0.209	0.82	89
08WR76	38.4589	-118.6742	1792	3.1	0.2	9	10	13	0.061	0.79	75
08WR77	38.4443	-118.6548	1786	27.8	1.7	39	234	76	2.606	0.66	47
08WR78	38.4422	-118.6459	1709	33.0	2.0	7	12	13	0.567	0.79	74
08WR79	38.5892	-118.7233	1442	2.8	0.2	31	47	14	0.022	0.66	45
08WR80	38.5802	-118.7189	1422	4.3	0.3	5	2	12	0.057	0.81	81
08WR81	38.5118	-118.6831	1526	10.1	0.6	25	44	58	0.232	0.69	51
08WR82	38.4618	-118.6920	2034	4.5	0.3	25	33	18	0.084	0.69	50
08WR85	38.4673	-118.6694	1722	3.3	0.2	18	18	2	0.094	0.77	68
08WR87	38.4376	-118.6554	1752	4.0	0.2	8	12	13	0.084	0.79	76
08WR88	38.4322	-118.6628	1818	3.6	0.2	10	21	17	0.128	0.80	80
09WR90	38.6477	-118.7687	1339	11.8	0.7	27	55	24	0.050	0.59	36
09WR91	38.3679	-118.5920	1885	2.8	0.2	7	11	5	0.088	0.83	98
09WR92	38.3713	-118.6385	2332	5.3	0.3	32	48	21	0.076	0.63	41
09WR93	38.3678	-118.6262	2244	2.8	0.2	26	43	18	0.079	0.71	54
09WR94	38.3680	-118.6170	2547	3.2	0.2	29	49	15	0.115	0.73	58
09WR95	38.3688	-118.6068	2024	3.0	0.2	27	45	13	0.108	0.72	56
09WR101	38.5013	-118.6629	1476	6.3	0.4	16	19	22	0.053	0.67	46
09WR102	38.4996	-118.6633	1541	6.7	0.4	10	13	21	0.039	0.67	46

Sample	Latitude	Longitude	Elevation	Age [Ma]	± (6%) [Ma]	U [ppm]	Th [ppm]	Sm [ppm]	He [ncc]	F_T	ESR
03WL40	38.3442	-118.5994	1938	4.17	0.3						
03WL41	38.3606	-118.6105	2494	3.20	0.2						
03WL42	38.3554	-118.6063	2403	3.30	0.2						
03WL43	38.3527	-118.6053	2312	4.04	0.2						
03WL44	38.3513	-118.6018	2260	3.82	0.2						
03WL45	38.3498	-118.6002	2196	3.80	0.2						
03WL46	38.3467	-118.5992	2080	3.30	0.2						

Table 3. Apatite (U-Th)/He age data for the southern Wassuk Range and Pine Grove Hills footwalls.

CHAPTER 3: Apatite (U-Th)/He Thermochronometry as an Innovative Geothermal Exploration Tool: A Case Study from the Southern Wassuk Range, Nevada

ABSTRACT

Unconventional, "blind" geothermal resources are now the focus of active geothermal exploration and their popularity follows the decline of exploration that previously exploited easily identifiable geothermal resources often manifested as hydrothermal deposits at the surface. Genetic occurrence models rely on an understanding of the structural and thermal processes that promote the generation of geothermal systems and have been used to focus regional-scale exploration for "blind" geothermal resources, and have been exceptionally useful in identifying resources in extensional settings. Extensional-type geothermal systems are complicated by the interrelation between footwall advection during exhumation, and the subsequent redistribution of heat by hydrothermal fluids in the hanging wall. The southern Wassuk Range hosts a moderate temperature extensional-type geothermal system and is thus ideal for studying this duality by analyzing a suite of footwall and hanging-wall apatite helium (AHe) thermochronologic samples. Hydrothermally reset AHe ages along the footwall range front suggests that the Hawthorne geothermal system (85° - 135° C) is long lived and has resided at a prominent structural boundary in the Wassuk Range footwall marked by localized advection and range-front deformation. In contrast, the presence of both hydrothermally reset and non-reset AHe ages from a ~1.4 km deep borehole in the hanging-wall basin infers that the geothermal plumbing system and current manifestation as a thermal anomaly are juvenile and are controlled by the generation of newly-formed faults in the hanging wall. AHe ages have been shown here to greatly enhance the focusing of regional-scale geothermal exploration efforts, and for the first time have been used to identify and estimate the temperature of unseen hydrothermal fluids and conduits.

1. INTRODUCTION

The thermal regimes of extensional tectonic settings are controlled by polarizing geologic processes where the geothermal gradient is raised in the footwalls of normal faults via isotherm advection during rapid exhumation and erosion and depressed in the hanging wall during burial and sedimentation (Elhers and Chapman, 1999). Hydrothermal fluids play an important role in the migration and redistribution of heat from the footwall to the hanging wall of normal faults. Fault and fracture networks in the footwall and along the range fronts provide conduits for the percolation of meteoric waters, which become heated by interaction with a thermally elevated footwall at depth, and subsequently migrate to the near surface through zones of localized structural and sedimentological permeability along the range front and hanging wall (Figure 1). Thermal anomalies at the near surface arise from the restricted migration of hot hydrothermal fluids, usually in the hanging wall, and are controlled by the presence of water, and the variable distribution of heat and fluid conduits. The temporal and spatial relationship between footwall advection and the resultant heating of the hanging wall and therefore, the presence of geothermal anomalies are poorly understood, and previous studies have primarily focused on controls such as the lateral distribution of permeability (e.g., Barton et al., 1998; Bartley and Glazner, 1985; Borgi, 2004; Monastero et al., 2005; Bertini et al, 2006; Faulds et al., 2006), rather than the along-strike variability of footwall advection (e.g., Elhers and Chapman, 1999; Elhers et al., 2001).

Geothermal exploration in extensional tectonic settings has classically relied on the surface expression of hydrothermal fluids (e.g., geysers, fumaroles, mud pots, tuffa deposits, etc.) (Benoit et al., 1982). Exploration challenges arise as the number of conventional discoveries decline. Genetic occurrence models (e.g., Coolbaugh et al., 2002; Blewitt et al., 2003; Sabin et al., 2005; Walker et al., 2005) have been employed in recent years to find “blind” geothermal resources (Sass et al., 1971) that

lack obvious geothermal surface manifestations. For extensional-type geothermal systems these models have focused geothermal exploration efforts by identifying a number of tectonic and structural trends associated with prolific discoveries. However, new innovative exploration techniques are necessary in order to further focus exploration efforts and to positively identify and exploit the presence of blind hydrothermal fluids.

Genetic Occurrence Models for Geothermal Exploration

After a quick look at the USGS geothermal favorability map of the conterminous United States (Figure 2), one may conclude that easily accessible geothermal resources lie across most of the western United States. This may once have been true, where discoveries of geothermal resources only required the finding of hydrothermal surface manifestations. Today the vast majority of obvious geothermal resources have been tapped and regional-scale exploration is now primarily model driven and requires an in-depth understanding of a region's structural and geologic history. These "blind" geothermal systems are exploration challenges and may make up to several times the known resources in the western United States (Benoit et al., 1982; Coolbaugh and Shevenell, 2004), and have the largest undiscovered resource potential. Geothermal genetic occurrence models have been used to promote the exploration of blind geothermal prospects through an understanding of the conductive and advective geologic processes that bring heat to the near surface. In general, these models show that utility-grade geothermal systems are commonly located above active plate boundaries or hot spots and are associated with high background heat flow (> 80 mW/m^2), recent volcanism, faulting, earthquakes, and high strain rates (> 10^{-15}/s) (Koenig and McNitt, 1983; Glazner et al., 1994; Walker and Whitmarsh, 1998; Wissian et al., 1999; Caskey and Wesnousky, 2000; Blewitt et al., 2002, 2003, 2005; Coolbaugh et al., 2002; Blackwell and Richard, 2004; Coolbaugh and Shevenell, 2004; Sabin, 2005; Walker et al., 2005; Kreemer et al., 2006; Bell and Ramelli, 2007, 2009; Hammond et al., 2007; Hickman et al., 2009).

Both magma- and extensional-type geothermal systems are present in the western United States and generally occur on the margins of the Great Basin where there is active extension and recent volcanism. Magma-type geothermal systems are heated and powered by the interaction of water with shallow-body intrusives and are the least common in the Great Basin and correlate with 1.5 Ma and younger silicic volcanic systems (Koenig and McNitt,1983; Wisian et al., 1999). Conversely, heat in extensional-type geothermal systems is mostly amagmatic and is related to high background heat flow, localized advection in the footwalls of normal faults, and deep circulation of hydrothermal fluids along associated range-front faults (Blackwell, 1983; Wissian et al., 1999; Walker, 2005). Extensional-type geothermal systems in the Basin and Range are focused around Neogene structures that fracture and extend already hot (85 ± 10 mWm^{-2}), attenuated crust (Blackwell, 1983). Additionally, these geothermal systems commonly occupy structurally complex zones (i.e., cross faults, transfer zones, ramps, releasing bends), as they tend to be zones of increased structural permeability and localized, rapid exhumation (Glazner et al., 1994; Barton et al., 1998; Walker and Whitmarsh, 1998; Caskey and Wesnouskey, 2000; Faulds et al., 2006; Hickman et al., 2009; Walker et al., 2005).

The Walker Lane belt (Stewart, 1988) is a northwest-striking belt of right-lateral transtension between the highly extended Basin and Range Province and the stable Sierra Nevada block, and hosts a number of structurally controlled geothermal systems. The Walker Lane is characterized by northwest- to northeast-striking normal, northwest-striking dextral, and northeast-striking sinistral-slip faults (Stewart, 1988, 1998; Hardyman and Oldow, 1991; Oldow, 1992; Wesnousky, 2005). Extensional-type geothermal systems in the Walker Lane are intimately related to Miocene and younger extensional structures. Geothermal systems are primarily associated with north-northeast-striking segments that are oriented roughly orthogonal to the Walker Lane's northwest - southeast extension direction. Because they are oriented orthogonal to the regional extension direction these structures receive maximized dilation and strain (Blewitt et al., 2003), effectively enhancing permeability and footwall

advection (Rowan and Wetlaufer, 1981; Koenig and McNitt, 1983; Coolbaugh et al., 2002; Faulds et al., 2003, 2004; Walker et al., 2005). Similarly, a number of extensional-type geothermal systems in the Walker Lane also occupy accommodation zones characterized by intersecting and/or overlapping fault strands as they too tend to be zones of increased fracture density and structural permeability (Glazner et al., 1994; Walker and Whitmarsh, 1998; Faulds et al., 2005, 2006; Hulen et al., 2005; Monastero, et al., 2005).

This study in the southern Wassuk Range, Nevada, attempts to address the duality of extensional-type geothermal systems by using apatite (U-Th)/He thermochronology (AHe) to address both the timing, distribution and magnitude of advection in the footwalls of normal faults, and the subsequent redistribution of heat by hydrothermal fluids in the hanging wall. Footwall AHe ages record the timing, rate, and along-strike variability of exhumation and therefore advection of the southern Wassuk Range footwall, which sources heat to a moderate-temperature geothermal system in the hanging wall. AHe ages from along the southern Wassuk Range front and from a ~1.4 km deep geothermal borehole in the hanging wall are used as markers for migrating hydrothermal fluids that become partially or completely reset during reheating. Not only does this work address the timing and formation of extensional-type geothermal anomalies and their plumbing systems, but also has important implications on the focusing of regional-scale geothermal exploration efforts as well as the utility of AHe ages in identifying potential down-hole hydrothermal fluid shows.

2. REGIONAL GEOLOGIC SETTING

The Wassuk Range

A long history of Cenozoic extension and tilting in the Wassuk Range has exposed kilometers-thick pre-extensional crustal sections composed primarily of granitic intrusive and associated wall rocks. Jurassic and Cretaceous granitic basement represents now dissected sections of Sierran magmatic arc

that intruded into Triassic to Lower Jurassic wall rocks (Dilles, 1992; Dilles and Gans, 1995; Surpless, 1999). Late Cretaceous to Paleogene erosion resulted in the formation of a prominent, continuous unconformity across Mesozoic Sierran intrusive and associated wall rocks throughout western Nevada and eastern California (e.g., Wernicke, 1992; Stockli et al., 2002; Van Buer et al., 2009). The Cretaceous – Paleogene upland surface is nonconformably overlain by Oligocene rhyolite ignimbrites (e.g., Mickey Pass Tuff and Singatse Tuff) and Miocene andesites (e.g., Lincoln Flat). Oligocene ignimbrites show large variations in thickness and are generally confined to paleovalleys (e.g., Surpless et al., 2002; Stockli et al., 2002; Henry, 2008). Oligocene ignimbrites in the Wassuk Range are overlain by pre-extensional Miocene andesites; except where Oligocene rocks are absent, Miocene andesites nonconformably overlie Mesozoic basement. These units are further overlain by the syn-tectonic Wassuk Group (12 - 8.5 Ma), deposited in fault-bounded basins (Axelrod, 1956; Gilbert and Reynolds, 1973; Dilles, 1992; McIntyre, 1990; Stewart, 1993; Dilles and Gans, 1995; Surpless, 1999; Stockli et al., 2002; Gorynski, Chapter 2).

Our understanding of the Wassuk Range faulting history is based primarily on detailed structural maps of tilted pre- and syn-extensional Neogene cover, and apatite (AHe) and zircon (ZHe) (U-Th)/He and apatite fission-track (AFT) data from the northern and central Wassuk Range (i.e., McIntyre, 1990; Dilles and Gans, 1995; Surpless, 1999; Stockli et al., 2002; Surpless et al., 2002; Stockli, 2005). The onset of rapid Miocene footwall exhumation occurred at ~15 Ma, as identified by AHe, ZHe, and AFT data (Stockli et al., 2002; Surpless et al., 2002; Stockli, 2005; Gorynski, Chapter 2). Throughout the Wassuk Range, Miocene extension was immediately preceded by the extrusion of the ~14.8 – 15.1 Ma Lincoln Flat andesite (Surpless, 1999; Surpless et al., 2002; Stockli et al., 2002; Dilles and Gans, 1995). Subsequent extension in the Wassuk Range was accommodated primarily by footwall rotation along high-angle, range-front faults, which variably tilted the overlying Lincoln Flat andesite and syn-extensional Wassuk Group. AHe data from the lowest structural depths of the exposed Wassuk Range

footwall identified a second cooling event starting at ~4 Ma related to footwall exhumation and normal faulting along the present-day range front and was accommodated by high-angle, east-dipping normal faults (Stockli et al., 2002; Gorynski, Chapter 2). Mio-Pliocene exhumation is consistent with mapped 7 Ma basaltic andesites that dip 8° - 12° to the west along the western flank of the central Wassuk Range (McIntyre, 1990; Surpless, 1999). Miocene and younger extension throughout the northern and central Wassuk Range resulted in ~60° -70° of cumulative footwall rotation and exposed ~8 - 10 km-thick crustal sections (Stockli et al., 2002; Surpless et al., 2002; Gorynski, Chapter 2).

The southern Wassuk Range structure is complicated because it is controlled by the termination of the Wassuk Range fault system into the Mina Deflection transfer zone (Figure 3). The Mina Deflection has acted as an important structural discontinuity since the Paleozoic but in the Miocene acted as a dextral antithetic accommodation zone and accommodated a polarity switch between the west-tilted Wassuk Range and east-tilted White Mountains to its north and south, respectively (Stockli et al., 2003; Oldow et al., 2008; Tincher and Stockli, 2009; Gorynski, Chapter 2). Four tilt blocks define the southern Wassuk Range footwall and bridge the highly tilted crustal sections of the northern and central Wassuk Range to the relatively flat-lying blocks in the Mina Deflection (Gorynski, Chapter 2). The present-day southern Wassuk Range front is defined by north-northwest-striking, moderate to steep, east-dipping normal faults, which are segmented in map view into right-stepping en-echelon strands. Range-bounding faults have been active since the Pliocene and into present day and accommodate slip rates of ~0.5 – 1 mm/yr (Wesnousky, 2005; Surpless, 2008; Bormann et al., 2010). Wassuk Range-front faults accommodate northwest-southeast-directed extension resulting from normal-dextral transtension along the Wassuk Range front (Oldow et al., 2001; Surpless, 2008; Bormann et al., 2010; Moeck et al., 2010). The effects of oblique transtension are enhanced at right steps along the range front, creating pull-apart structures consisting of a series of northeast-oriented normal faults in the Wassuk Range hanging wall (Bell and Hinz, 2010; Hinz et al., 2010; Gorynski, Chapter 2).

Hawthorne Geothermal Anomaly

A moderate-temperature geothermal system resides in the hanging wall of the southern Wassuk Range and underlies the Army Hawthorne Ammunition Depot lands near Hawthorne, Nevada (Figure 4). Its presence has been known since the discovery of hydrothermal fluids in water wells in the 1940s (Trexler et al., 1981). Thermally elevated shallow groundwater throughout the basin was confirmed by the subsequent drilling of water wells and 2m temperature depth probe surveys (Trexler et al., 1981) that encountered temperatures approaching ~100° C. Because the anomaly lies on military lands, continued geothermal exploration has been carried out by the Navy Geothermal Program Office (GPO) at China Lake, CA, who have conducted a plethora of thermal, structural, geophysical and geochemical studies in order to assess the thermal magnitude and extent of the Hawthorne geothermal system (HGS) and its geologic controls (i.e., Bell and Hinz, 2010; Bormann, et al., 2010; Gorynski et al., 2010; Hinz et al., 2010; Kell-Hills et al., 2010; Kratt et al., 2010; Lazaro et al., 2010; Moeck et al., 2010; Penfield et al., 2010; Shoffner, et al., 2010).

Three blind geothermal anomalies are recognized in the HGS and are identified by anomalously high maximum well temperatures (Figure 4), well temperature gradients, 2m temperature gradient-hole surveys (Trexler et al., 1981; Kratt et al., 2010), total dissolved solids (Penfield et al., 2010) and cation geothermometry (Penfield et al., 2010). A fourth geothermal anomaly lies ~4 - 5 km NE of Hawthorne (Figure 4) and is not blind and is marked by both Quaternary tuffa deposits along hanging-wall faults and a 2m temperature gradient-hole anomaly (Heinz et al., 2010; Kratt et al., 2010). Although some have speculated on the presence of magmatic sills in 3D seismic data from the Wassuk Range hanging wall (i.e., Kell-Hills et al., 2010), most accept that heat is sourced from tectonic advection during rapid footwall exhumation. Meteoric waters are heated through interaction with the thermally elevated

Wassuk Range footwall, which then circulate and migrate along high-angle range-front and hanging-wall faults to the near surface.

This study focuses on the formation and lateral extent of geothermal anomaly A in the HGS (Figure 4). Geothermal anomaly A parallels the eastern flank of the Wassuk Range footwall and is nested within a prominent right, en-echelon step in the range-front system. Here, northeast-striking normal fault planes within range-front pull-apart structures are highly dilational and shearing and therefore promote the circulation of hot hydrothermal fluids through this spatially dense network of hanging-wall faults (Moeck et al., 2010). Like many geothermal systems in the Walker Lane, anomaly A is associated with high-angle, recent to active extensional structures with a north to northeast strike, and a high Holocene slip rate (0.5-1 mm/yr) (Bell and Hinz, 2010; Bormann et al., 2010; Hinz et al., 2010). In addition to its structural controls, Anomaly A further correlates with one of the largest drainages in the southern Wassuk Range, and is therefore associated with a rather thick pile of sediment and large hydrothermal circulation cell.

The presence of a geothermal resource associated with anomaly A was further supported by the drilling of two geothermal test holes, HWAAD-2A and HWAAD-3, in 2008 and 2009 (Figure 4). The Navy GPO drilled both holes to depths of > 1200 m and encountered temperatures in excess of 80 °C. Results from HWAAD-2A are most promising, where drilling reached a total depth of ~1430 m and a bottom hole equilibrated temperature of ~113 °C. Similar temperatures were encountered in maximum-reading-thermometer (MRT) measurements that read between ~104 °C and ~118 °C during drilling, and post-drilling geophysical logs that revealed temperatures of ~103 °C and ~113 °C at depths of ~300 m and ~760 m, respectively (Lazaro et al., 2010).

3. METHODOLOGY

Apatite (U-Th)/He Thermochronology

AHe dating is a widely applied thermochronometric technique. ^{4}He in apatite is produced from the radioactive decay of ^{238}U, ^{235}U, ^{232}Th, and ^{147}Sm. Retention of radiogenic ^{4}He in apatite is regulated by temperature (Zeitler et al., 1987, Lippolt et al., 1994: Wolf et al., 1996), where ^{4}He completely diffuses out of the apatite crystal at temperatures above 80 °C, is completely retained below 40 °C and partially retained between 40° - 80 °C (termed the Partial Retention Zone (PRZ)) (Wolf et al., 1998). The thermal sensitivity of this system is lower than that of any other isotopic thermochronometer and can measure processes in the uppermost ~ 1 - 3 km of the crust, assuming a mean annual surface temperature of 10 ± 5 °C and a geothermal gradient of 25 °C/km, (Stockli, 2005). As seen with apatite fission track, the low-temperature sensitivity of the AHe thermochronometer allows for the assessment of small-scaled heating and cooling events related to structural, erosional and hydrothermal processes in the uppermost crust (Farley and Stockli, 2002; Elhers and Farley, 2003; Stockli, 2005). (U-Th)/He thermochronometry has been applied to a number of extensional studies in order to address the timing and rate of footwall exhumation and to assess the pre-extensional thermal state of the crust. This method is particularly useful when footwall rotation during extension exposes kilometers-thick sections of crust and when paired with mapped pre- and syn-extensional cover sequences can provide a crucial structural context for the interpretation of pre-extensional isotherms that are preserved in fossil partial retention and annealing zones (e.g., Miller et al., 1999; Stockli et al., 2002; Surpless et al., 2002; Stockli, 2005).

The southern Wassuk Range is the home to an extensional-type geothermal system and is thus an ideal location to study the interaction and timing between isotherm advection in the footwalls of normal faults and the subsequent conductive heating of the hanging-wall basin. Approximately 100 AHe

samples were collected from the southern Wassuk Range footwall, and cover the entire upper-crustal section exposed during Miocene and younger tilting and extension (Figure 4). AHe ages that result from the cooling of the southern Wassuk Range footwall during extension can be used to identify areas of localized footwall exhumation and therefore advection. Although the vast majority of AHe ages from the Wassuk Range footwall result from cooling during exhumation, anomalously young AHe ages along the range front will also be used to identify areas that underwent late-stage reheating and would thus identify areas of hydrothermal fluid migration (e.g., Gorynski et al., 2010). Additional samples were collected from the ~1.4 km deep HWAAD-2a geothermal borehole in the hanging-wall basin of the southern Wassuk Range. As most of the samples from the HWAAD-2a borehole are at temperatures in excess of 80° C, AHe ages can effectively address the long-term conductive thermal equilibration of the Hawthorne geothermal anomaly, its plumbing system and the hanging-wall basin. Furthermore, AHe age versus depth distributions will be compared to a number of temperature logs and readings collected from the borehole in order to assess their utility in accurately depicting the thermal character of the borehole and the applicability of AHe ages in identifying potential hydrothermal fluid conduits.

Forward and inverse modeling of time-temperature (T-t) histories for (U-Th)/He datasets is now standard practice, and provides statistically robust time and temperature estimates for individual samples. AHe and ZHe data (Gorynski, Chapter 2) for individual samples from footwall transects were inverse-modeled using the in-house *HeMP* software (Hager and Stockli, 2009). Model-derived T-t histories furnished pre-extensional temperature estimates for individual samples, and when placed in a palinspastically restored configuration yielded geothermal gradient estimates and therefore estimates on footwall advection (e.g., Stockli et al., 2002; Stockli, 2005). Forward modeling using HeFTy (Ketcham, 2005) evaluated a number of isothermal reheating scenarios for samples that underwent late-stage, hydrothermal reheating, and were therefore used to produce a spectrum of temperature estimates for hydrothermal fluids.

4. RESULTS

Structure of the Southern Wassuk Range Footwall

Range-front faults in the central and southern Wassuk Range are disconnected in map view by discrete northeast-directed en-echelon steps that mark the boundaries between differentially tilted footwall blocks (Gorynski, Chapter2). Three different tilt blocks are recognized in the central and southern Wassuk Range, and are (from N to S) the Mt. Grant, Coryville, and Lucky Boy blocks (Figure 4). The three northern blocks are geographically bound by northerly striking, east-dipping, high-angle normal faults on their eastern flanks, and are separated by northeast-striking sinistral scissor faults (Figure 3). Tilting is greatest in the Mt. Grant block at ~60° and is consistent with titling and fault-block rotation documented in the northern Wassuk Range (McIntyre, 1990; Dilles and Gans, 1999; Surpless 1999; Surpless et al., 2002; Stockli et al., 2002). Degree of fault-block rotation decreases southward into the Coryville (~20-40°), Lucky Boy (~20-0°) and Anchorite Hills (< 5°) blocks. Abrupt tilt discontinuities between blocks are accommodated by northeast-striking sinistral scissor faults, which are responsible for the systematic southward decrease in footwall rotation. Similarly, the thickness of exposed crust decreases towards the southern Wassuk Range so that cumulative extension and fault-block rotation have exposed paleodepths of ~9 km in the Mt. Grant block and < 4 km in the Lucky Boy and Anchorite Hills blocks.

AHe Thermochronology of the Southern Wassuk Range footwall

AHe footwall transects were collected across the Mt. Grant, Coryville and Lucky Boy blocks of the southern Wassuk Range and sampled the entire exposed crustal section (Figures 3 - 6). AHe ages document the cooling history of the southern Wassuk Range footwall throughout most of the Cenozoic. Two inflections in the AHe age versus Mio-Pliocene paleodepth plots for transects from the Mt. Grant and Coryville blocks (Figures 4, 5) are recognized at ~15 Ma and ~3 – 5 Ma, and record the onset of rapid

cooling for the southern Wassuk Range footwall. These transects have also preserved the fossil Mio-Pliocene AHe PRZ and therefore the 40° C and 80° C isotherms. Mio-Pliocene AHe ages from the southernmost Lucky Boy block did not sample the Mio-Pliocene AHe PRZ. These ages are mostly invariant at ~3 -5 Ma and are inferred to have resided directly below the Mio-Pliocene AHe PRZ, and therefore, record the onset of rapid cooling. Two AHe ages of 2.8 ± 0.2 and 2.6 ± 0.2 Ma from the range front of the Mt. Grant block are anomalously young with respect to their position on the AHe age versus paleodepth profile, and document a later-stage reheating event (Figure 5).

Along-strike AHe ages were taken from along the Wassuk Range front and sample from 38.645° to 38.345° N latitude and represent Pliocene paleodepths of ~2 - 4 km (Figure 6). Range-front cooling ages span the entire Cenozoic, ranging between 2.6 ± 0.2 and 77 ± 4.6 Ma. AHe samples from along the range front of the Coryville and Lucky Boy blocks are anomalously old and disagree with larger-scale, eastward younging trends. These samples were likely taken from structurally detached slivers of the southern Wassuk Range. When samples from the structurally intact Wassuk Range footwall block alone are considered, ages are predominantly late Miocene to Pliocene. Footwall AHe cooling age patterns are analogous to those in the entire dataset and show an overall southward younging trend with Pliocene AHe cooling ages (~3-5 Ma) mimicking the latitudinal extent of the Hawthorne geothermal system (Figure 8). An inflection in the AHe age versus along-strike distance profile occurs at ~25 - 30 km and ~3 - 4 Ma, and correlates with the location of a northeast-striking cross fault and a predominate right en-echelon step between the Mt. Grant and Coryville blocks along the Wassuk Range front.

AHe Thermochronology of the Southern Wassuk Range Hanging Wall and HWAAD-2 Borehole

For a more detailed summary of the Navy's 2008 and 2009 slim-hole drilling campaign near Hawthorne, Nevada see Lazaro et al., (2010).

The HWAAD-2A geothermal well drilled to a depth of ~1.4 km in the Walker Lake basin in the hanging wall of the southern Wassuk Range and reached an equilibrated bottom-hole temperature of 113 °C (Figures 3, 8). HWAAD-2A encountered ~350 m of granitic alluvial fan sediments before penetrating into intensely fractured Mesozoic basement or coarse, consolidated, granitic fanglomerate. MRT readings acquired from a wireline log recorded on an average spacing of ~28 m and measured temperatures between 30° C and 116 °C. An apparent logging malfunction prevented data acquisition between 540 m and 800 m. Despite increasing temperatures with depth at a rate of ~74 °C/km, the HWAAD-2A borehole is characterized by thermal heterogeneities marked in the MRT log by 10 – 100 m long temperature spikes with vertically adjacent measurements differing by almost 50%. Temperature-spike gradients of > 1500° C/km are recorded over 10s of meters, but in general temperatures increased steadily with depth at a rate of ~74 °C/km (R^2 = 0.83). Four temperature spikes were identified in the MRT log and are defined here as temperatures in excess of 80 °C resulting from an increase in temperature at a rate of > 400 °C/km between sampling points. The three uppermost temperature spikes are confined to ~50 - 200 m intervals, and all record maximum temperatures of 100 ± 2 °C. The deepest temperature spike reaches a maximum temperature of 116 °C and maintains temperatures in excess of 100 °C into the bottom of the geothermal well.

45 datable apatite grains were acquired from 10 intervals and spanned the entire borehole below 400 m. AHe dates range between 0 and 19 Ma and show variable scatter within each interval, with %RSD values ranging from 54% to 118%. Young mean AHe ages (< 2.5 Ma) with minimal scatter (100 ± 20 %RSD) correlate with temperature spikes (> 80 °C) in the MRT log, whereas older mean AHe ages (> 2.5 Ma) with significant scatter (> 120 or < 80, %RSD) correlate with low MRT values (< 80 °C) (Figure 9). Mismatches in this correlation occur only in regions where either the MRT log or AHe dataset are absent. Interval AHe age and scatter characteristics are vertically distinguishable and imply precision on the scale of 10s of meters and insignificant sample mixing during drilling.

5. INTERPRETATION OF APATITE (U-Th)/He THERMOCHRONOMETRIC DATA

Thermal Evolution of the Southern Wassuk Range Footwall

The middle Miocene and earlier tectonic history of the southern Wassuk Range is important because it set up the structural configuration utilized during Mio-Pliocene and younger "Walker Lane style" deformation, and therefore influences the location of the present-day geothermal anomalies in the hanging-wall basin. AHe ages from the southern Wassuk Range footwall record the onset of rapid footwall exhumation beginning at ~15 Ma. This episode of footwall exhumation is consistent with extension and tilting throughout the Wassuk Range, documented by other thermochronometric and structural datasets (i.e., McIntyre, 1990; Dilles and Gans, 1995; Surpless et al., 2002; Stockli et al., 2002; Krugh, 2008; Gorynski, Chapter 2). Middle Miocene east-west extension was accommodated primarily by footwall rotation along east-dipping, high-angle normal faults. Tilting and extension were variable in the southern Wassuk Range, and systematically decrease towards the south, from tilt block to tilt block, into the Mina Deflection accommodation zone. Differential tilting of the southern Wassuk Range footwall is responsible for the creation of northeast-striking sinistral scissor faults between tilt blocks, and right, en-echelon steps along the range front.

The onset of a second episode of rapid footwall exhumation is recorded at ~3 - 5 Ma across the entire Wassuk Range and resulted from northwest-southeast-directed extension and transtension documented throughout the central Walker Lane region (e.g., Stockli et al., 2002, 2003; Tincher and Stockli, 2009). The Pliocene AHe age signal extends kilometers back into the southern Wassuk Range and is significantly greater than previously recorded in the central Wassuk Range (i.e., Stockli et al., 2002; Surpless et al., 2002). In the study area alone, Pliocene AHe cooling ages towards the south characterize increasingly thicker sections of crust, and therefore entail a period of exhumation that was chiefly focused in the southern Wassuk Range. Minimal Miocene fault-block rotation in the Coryville and Lucky

Boy blocks promoted the reactivation of their moderately dipping range-front faults during Pliocene transtension. In contrast, shallow dipping range-front faults in the Mt Grant block were abandoned during Pliocene extension, and were further rotated to sub-horizontal orientations by newly-formed, high-angle, range-front faults. Even so, the southern two blocks were not devoid of Pliocene range-front structures, as seen by the juxtaposition of Late Jurassic to Miocene and Pliocene AHe ages along the eastern edge of the Coryville and Lucky Boy blocks (Figure 10).

Because the Walker Lane continues to undergo dextral transtension, it is important to understand the style of Mio-Pliocene and younger exhumation, extension and footwall advection in order to confidently predict and characterize the distribution of extensional-type geothermal systems. Mio-Pliocene AHe ages from the southern Wassuk Range footwall record the onset of northwest-southeast-directed, "Walker Lane style" extension in the Wassuk Range at ~3 - 5 Ma (Gorynski, Chapter 2). Northwest-southeast-directed extension resulted in normal-dextral transtension along the Wassuk Range front and effectively focused extension and exhumation at the en-echelon right steps along the range front and along the southern terminus of the Lucky Boy block, where the range-front system strikes approximately northeast. Young AHe ages reflect this trend and are focused along the southeast corners of the three footwall tilt blocks and all along the southernmost Lucky Boy block at the Whisky Flat pull-apart structure (Figure 10). Releasing bends formed at the southeast corners of the Mt Grant and Coryville blocks (Hinz et al., 2010; Bell and Hinz, 2010) and therefore localize exhumation, marked again by young AHe ages. In the Lucky Boy block, exhumation localized along its NE oriented segments at the very southern terminus of the Wassuk Range, as slip is enhanced on structures oriented orthogonal to a northwest-southeast extension direction (Figure 11).

Temperature estimates throughout the Neogene for samples from the Mt. Grant and Coryville blocks were derived from inverse-modeled T-t histories (Gorynski, Chapter 2). Model-derived

temperatures were plotted versus their respective pre-extensional paleodepths and record an increase in the geothermal gradient between ~15 and ~6 Ma (Figure 12). This increase in the geothermal gradient throughout the Miocene is attributed to footwall advection that accompanied extension and tilting of the southern Wassuk Range footwall at ~15 Ma and ~3 – 5 Ma and is most evident in the Mt Grant block, where the geothermal gradient increased 8 ± 7 °C/km between 15 Ma and 6 Ma (Figures 11). The most recent exhumation event in the Wassuk Range began at ~3 - 5 Ma and most likely raised the geothermal gradient to its regional present-day value of ~35 ± 5 °C/km. The pattern of young (< 5 Ma) AHe ages along the Wassuk Range front (Figure 8, 9, 10) implies that Pliocene faulting, exhumation and advection were focused at pull-apart structures along the SE corners of tilt blocks and at the southern terminus of the Wassuk Range, a pattern of deformation that continues today (Bormann et al., 2010; Hinz et al., 2010; Moeck et al., 2010).

Some anomalously young AHe ages occur along the southern Wassuk Range front and likely resulted from later-stage reheating during interaction with hot hydrothermal fluids (Figures 4, 7). Anomalously young AHe ages from the southern Wassuk Range footwall are generally recognized as ages that are ≤ 3 Ma, but may be any age that significantly deviates in a younging direction from the expected AHe age versus paleodepth profile. This is most evident along the range front of the Mt. Grant block where a few AHe ages are significantly younger then the surrounding ages for a given paleodepth (Figure 5). Inverse modeling (Ketcham, 2005) of these AHe ages furnished T-t histories which require a variety of late-stage (0 - 3 Ma) reheating events (Figure 13A). Reheating scenarios were forward modeled (Ketcham, 2005) for an array of isothermal-holding times and temperatures and furnished temperature estimates for reheating/hydrothermal fluids between ~70° – 155° C since 3 Ma (Figure 13B). The ephemeral nature of hydrothermal fluid pathways restricts isothermal holding to durations on the order of 0.01 – 0.1 Myr, thus refining our model-derived temperature estimates for reheating (i.e., hydrothermal fluids) to ~85° - 135° C. These estimates are compatible with cation geothermometry

temperature estimates of ~86° – 180° C across the entire HGS (Penfield et al., 2010). Furthermore, because these samples were not likely reheated at the surface and are currently being exhumed at a rate of ~1 km/Myr (Surpless, 2008; Bormann et al., 2010), these data suggest that the HGS is long lived and although likely episodic, has a lifespan on the order of 0.1 – 1 Myrs.

Thermal Evolution of the Southern Wassuk Range Hanging Wall and HWAAD-2A Borehole

AHe ages from the HWAAD-2A borehole are middle Miocene to recent in age and fall into two age populations, 0 to 2.5 Ma and 2.5 to 19 Ma. Partially and completely reset AHe borehole ages (0 - 2.5 Ma) are significantly younger than those seen in the southern Wassuk Range footwall and likely result from a post 3 Ma reheating event. The correlation between zones of completely and partially reset AHe ages with temperature spikes in the MRT log suggests that reheating resulted from the interaction of samples with hot hydrothermal fluids. Hydrothermal fluid migration was confined to small (meter-scale) pathways, as seen in the presence of vertically adjacent zones of completely reset and non-reset AHe ages with as little as ~10 m of separation (Figure 9).

The geothermal gradient in the HWAAD-2A borehole (~74 °C/km) is likely young and is anomalously high with respect to the rest of the hanging-wall basin (35 ± 10° C /km). A geothermal gradient of ~74° C/km with a surface temperature of 10° ± 5° C entails a shallow modern AHe PRZ at depths between ~0.4 and 1 km. However, the presence of non-zero AHe ages at the bottom of the HWAAD-2A borehole (~1.4 km) negates this conclusion and therefore the longevity of this hanging-wall anomaly. Instead, the lagged thermal response of helium diffusion in apatite preserves a window into the maturation of a juvenile geothermal anomaly. Conductive heating of the southern Wassuk Range hanging wall and the Hawthorne geothermal anomalies is segmented with depth and is restricted to structurally and/or sedimentologically permeable zones. Over time, conductive cooling of hydrothermal

fluid pathways by heating of the surrounding wall rock should annihilate temperature spikes with depth resulting in a mature, elevated, and thermally equilibrated geothermal anomaly.

6. DISCUSSION

The Role of Footwall Advection in Sourcing Heat to Extensional-Type Geothermal Systems

Exploration for blind, extensional-type geothermal systems classically focuses on structurally enhanced geothermal reservoirs, and neglects their laterally variable sources. In extensional-type geothermal systems, heat is passively advected to the surface in the footwalls of normal faults during extension and unroofing. Heterogeneity in advective heat transport along the range front is expected, given the along-strike tectonic variability of these processes. The mapping of pre-extensional isotherms exposed in the footwalls of normal faults and defined by the upper and lower limits of the Miocene and Mio-Pliocene AHe PRZs, coupled with detailed structural data, allows for the quantitative analysis of advective heat transport during extension (Figure 10, 11).

Fault strike and fault-block rotation in the southern Wassuk Range are laterally variable and are shown here to greatly influence the along-strike variability of advection in extensional tectonic settings. Two episodes of rapid exhumation in the Wassuk Range starting at ~15 Ma and ~3 - 5 Ma, respectively, exhibit markedly different styles of deformation and are used to exemplify this point. Exhumation starting at ~15 Ma resulted from east-west directed extension and was accommodated primarily through fault-block rotation. Tilting of the southern Wassuk Range footwall decreases towards the south yet is partitioned into three discrete blocks that show little internal variability. Of these, the northernmost block (Mt. Grant Block) experienced the greatest degree of Miocene tilting (~50°), and the greatest discernable increase in geothermal gradient (8 ± 7 °C/km). Increased tilting exhumed structurally deeper paleodepths and isotherms, which focused along the range front. Differential tilting of the Wassuk Range footwall also resulted in the formation of right en-echelon steps along the range

front, marked by northeast-striking scissor faults which separate tilt blocks. A second episode of footwall exhumation starting at ~3 – 5 Ma resulted from northwest-southeast directed extension, which in turn generated dextral transtension along the Wassuk Range front. Young AHe ages (3 – 5 Ma) are focused along the SE corners of tilt blocks, defined by right en-echelon steps along the range front, and also at the southern terminus of the Wassuk Range (Figures 9, 10). Exhumation and advection are similarly focused at these range-front pull-apart structures and along the southern Wassuk Range, where fault strike becomes more northeasterly and roughly orthogonal to the overall northwest-southeast extension direction, zones that are also characterized by increased fracture density and dilation.

Thermal Evolution and Longevity of an Extensional-Type Geothermal System

The HGS, although likely episodic, has been around since the onset of dextral transtension along the Wassuk Range front, which was responsible for the focusing of advective heat and formation of structural fluid conduits. The presence of reset AHe ages along the present-day range front resulted from the interaction of footwall samples with hot (85° - 135° C) hydrothermal fluids, and provide some time constraints on the longevity of the HGS, whose lifespan is on the order of 0.1 – 1 Myr. Present-day geothermal anomalies and plumbing systems in the hanging wall are much younger than the entire geothermal system itself. The presence of non-reset AHe ages at the bottom of the ~1.4 km deep HWAAD-2A borehole and completely reset AHe ages at shallower discrete intervals suggests that the geothermal anomaly is not conductively equilibrated and is therefore juvenile. This time discrepancy between hydrothermal reheating of the footwall and the subsequent reheating of the hanging-wall basin reinforces the complex duality of extensional-type geothermal systems that requires not only advective heat transport in the footwalls of normal faults, but demands the continuous production of structural fluid conduits. These processes are intimately related and are exemplified in the southern

Wassuk Range where Mio-Pliocene and younger transtension focuses both heat via footwall advection, and faults at range-front pull-apart structures; and although the HGS has likely resided in and around these structures, its current manifestation as thermal anomalies in the hanging wall has shifted through time following the development of new hanging-wall and range-front structures.

Apatite (U-Th)/He Thermochronometry as a Geothermal Exploration Tool

Cooling ages greatly enhance regional-scale exploration for blind geothermal resources. AHe thermochronometric data have been shown here to 1) help identify areas of significant hydrothermal fluid migration at the surface and within boreholes; 2) estimate temperatures for hydrothermal fluids; 3) identify zones of localized advection; and 4) locate structural complexities such as range-front faults and accommodation zones that are associated with increased structural permeability. Furthermore, this dataset and its geothermal exploration implications may be accurately represented by a suite of range-front samples collected on a 1 - 3 km spacing (Figure 8). Therefore, AHe thermochronometry becomes an accurate, easy, and inexpensive addition to standard regional-scale geothermal exploration practices.

AHe data from the HWAAD-2A geothermal borehole in the southern Wassuk Range hanging-wall basin has important implications on the utility of AHe thermochronometry in assessing the long-term conductive equilibration of geothermal boreholes, the identification of hydrothermal fluid shows, and the pragmatism of borehole temperature logs. Hydrothermally reset AHe ages in the HWAAD-2A borehole correlate with temperature spikes in the MRT log, but show no correlation with post-drilling geophysical temperature logs (Figure 9). Although post-drilling geophysical temperature logs have important implications during the development of geothermal fields, our data suggests that MRT logs more accurately depict the thermal character of geothermal anomalies and the surrounding hanging-wall basin and therefore should be more readily applied during geothermal exploration. This is particularly true in young geothermal systems, where geothermal anomalies are not likely conductively equilibrated.

7. CONCLUSIONS

Geothermal systems require the presence of heat, water and structural or sedimentological fluid conduits. Therefore, exploration for "blind" geothermal resources that lack obvious hydrothermal surface expressions requires an in-depth understanding of the geologic processes that generate heat and permeability. Genetic occurrence models have been employed in recent years to focus exploration for extensional-type geothermal systems to areas that are undergoing active extension and are characterized by dense fault and fracture networks (e.g., accommodation zones). AHe thermochronometric ages can be used in conjunction with genetic occurrence models to further focus geothermal exploration efforts by identifying areas that have been hottest most recently, either by the rapid unroofing and exhumation of footwalls in normal faults or the flow of hot hydrothermal fluids along range-front and hanging-wall faults. More importantly, an along-strike footwall transect of AHe ages will also help resolve structural complexities and identify cross-fault structures (Figure 8), which are often associated with geothermal systems (e.g., Walker and Whitmarsh, 1998; Faulds et al., 2005, 2006; Hulen et al., 2005; Monastero, et al., 2005). This method has successfully been retroactively applied to a known extensional-type geothermal system in the hanging wall of the southern Wassuk Range.

AHe ages from the southern Wassuk Range footwall and a geothermal borehole in the hanging-wall basin shed light on the interplay between footwall advection of heat and its subsequent redistribution in the hanging wall by flowing hydrothermal fluids through fault and fracture networks. Hydrothermally reset AHe ages along the modern footwall range front denote the presence of a long-lived geothermal system in the southern Wassuk Range, however its current structural plumbing system and manifestation as geothermal anomalies in the hanging wall are more recent as is evident by the presence of both hydrothermally reset and non-reset ages from the ~1.4 km HWAAD-2A borehole. The hanging-wall geothermal anomalies are therefore ephemeral in nature and their location and lifespan are dictated by the generation of young and newly formed faults in the hanging-wall basin. We propose

a modified workflow for extensional-type geothermal exploration that begins first with regional-scale geologic reconnaissance using genetic occurrence models, followed by a detailed thermochronometric analysis of the active range front, and finally detailed structural mapping of active and recent structures before the drilling of geothermal temperature and gradient holes.

8. CONTINUED EXPLORATION

In addition to continued exploration at the en-echelon step between the range front of the Mt. Grant and Coryville blocks, we propose that future exploration efforts in the southern Wassuk Range should focus along the range front of the southernmost Lucky Boy block at the Whisky Flat pull apart (Figure 4). Like the pull-apart structure between the Mt. Grant and Coryville blocks, the curvilinear fault trace along the southern Lucky Boy block is defined by young AHe ages (Figure 10), and has been the focus of footwall advection and fault dilation since the onset of transtensional deformation in the Mio-Pliocene. Furthermore, a cross-fault separates the Lucky Boy block from the Anchorite Hills, and is likely characterized by a dense network of faults and fractures and therefore increased structural permeability.

Chapter 3: REFERENCES

Axelrod, D., 1956, Mio-Pliocene floras from west-central Nevada: California University Publications Geological Society, v. 33, p. 1-322.

Barton, C., Hickman, S., Morin, R., Zoback, M., and Benoit, D., 1998, Reservoir-scale fracture permeability in the Dixie Valley, Nevada, geothermal field: SPE/ISRM Rock Mechanics in Petroleum Engineering, p. 47371-47380

Bell, J., and Ramelli, A., 2007, Active Faults and Neotectonics at Geothermal Sites in the Western Basin and Range: Preliminary Results: Geothermal Resources Council Transactions, v. 31, p. 375-378.

Bell. J., and Remelli, A., 2009, Active Fault Controls at High-Temperature Geothermal Sites: Prospecting for New Faults: Geothermal Resource Council Transactions, v. 33, p. 425-429.

Bell, J.W., and Hinz, N., 2010, Young Walker Basin faults provide new insights into structural relations controlling geothermal potential at the Hawthorne army weapons depot, central Nevada: Geothermal Resources Council Transactions, v. 34, p. 751-754.

Benoit, W.R., Hiner, J.E., and Forest, R.T., 1982, Discovery and geology of the Desert Peak Geothermal Field: A case history, NV Bureau of Mines & Geology, pp. 7.

Blackwell, D., 1983, Heat flow in the northern Basin and Range province: The role of heat in the development of energy and mineral resources in the Northern Basin and Range province: Geothermal Resources Council Special Report, v. 13, p. 81-92.

Blackwell, D., and Richards, M., 2004, Geothermal Map of North America, 1 sheet, scale 1: 6,500,000: American Association of Petroleum Geologists, Tulsa, OK, available at< http://www. smu. edu/geothermal/heatflow/geothermal_all_us_clipped_150dpi_pagesize_leg end. gif.

Blewitt, G., Coolbaugh, M., Holt, W., Kreemer, C., Davis, J., and Bennett, R., 2002, Targeting of potential geothermal resources in the Great Basin from regional relationships between geodetic strain and geological structures: Geothermal Resources Council Transactions, v. 26, p. 523-526.

Blewitt, G., Coolbaugh, M., Sawatzky, D., Holt, W., Davis, J., and Bennett, R., 2003, Targeting of potential geothermal resources in the Great Basin from regional to basin-scale relationships between geodetic strain and geological structures: Geothermal Resources Council Transactions, v. 27, p. 3-8.

Blewitt, G., Hammond, W., and Kreemer, C., 2005, Relating geothermal resources to Great Basin tectonics using GPS: Geothermal Resources Council Transactions, v. 29, p. 331-335.

Bormann, J., Wesnousky, S.G., Hammond, W.C., and Sarmiento, A., 2010, Holocene Earthquakes on the Wassuk Range fault zone: paleoseismic observations from the rose creek fan and regional geodetic observations, Hawthorne, Nevada, USA: Geothermal Resources Council Transactions, v. 34, p. 755-760.

Caskey, S., and Wesnousky, S., 2000, Active faulting and stress redistributions in Dixie Valley, Beowawe, and Bradys geothermal fields: Implications for geothermal exploration in the Basin and Range: 25th workshop on Geothermal Reservoir Engineering, Stanford University, p. 24-26.

Coolbaugh, M., Arehart, G., Faulds, J., and Garside, L., 2005, Geothermal systems in the Great Basin, western United States: Modern analogues to the roles of magmatism, structure, and regional tectonics in the formation of gold deposits, p. 1063.

Coolbaugh, M., and Shevenell, L., 2004, A method for estimating undiscovered geothermal resources in Nevada and the Great Basin: Geothermal Resources Council Transactions, v. 28, p. 13.

Coolbaugh, M., Taranik, J., Rains, G., Shevenell, L., Sawatzky, D., Bedell, R., and Minor, T., 2002, A geothermal GIS for Nevada: defining regional controls and favorable exploration terrains for extensional geothermal systems: Geothermal Resources Council Transactions, p. 485-490.

Dilles, J., 1989, Late Cenozoic normal and strike-slip faults, northern Wassuk Range: Geological Society of America Abstracts, v. 21, p. 73.

Dilles, J., 1992, Cenozoic normal and strike-slip faults in the northern Wassuk Range, western Nevada: Walker Lane Symposium Proceedings, p. 114-136.

Dilles, J., and Wright, J., 1988, The chronology of early Mesozoic arc magmatism in the Yerington district of western Nevada and its regional implications: Bulletin of the Geological Society of America, v. 100, p. 644-653.

Dilles, J., and Gans, P., 1995, The chronology of Cenozoic volcanism and deformation in the Yerington area, western Basin and Range and Walker Lane: Geological Society of America Bulletin, v. 107, p. 474-486.

Ehlers, T., and Chapman, D., 1999, Normal fault thermal regimes: conductive and hydrothermal heat transfer surrounding the Wasatch fault, Utah: Tectonophysics, v. 312, p. 217-234.

Ehlers, T., Armstrong, P., and Chapman, D., 2001, Normal fault thermal regimes and the interpretation of low-temperature thermochronometers: Physics of the Earth and Planetary Interiors, v. 126, p. 179-194.

Ehlers, T., and Farley, K., 2003, Apatite (U–Th)/He thermochronometry: methods and applications to problems in tectonic and surface processes: Earth and Planetary Science Letters, v. 206, p. 1-14.

Farley, K., and Stockli, D.F., 2002, (U-Th)/He dating of Phosphates: Apatite, Monazite, and Xenotime: Review in Mineralogy and Geochemistry, v. 48, p. 559-577.

Faulds, J., Garside, L., and Oppliger, G., 2003, Structural Analysis of the Desert Peak-Brady Geothermal Field, Northwestern Nevada: Implications for understanding linkages between northeast-trending structures and geothermal reservoirs in the Humboldt structural zone: Geothermal Resources Council Transactions, v. 27, p. 859.

Faulds, J., Coolbaugh, M., Blewitt, G., and Henry, C., 2004, Why is Nevada in hot water? Structural controls and tectonic model of geothermal systems in the northwestern Great Basin: Geothermal Resources Council Transactions, v. 28, p. 649-654.

Faulds, J.E., Coolbaugh, M., and Ramelli, A., 2005, Geologic reconnaissance of the Salt Wells geothermal field: preliminary assessment of structural controls; Internal report for Amp Resources, Inc.; Prepared by the University of Nevada, Reno, p. 1-8.

Faulds, J., Coolbaugh, M., Vice, G., and Edwards, M., 2006, Characterizing structural controls of geothermal fields in the northwestern Great Basin: A progress report: Geothermal Resources Council Transactions, v. 30, p. 69-76.

Fitzgerald, G., Fryzell, J.E., and Wernicke, B.P., 1991, Miocene crustal extension and uplift in southeastern Nevada: Constraints from fission track analysis: Geology, v. 19, p. 1013-1016.

Foster, D.A., Howard, K.A., and John, B.E., 1994, Thermochronological constraints on the development of metamorphic core complexes in the lower Colorado River area: Eighth International Conference on Geochronology, Cosmochronology, and Isotope Geology U.S. Geol. Surv. Circ., 1107, p. 103.

Gilbert, C., and Reynolds, M., 1973, Character and chronology of basin development, western margin of the Basin and Range province: Geological Society of America Bulletin, v. 84, p. 2489-2510.

Glazner, A., Walker, J., Bartley, J., Coleman, D., and Taylor, W., 1994, Igneous activity at releasing bends and transfer zones in extensional systems: Implications for site and mode of geothermal activity: Geothermal Resources Council Transactions, v. 18, p. 7-9.

Gorynski, K.E., Stockli, D.F., Walker, J.D., and Sabin, A., 2010, Application of (U-Th)/He thermochronometry as a geothermal exploration tool in extensional tectonic settings: the Wassuk Range, Hawthorne, Nevada: Geothermal Resources Council Transactions, v. 34, p. 685-688.

Hammond, W., Kreemer, C., and Blewitt, G., 2007, Exploring the Relationship between Geothermal Resources and Geodetically Inferred Faults Slip Rates in the Great Basin: Geothermal Resources Council Transactions, v. 31, p. 391-395.

Hardyman, R., and Oldow, J., 1991, Tertiary tectonic framework and Cenozoic history of the central Walker Lane, Nevada, Volume 1, p. 279-301.

Henry, C., 2008, Ash-flow tuffs and paleovalleys in northeastern Nevada: Implications for Eocene paleogeography and extension in the Sevier hinterland, northern Great Basin: Geosphere, v. 4, p. 1-35.

Hickman, S., Barton, C., Zoback, M., Morin, R., Sass, J., and Benoit, R., 2009, In situ stress and fracture permeability along the Stillwater fault zone, Dixie Valley, Nevada: International Journal of Rock Mechanics and Mining Sciences, v. 34, p. 414-414.

Hinz, N.H., Faulds, J.E., Moeck, I., Bell, J.W., and Oldow, J.S., 2010, Structural controls of three blind geothermal resources at the Hawthorne ammunition depot, west-central Nevada: Geothermal Resources Council Transactions, v. 34, p. 785-790.

Hulen, J., Nash, G., and Deymonaz, J., 2005, Geology of the Emigrant geothermal prospect: Esmeralda County, Nevada: Geothermal Resources Council Transactions, v. 29, p. 369-380.

Kell-Hills, A., Louie, J.N., Kent, G., Pullammanappallil, S., Sabin, A., and Lazarro, M., 2010, A revised interpretation of 3d seismic data, Hawthorne army depot, Nevada: faulted-basin reflections or sill intrusions?: Geothermal Resources Council Transactions, v. 34, p. 869-872.

Ketcham, R., 2005, Forward and inverse modeling of low-temperature thermochronometry data: Reviews in Mineralogy and Geochemistry, v. 58, p. 275-314.

Kistler, R.W., and Peterman, Z.E., 1973, Variations in Sr, Rb, K, Na, and initial Sr87/Sr86 in Mesozoic granitic rocks and intruded wall rocks in central California: Geological Society of America Bulletin, v. 84, p. 3489-3512.

Koenig, J., and McNitt, J., 1983, Controls on the location and intensity of magmatic and non-magmatic geothermal systems in the Basin and Range province: Geothermal Resources Council, Special Report, pp. 93.

Kratt, C., Sladek, C., and Coolbaugh, M., 2010, Boom and bust with the latest 2m temperature surveys: dead horse wells, Hawthorne army depot, terraced hills, and other areas in Nevada: Geothermal Resources Council Transactions, v. 34, p. 567-574.

Kreemer, C., Blewitt, G., and Hammond, W., 2006, Using geodesy to explore correlations between crustal deformation characteristics and geothermal resources: Geothermal Resources Council Transactions, v. 30, p. 441-446.

Krugh, W.C., 2008, Low-temperature thermochronologic constraints on fault array evolution and patterns of range-scale denudation: Ph.D. Thesis; ETH Zurich; Zurich, Switzerland, p.1- 190.

Lachenbruch, A., and Sass, J., 1977, Heat flow in the United States and the thermal regime of the crust: The Earth's Crust, p. 626-675.

Lazaro, M., Page, C., Tiedeman, A., Sabin, A., Bjornstad, S., Alm, S., Meade, D., Shoffner, J., Mitchell, K., and Crowder, B., 2010, United States department of the Navy geothermal exploration leading to shallow and intermediate/deep drilling at Hawthorne ammunition depot, Hawthorne, NV: Geothermal Resources Council Transactions, v. 34, p. 595-598.

Lippolt, H., Leitz, M., Wernicke, R., and Hagedorn, B., 1994, (Uranium+ thorium)/helium dating of apatite: experience with samples from different geochemical environments: Chemical Geology, v. 112, p. 179-191.

McIntyre, J., 1990, Late Cenozoic structure of the central Wassuk Range, Mineral County, Nevada: Oregon State University; M.S. Thesis; Bend, Oregon; pp. 120.

McKenna, J., and Blackwell, D., 2004, Numerical modeling of transient Basin and Range extensional geothermal systems: Geothermics, v. 33, p. 457-476.

Micklethwaite, S., and Cox, S.F.,, 2004, Fault-segment rupture, after-shock-zone fluid flow, and mineralization: Geology, v. 32, p. 813-816.

Miller, E., Dumitru, T., Brown, R., and Gans, P., 1999, Rapid Miocene slip on the Snake Range–Deep Creek Range fault system, east-central Nevada: Geological Society of America Bulletin, v. 111, p. 886-905.

Moeck, I., Hinz, N.H., Faulds, J.E., Bell, J.W., Kell-Hills, A., and Louie, J.N., 2010, 3D Geological mapping as a new method in geothermal exploration: a case study from central Nevada: Geothermal Resources Council Transactions, v. 34, p. 807-811.

Monastero, F., Katzenstein, A., Miller, J., Unruh, J., Adams, M., and Richards-Dinger, K., 2005, The Coso geothermal field: A nascent metamorphic core complex: Geological Society of America Bulletin, v. 117, p. 1534-1553.

Oldow, J., 1992, Late Cenozoic displacement partitioning in the northwestern Great Basin, p. 17–52.

Oldow, J., Aiken, C., Hare, J., Ferguson, J., and Hardyman, R., 2001, Active displacement transfer and differential block motion within the central Walker Lane, western Great Basin: Geology, v. 29, p. 19-22.

Oldow, J., Geissman, J., and Stockli, D., 2008, Evolution and strain reorganization within late Neogene structural stepovers linking the central Walker Lane and northern Eastern California shear zone, western Great Basin: International Geology Review, v. 50, p. 270-290.

Penfield, R., Zehner, R., Coolbaugh, M., Shevenell, L., Hastings, J., Johnson, G., Snyder, W., Morgos, D., Kurz, K., Sabin, A., Lazaro, M., Bjornstad, S., and Halsey, G., 2010, Geothermal site assessment using the national geothermal data system (NGDS), with examples from the Hawthorne ammunition depot area: Geothermal Resources Council Transactions, v. 34, p. 709-714.

Proffett, J., 1977, Cenozoic geology of the Yerington district, Nevada, and implications for the nature and origin of Basin and Range faulting: Geological Society of America Bulletin, v. 88, p. 247-266.

Reheis, M.C., and Sawyer, T.L., 1997, Late Cenozoic history and slip rates of the Fish Lake Valley, Emigrant Peak, and Deep Springs fault zones, Nevada and California: Geological Society of America Bulletin, v. 109, p. 280-299.

Rowan, L., and Wetlaufer, P., 1981, Relation between regional lineament systems and structural zones in Nevada: AAPG Bulletin, v. 65, p. 1414-1432.

Sabin, A., Walker, J.D., Unruh, J., and Combs, J., 2005, Kinematic and dynamic studies: genetic occurrence models for geothermal prospecting: Report for Contract No. N68936-04-C-0057 (US Navy).

Sass, J., Lachenbruch, A., Munroe, R., Greene, G., and Moses Jr, T., 1971, Heat flow in the western United States: Journal of Geophysical Research, v. 76, p. 6376-6413.

Shoffner, J.D., Li, Y., Hinz, N., Sabin, A., Lazaro, M., and Alm, S., 2010, Understanding fault characteristics and sediment depth for geothermal exploration using 3d gravity inversion in Walker Valley, Nevada: Geothermal Resources Council Transactions, v. 34, p. 633-636.

Stewart, J., 1988, Tectonics of the Walker Lane belt, western Great Basin: Mesozoic and Cenozoic deformation in a zone of shear: Metamorphism and crustal evolution of the western United States, v. 7, p. 683–713.

Stewart, J., 1998, Regional characteristics, tilt domains, and extensional history of the later Cenozoic Basin and Range province, western North America: Geological Society of America Special Papers, v. 323, p. 47-74.

Stewart, J.H., Carlson, J.E., Tingley, S.L., Survey, G., Mines, N.B.o., and Geology, 1977, Geologic map of Nevada, Nevada Bureau of Mines and Geology, University of Nevada.

Stockli, D.F., 1999, Regional timing and spatial distribution of Miocene extension in the northern Basin and Range Province: Ph.D. Thesis; Stanford University; Stanford, California, pp. 239.

Stockli, D., 2005, Application of low-temperature thermochronometry to extensional tectonic settings: Reviews in Mineralogy and Geochemistry, v. 58, p. 411-448.

Stockli, D., Surpless, B., Dumitru, T., and Farley, K., 2002, Thermochronological constraints on the timing and magnitude of Miocene and Pliocene extension in the central Wassuk Range, western Nevada: Tectonics, v. 21, p. 1028-1047.

Stockli, D., Dumitru, T., McWilliams, M., and Farley, K., 2003, Cenozoic tectonic evolution of the White Mountains, California and Nevada: Geological Society of America Bulletin, v. 115, p. 788-816.

Surpless, B., 2008, Modern strain localization in the central Walker Lane, western United States: Implications for the evolution of intraplate deformation in transtensional settings: Tectonophysics, v. 457, p. 239-253.

Surpless, B., Stockli, D., Dumitru, T., and Miller, E., 2002, Two-phase westward encroachment of Basin and Range extension into the northern Sierra Nevada: Tectonics, v. 21, p. 1002-1015.

Surpless, B.E., 1999, Tectonic evolution of the northern Sierra Nevada-Basin and Range transition zone; a study of crustal evolution in extensional provinces: United States: Ph.D. Thesis; Stanford University; Stanford, California, pp. 340.

Svarc, J., Savage, J., Prescott, W., and Ramelli, A., 2002, Strain accumulation and rotation in western Nevada, 1993–2000: Journal of Geophysical Research, v. 107, p. 2090.

Tincher, C.R., and Stockli, D.F., 2009, Cenozoic volcanism and tectonics in the Queen Valley area, Esmeralda County, western Nevada: Late Cenozoic structure and evolution of the Great Basin-Sierra Nevada transition, p. 255-274.

Trexler, D., Koeing, B., Flynn, T., Bruce, J., and Ghusn Jr, G., 1981, Low-to-moderate temperature geothermal resource assessment for Nevada: Area specific studies, final report for the period June 1, 1980-August 30, 1981, DOE/NV/10039-3, Nevada Bureau of Mines and Geology, University of Nevada, Reno, NV. pp 226.

Van Buer, N., Miller, E., and Dumitru, T., 2009, Early Tertiary paleogeologic map of the northern Sierra Nevada batholith and the northwestern Basin and Range: Geology, v. 37, p. 371-374.

Walker, J.D., and Whitmarsh, R.S., 1998, A tectonic model for the Coso geothermal area: Proceedings Geothermal Program Review, XVI, A strategic plan for geothermal Research, U.S. Department of Energy Report DOE/EE-0188, p. 17-24.

Walker, J.D., Sabin, A., Unruh, J., Combs, J., and Monastero, F., 2005, Development of genetic occurrence models for geothermal prospecting: Geothermal Resources Council Transactions, v. 29, p. 309-314.

Wernicke, B., 1992, Cenozoic extensional tectonics of the US Cordillera: The Cordilleran orogen: Conterminous US: Boulder, Colorado, Geological Society of America, Geology of North America, v. 3, p. 553–581.

Wesnousky, S., 2005, Active faulting in the Walker Lane: Tectonics, v. 24, p. 3009-3044.

Wisian, K., Blackwell, D., and Richards, M., 1999, Heat flow in the western United States and extensional geothermal systems: 24th workshop on Geothermal Reservoir Engineering, Stanford University. p. 25-27.

Wolf, R., Farley, K., and Silver, L., 1996, Helium diffusion and low-temperature thermochronometry of apatite: Geochimica et Cosmochimica Acta, v. 60, p. 4231-4240.

Wolf, R., Farley, K., and Kass, D., 1998, Modeling of the temperature sensitivity of the apatite (U-Th)/He thermochronometer: Chemical Geology, v. 148, p. 105-114.

Zeitler, P., Herczeg, A., McDougall, I., and Honda, M., 1987, U-Th-He dating of apatite: A potential thermochronometer: Geochimica et Cosmochimica Acta, v. 51, p. 2865-2868.

Chapter 3: FIGURES AND TABLES

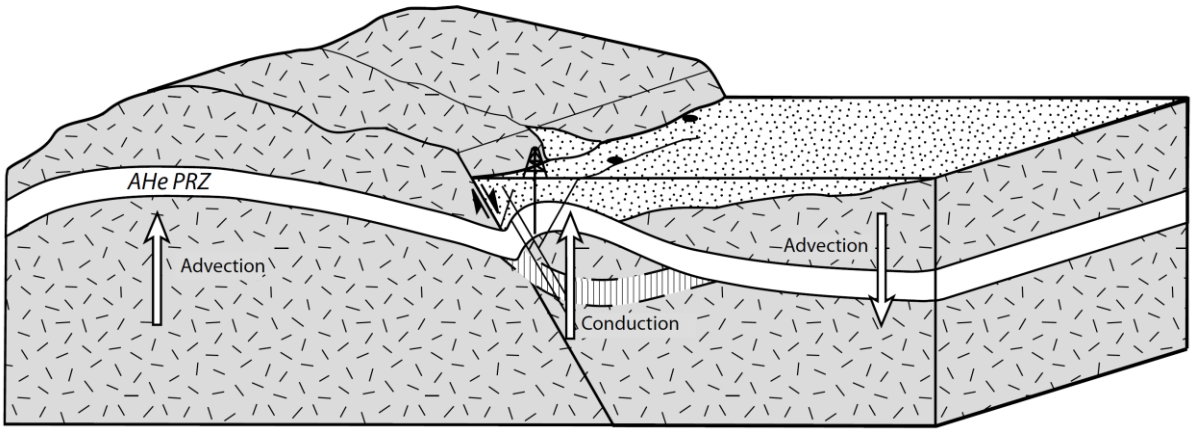
AHe PRZ
Advection
Advection
Conduction

Figure 1. Block diagram adapted from Ehlers et al.,(2001) showing the thermal characterization of normal faults where isotherms, represented here as the AHe PRZ, are advected upward in rapidly exhumed footwalls of normal faults, and are depressed in the hanging wall. An elevated AHe PRZ in the hanging wall is also shown and correlates with the conductive heating of the hanging wall through interaction with advecting hydrothermal fluids along fault and fracture networks.

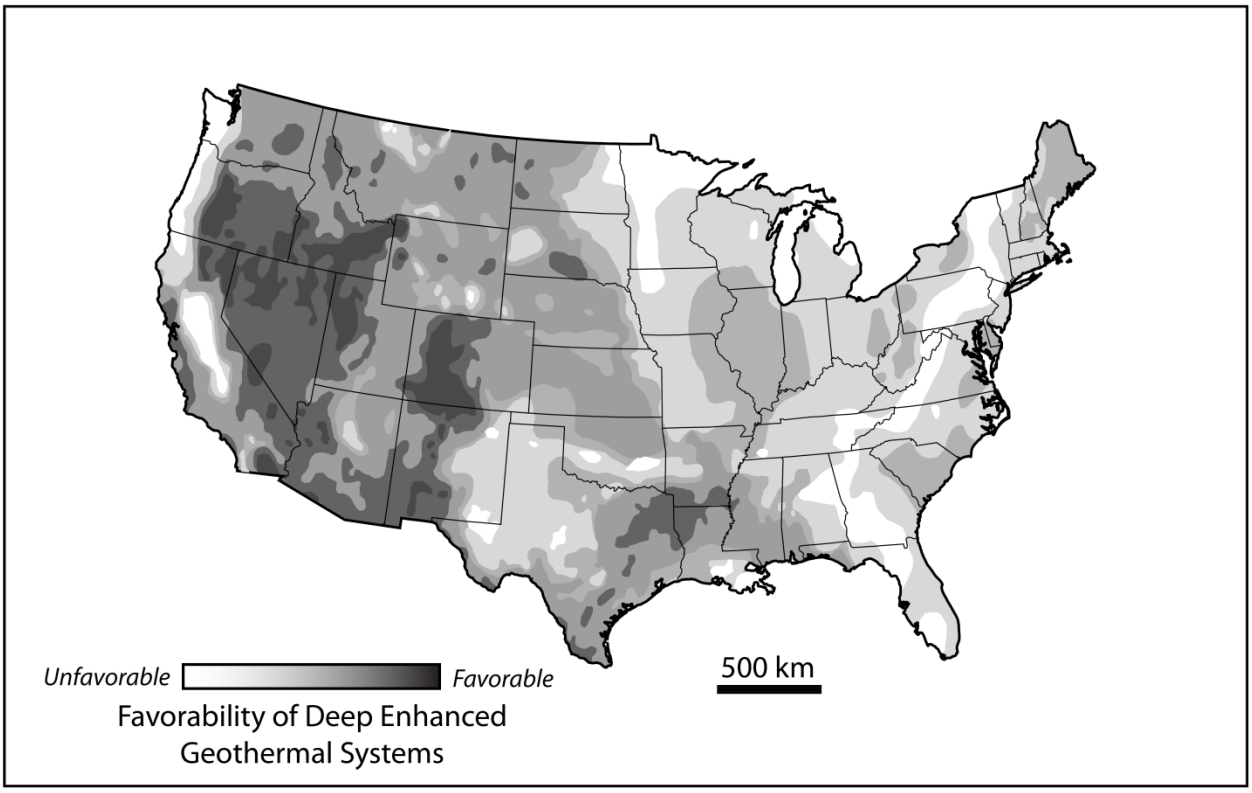
Unfavorable
Favorable
500 km
Favorability of Deep Enhanced
Geothermal Systems

Figure 2. Geothermal exploration favorability map of the conterminous United States (Roberts, 2009). Darker regions designate areas of increased favorability, which cover much of the western United States. Despite that much of the west appears to have easily accessible geothermal resources, these resources actually remain hidden. Genetic occurrence models have been used in conjunction with other exploration techniques to focus regional-scale geothermal exploration efforts.

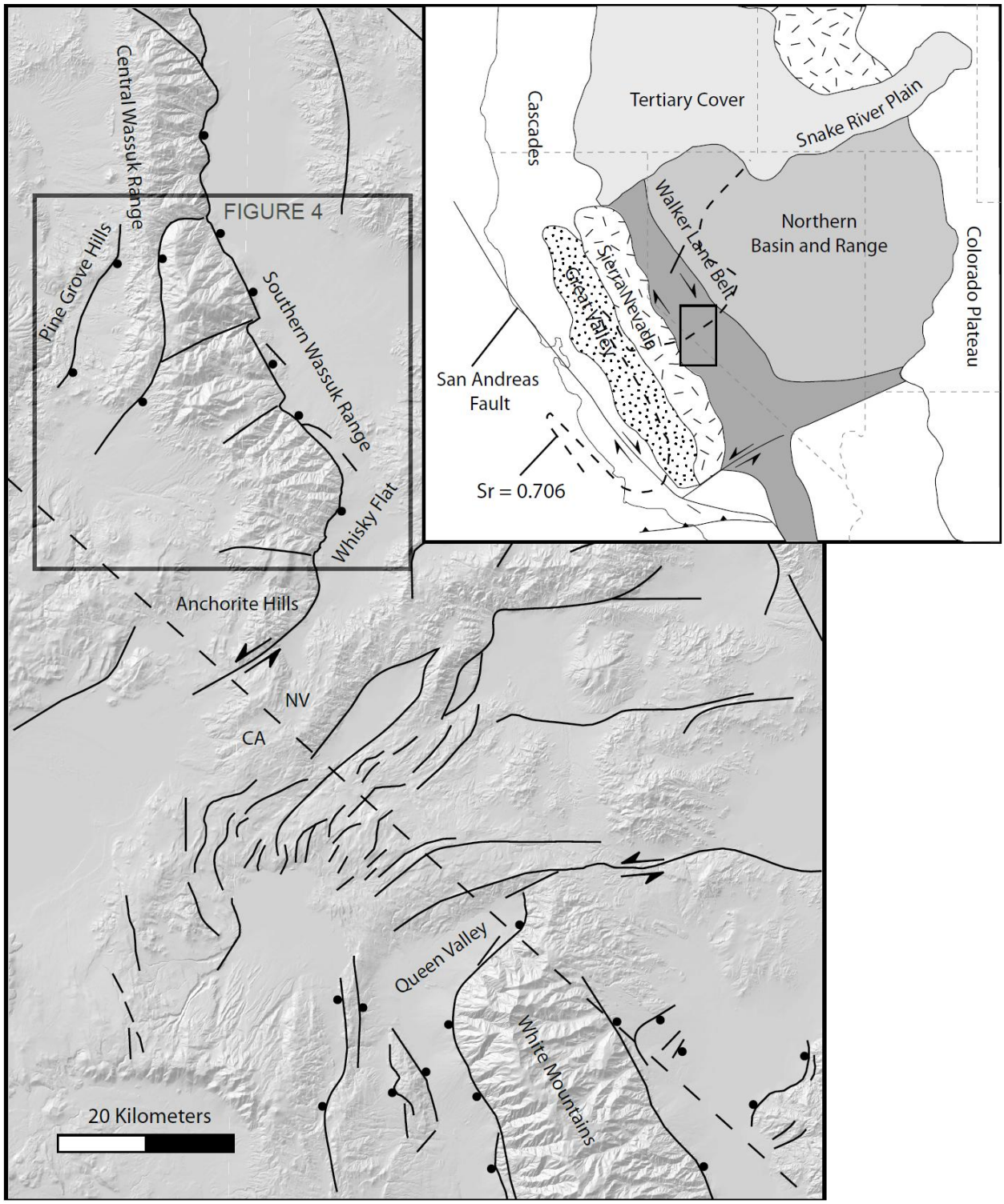
Central Wassuk Range
FIGURE 4
Pine Grove Hills
Southern Wassuk Range
Whisky Flat
Anchorite Hills
NV
CA
Queen Valley
White Mountains
20 Kilometers
Cascades
Tertiary Cover
Snake River Plain
Walker Lane Belt
Northern
Basin and Range
Colorado Plateau
Sierra Nevada
Great Valley
San Andreas
Fault
Sr = 0.706

Figure 3. Digital elevation model of the central Walker Lane belt with major late Cenozoic faults (modified after Stewart, et al., 1977; Oldow, 1992; Rehis and Sawyer, 1997; Stockli et al., 2003). The west-tilted Wassuk Range footwall and east-tilted White Mountains footwall are separated by the east-west trending faults of the Mina Deflection. Insert map shows the location of the study area with respect to the western margin of the North American craton, as defined by the $^{87}Sr/^{86}Sr$ 0.706 line (Kistler and Peterman, 1973; Oldow et al., 2008).

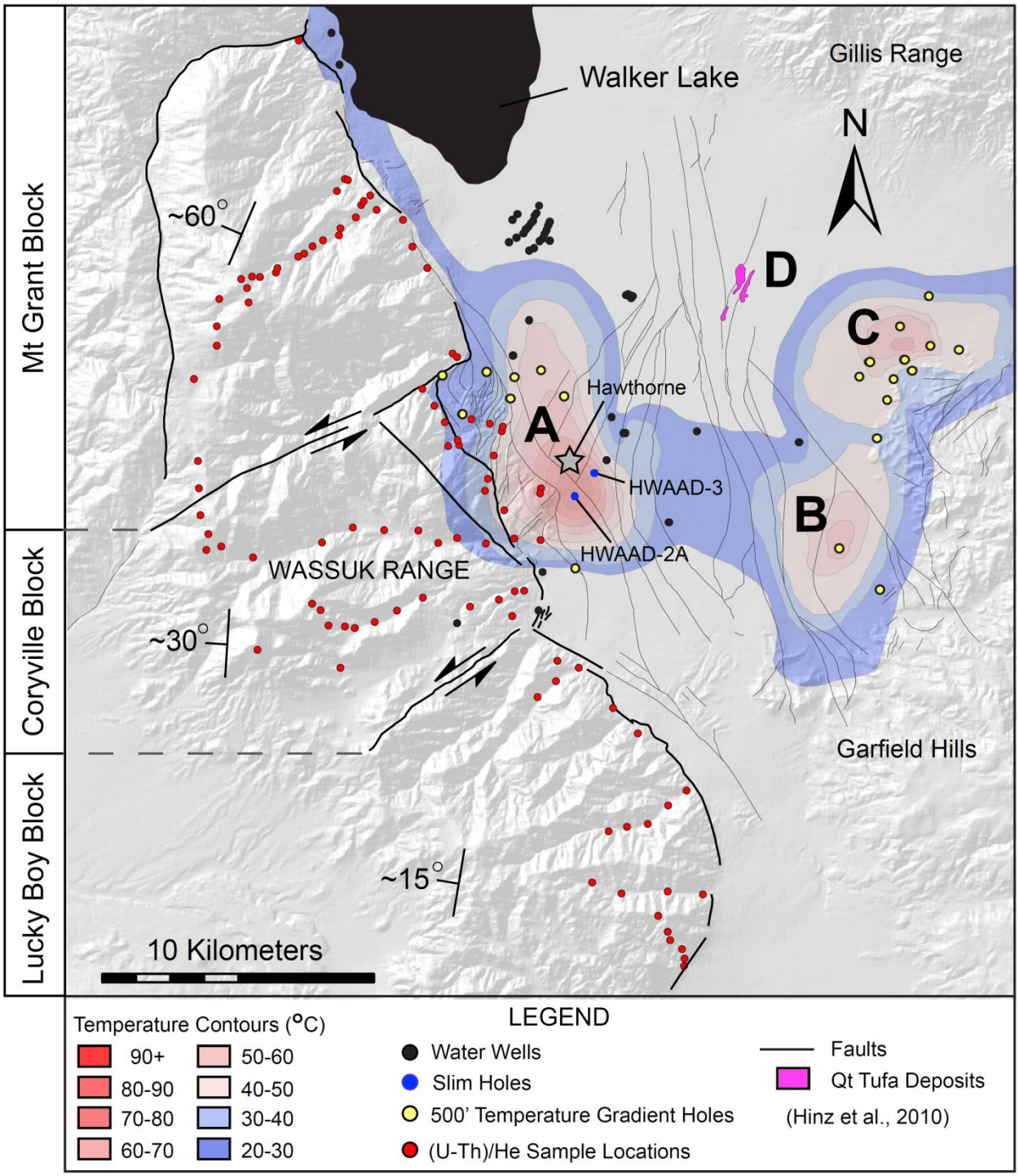
Mt Grant Block
Coryville Block
Lucky Boy Block
Walker Lake
Gillis Range
N
~60°
D
C
A
Hawthorne
HWAAD-3
HWAAD-2A
B
WASSUK RANGE
~30°
Garfield Hills
~15°
10 Kilometers
Temperature Contours (°C)
90+
80-90
70-80
60-70
50-60
40-50
30-40
20-30
LEGEND
Water Wells
Slim Holes
500' Temperature Gradient Holes
(U-Th)/He Sample Locations
Faults
Qt Tufa Deposits
(Hinz et al., 2010)

Figure 4. DEM of the Southern Wassuk Range overlain with footwall (U-Th)/He sample locations and the contoured Hawthorne Geothermal Anomalies in the hanging wall. Three of the Hawthorne geothermal anomalies (A,B,C) are blind and correlate with structures in the hanging-wall fault system (from Heinz et al., 2010) and with transfer zones along the Wassuk Range front. NE-SW striking transfer zones in the footwall mark the boundaries between the (from N to S) Mt. Grant, Coryville, and Lucky Boy tilt blocks. A fourth geothermal anomaly (D) is not blind and is associated with Quaternary tuffa deposits along hanging-wall faults (Heinz et al., 2010).

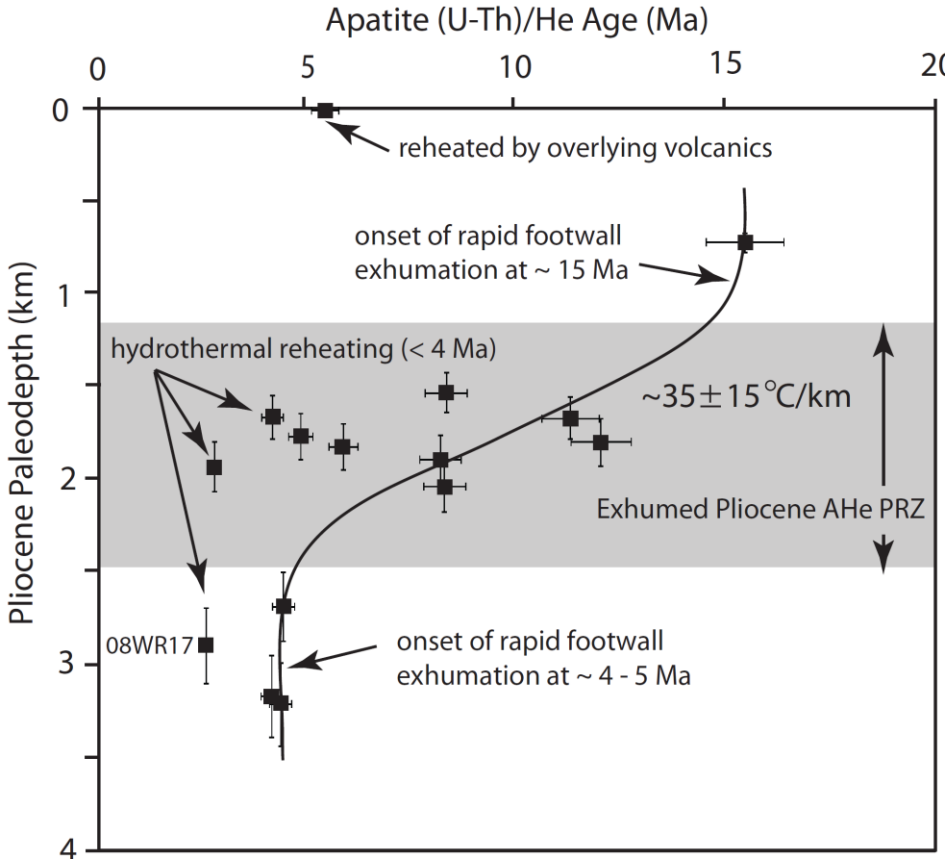
Apatite (U-Th)/He Age (Ma)
0
5
10
15
20
Pliocene Paleodepth (km)
0
1
2
3
4
reheated by overlying volcanics
onset of rapid footwall
exhumation at ~ 15 Ma
hydrothermal reheating (< 4 Ma)
~35±15°C/km
Exhumed Pliocene AHe PRZ
08WR17
onset of rapid footwall
exhumation at ~ 4 - 5 Ma

Figure 5. Apatite helium age vs. paleodepth plot for the Mt. Grant block in the southern Wassuk Range. Inflections in the age-paleodepth plot at ~4-5 and ~15 Ma mark the onset of rapid footwall exhumation. Scatter in the AHe age-paleodepth plot is accredited to hydrothermal reheating along Wassuk Range range-front faults. The Pliocene AHe PRZ is preserved and provides a rough estimate for the Pliocene geothermal gradient.

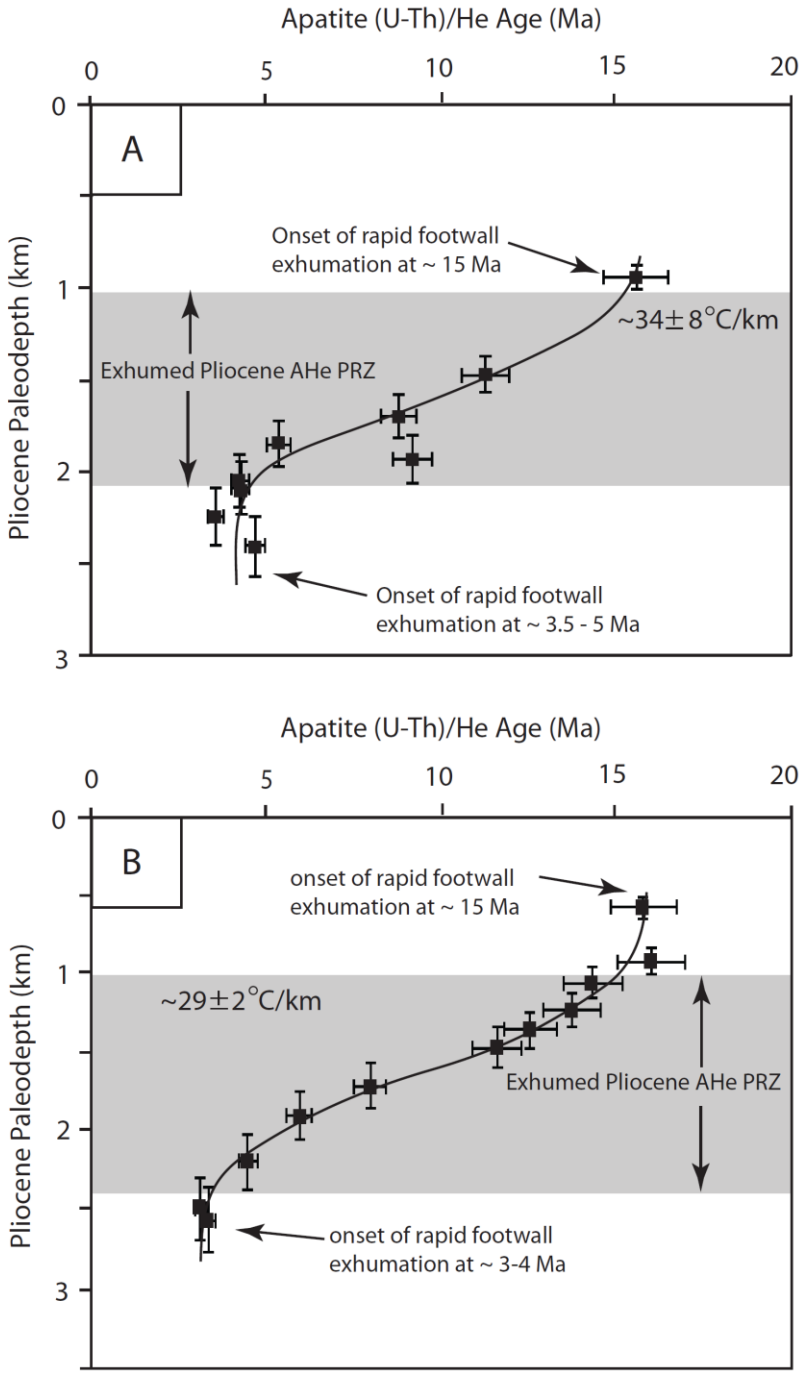
Apatite (U-Th)/He Age (Ma)
0
5
10
15
20
A
Onset of rapid footwall
exhumation at ~ 15 Ma
~34±8°C/km
Exhumed Pliocene AHe PRZ
Onset of rapid footwall
exhumation at ~ 3.5 - 5 Ma
Pliocene Paleodepth (km)
0
1
2
3
Apatite (U-Th)/He Age (Ma)
0
5
10
15
20
B
onset of rapid footwall
exhumation at ~ 15 Ma
~29±2°C/km
Exhumed Pliocene AHe PRZ
onset of rapid footwall
exhumation at ~ 3-4 Ma
Pliocene Paleodepth (km)
0
1
2
3

Figure 6. Apatite helium age vs. paleodepth plots for the Coryville block in the southern Wassuk Range. Inflections in the age-paleodepth plot at ~3.5-5 and ~15 Ma [A] and ~3-4 and ~15 Ma [B] mark the onset of rapid footwall exhumation. Both age-paleodepth profiles have preserved the Pliocene AHe PRZ, which provides a rough estimate for the Pliocene geothermal gradient.

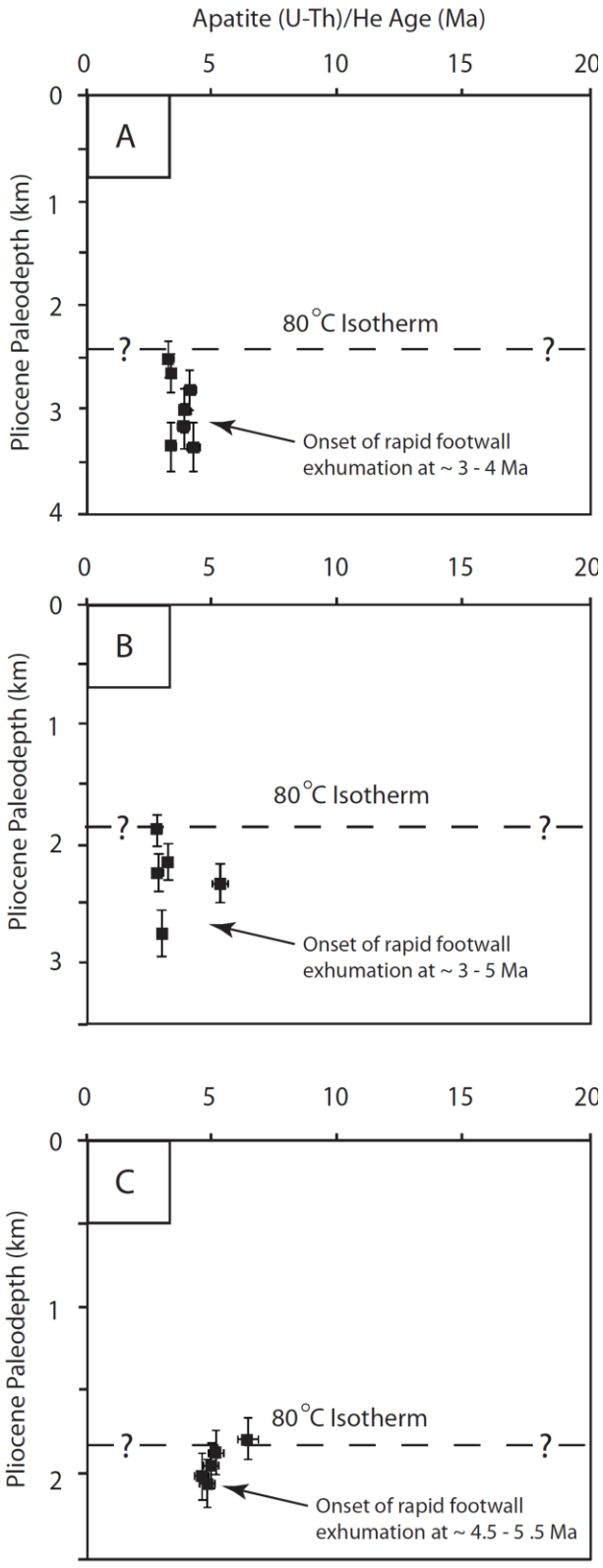
Apatite (U-Th)/He Age (Ma)
0
5
10
15
20
A
Pliocene Paleodepth (km)
0
1
2
3
4
80°C Isotherm
?
?
Onset of rapid footwall
exhumation at ~ 3 - 4 Ma
B
Pliocene Paleodepth (km)
80°C Isotherm
Onset of rapid footwall
exhumation at ~ 3 - 5 Ma
C
Pliocene Paleodepth (km)
80°C Isotherm
Onset of rapid footwall
exhumation at ~ 4.5 - 5 .5 Ma

Figure 7. Apatite helium age vs. paleodepth plots for the Lucky Boy block in the southern Wassuk Range. Inflections in the age-paleodepth plot at ~3-4 [A], ~3-5 [B]. and ~4.5-5.5 Ma [C] mark the onset of rapid footwall exhumation. Because no samples were taken from the shallowest structural paleodepths the Pliocene AHe PRZ is not preserved, nor are ages that record rapid footwall exhumation at ~15 Ma exhibited elsewhere throughout the Wassuk Range. Nevertheless, a maximum depth for the Pliocene 80° C isotherm can be estimated.

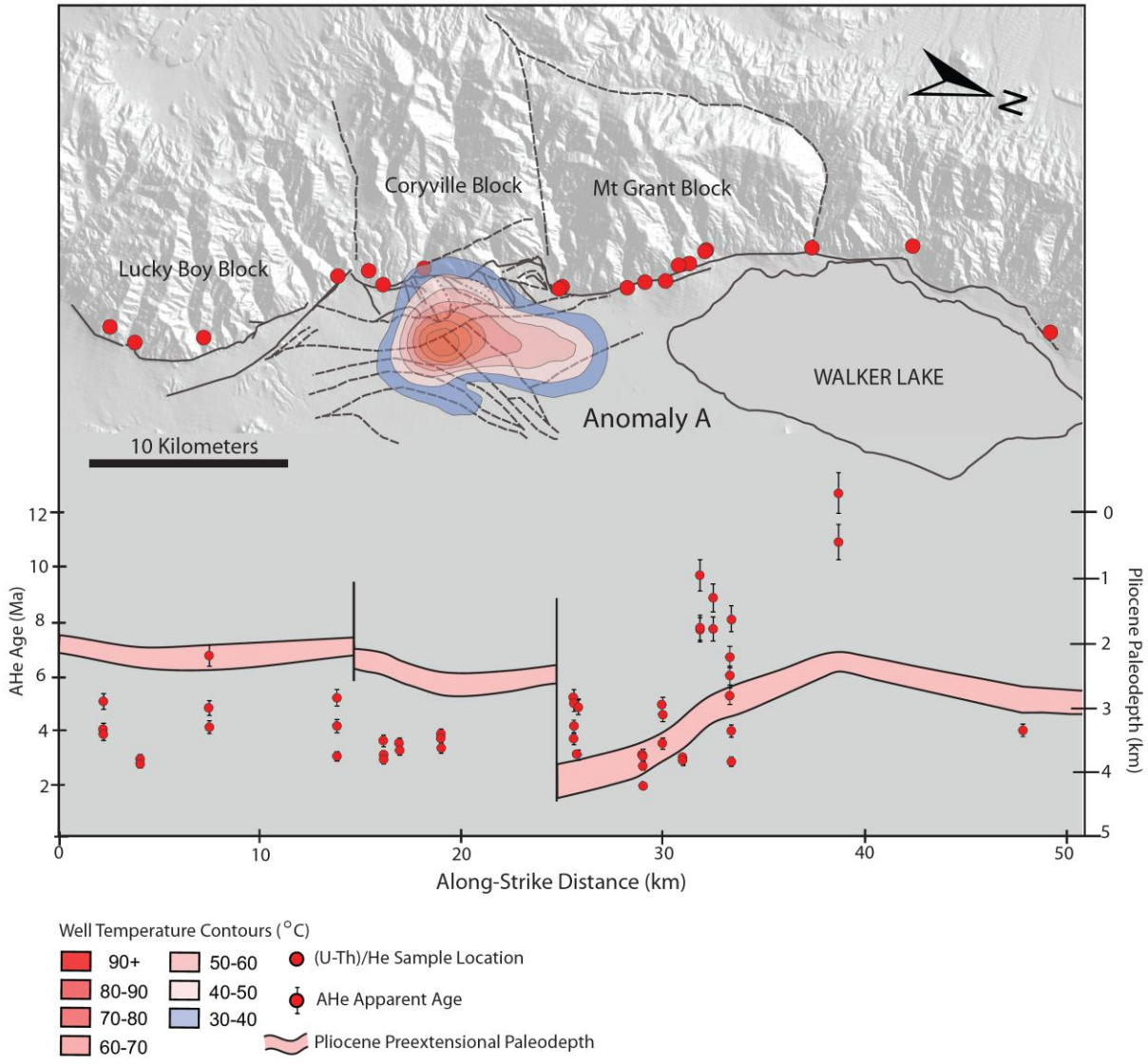
N
Coryville Block
Mt Grant Block
Lucky Boy Block
WALKER LAKE
Anomaly A
10 Kilometers
AHe Age (Ma)
Pliocene Paleodepth (km)
Along-Strike Distance (km)
Well Temperature Contours (°C)
90+
80-90
70-80
60-70
50-60
40-50
30-40
(U-Th)/He Sample Location
AHe Apparent Age
Pliocene Preextensional Paleodepth

Figure 8. DEM of the southern Wassuk Range showing the location of along-strike, footwall apatite (U-Th)/He sample locations, the Hawthorne geothermal anomaly A, and range-front structures (Heinz et al., 2010). Footwall AHe ages and Pliocene pre-extensional paleodepths are plotted versus along-strike distance. The location of young (< 4 Ma) AHe ages correlate with the location of the geothermal anomaly. An inflection in the AHe age versus along-strike distance profile occurs at ~25 – 30 km and is coincident with the boundary between the Mt. Grant and Coryville block, marked by a NE-SW-striking cross fault and an en echelon step in the range front.

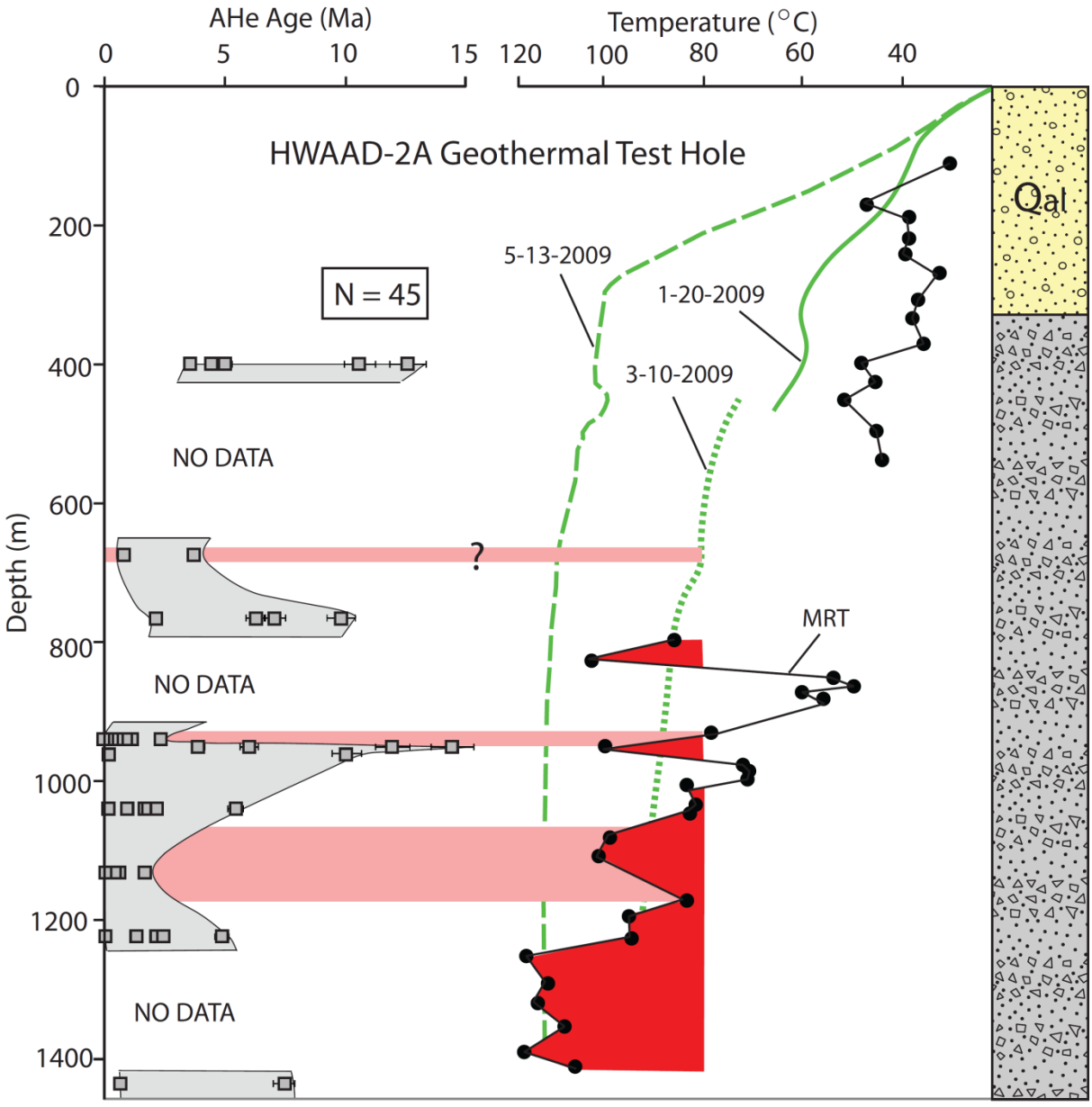
AHe Age (Ma)
0
5
10
15
Temperature (°C)
120
100
80
60
40
0
200
400
600
800
1000
1200
1400
Depth (m)
HWAAD-2A Geothermal Test Hole
Qal
5-13-2009
1-20-2009
3-10-2009
N = 45
NO DATA
?
MRT
NO DATA
NO DATA

Figure 9. Well temperature and AHe age data from the HWAAD-2A borehole in the Wassuk Range hanging wall. Zones defined by partially and completely reset detrital AHe ages correlate with depth of temperature spikes (highlighted red) in the MRT log. These zones are interpreted as hydrothermal fluid migration pathways. The absence of correlation between AHe ages and down-hole temperature readings (green) implies the presence of a youthful geothermal anomaly.

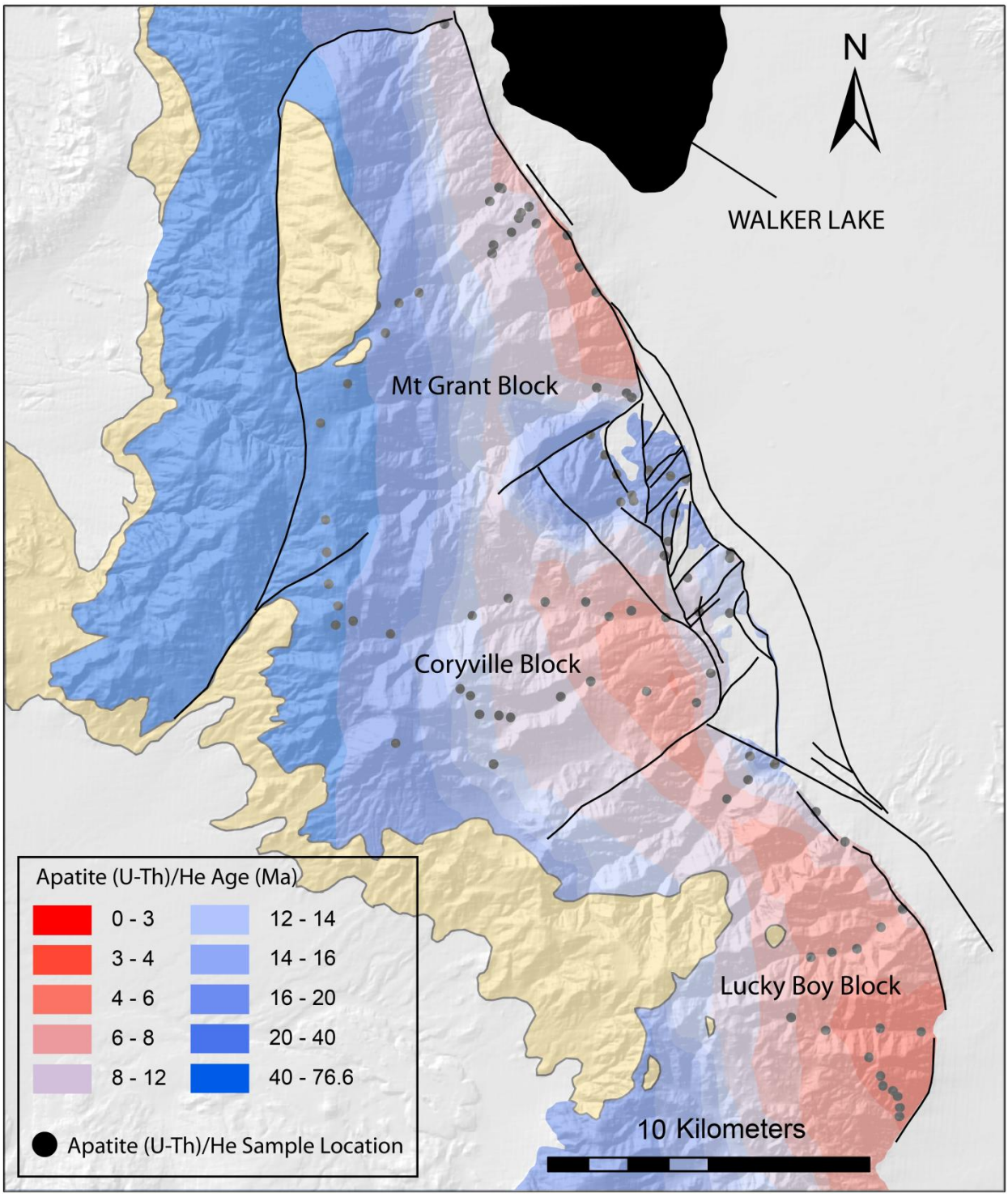
N
WALKER LAKE
Mt Grant Block
Coryville Block
Lucky Boy Block
Apatite (U-Th)/He Age (Ma)
0 - 3
3 - 4
4 - 6
6 - 8
8 - 12
12 - 14
14 - 16
16 - 20
20 - 40
40 - 76.6
Apatite (U-Th)/He Sample Location
10 Kilometers

Figure 10. AHe age contour map (ordinary kringing) for the southern Wassuk Range footwall. Young ages (≤ 4 Ma) along the Wassuk Range front define the along-strike variability of Pliocene exhumation that was primarily focuses along the SE corners of tilt blocks, and also at the southern terminus of the Wassuk Range. Similarly, Pliocene cooling ages also coincident with the location of Hawthorne geothermal anomaly A. The juxtaposition of Pliocene against Cretaceous to Miocene cooling ages on the eastern margin of the Coryville block links with mapped (Heinz et al., 2010) and previously unidentified range-front faults.

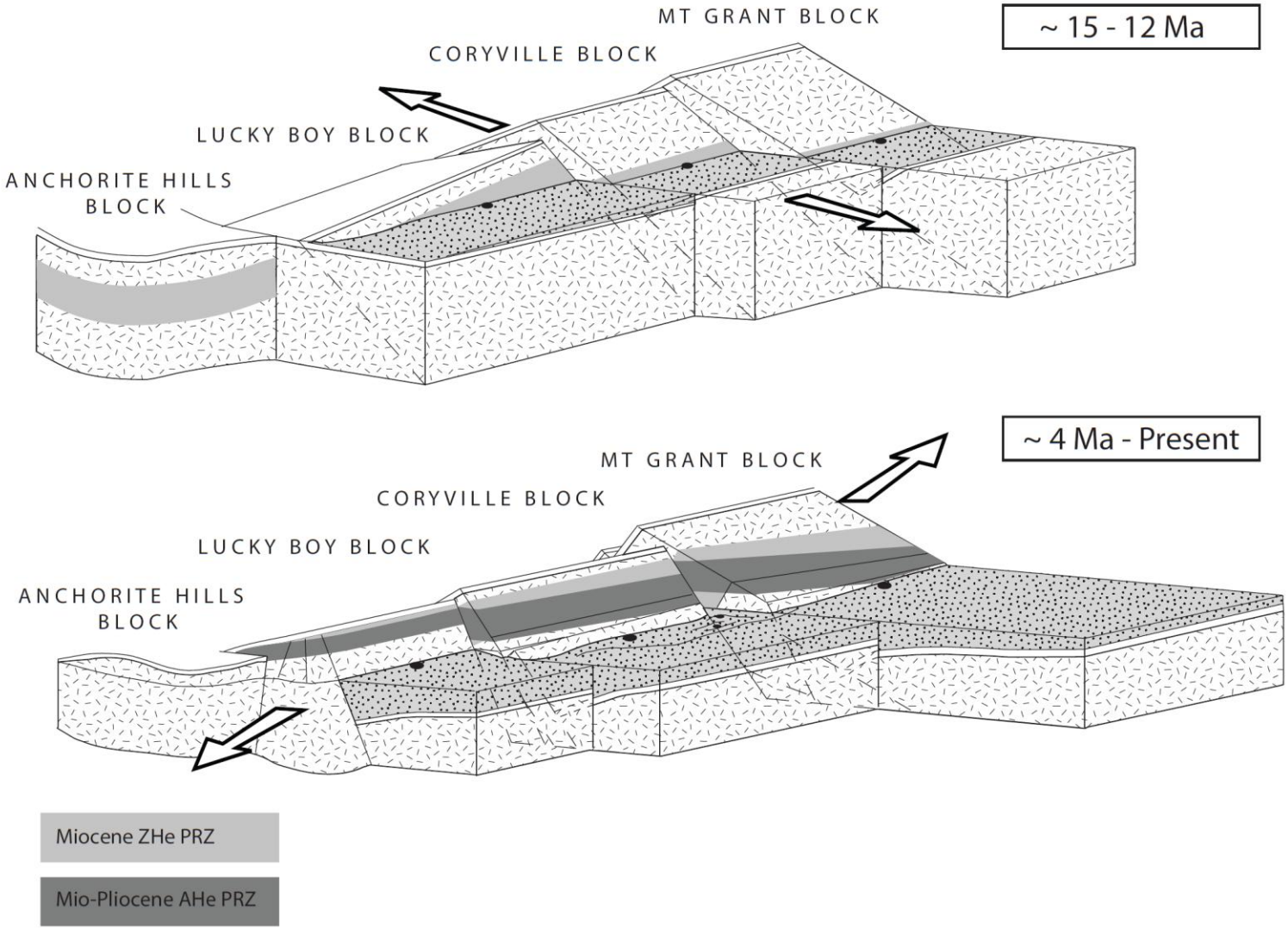
MT GRANT BLOCK
~ 15 - 12 Ma
CORYVILLE BLOCK
LUCKY BOY BLOCK
ANCHORITE HILLS BLOCK
~ 4 Ma - Present
MT GRANT BLOCK
CORYVILLE BLOCK
LUCKY BOY BLOCK
ANCHORITE HILLS BLOCK
Miocene ZHe PRZ
Mio-Pliocene AHe PRZ

Figure 11. Schematic block diagram reconstructions of the southern Wassuk Range based on the tilting of pre and syn-extensional volcanic rocks (Gorynski, Chapter 2), as well as apatite and zircon helium age mapping. E-W directed tilting in the Miocene was chiefly focused in the Mt. Grant block exposing the greatest structural paleodepths and pre-extensional isotherms. A second episode of tilting at ~4-5 Ma resulted from NW-SE directed extensional and focused young AHe and ZHe ages at the SE corners of tilt blocks, and at the southern terminus of the Wassuk Range.

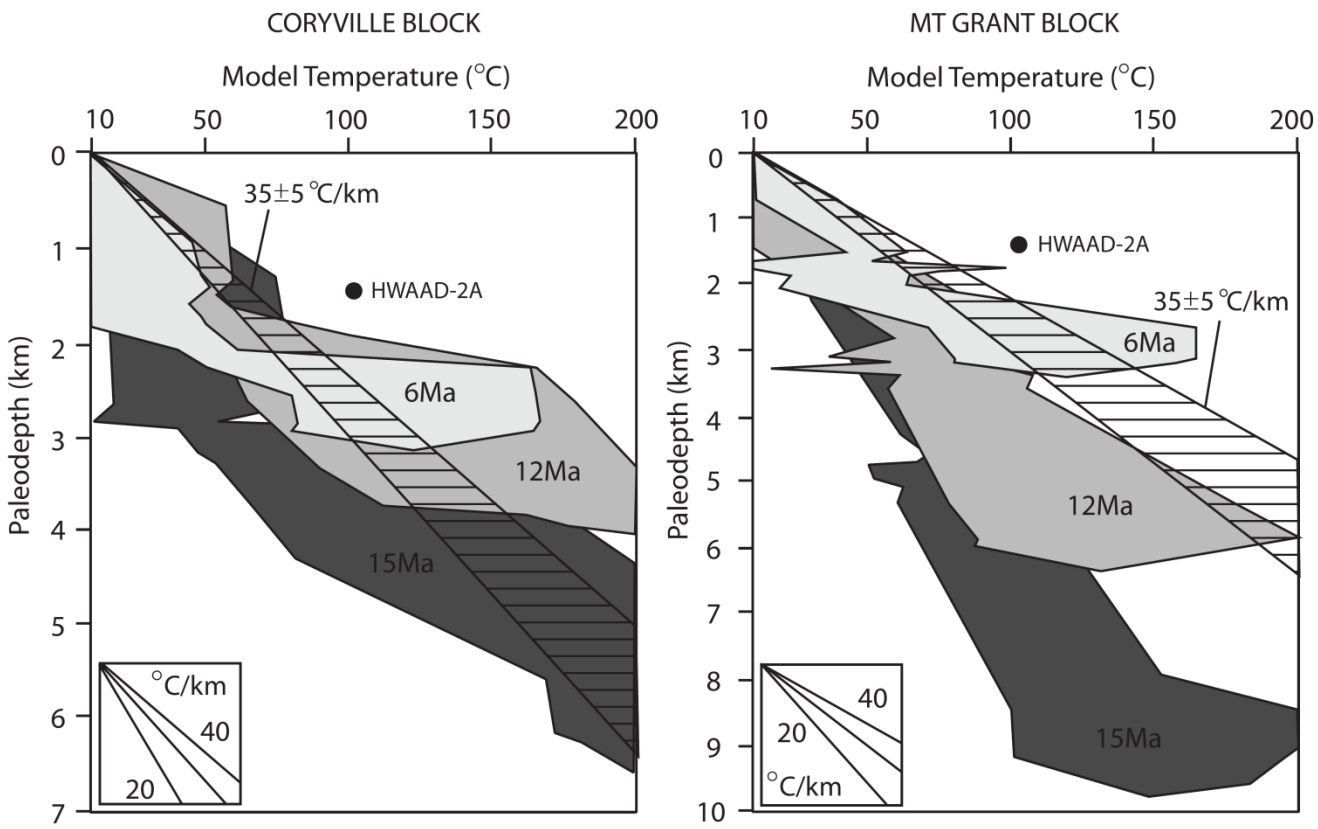
CORYVILLE BLOCK
Model Temperature (°C)
10
50
100
150
200
Paleodepth (km)
0
1
2
3
4
5
6
7
35±5 °C/km
HWAAD-2A
6Ma
12Ma
15Ma
°C/km
40
20
MT GRANT BLOCK
Model Temperature (°C)
10
50
100
150
200
Paleodepth (km)
0
1
2
3
4
5
6
7
8
9
10
HWAAD-2A
35±5 °C/km
6Ma
12Ma
15Ma
40
20
°C/km

Figure 12. Model temperature vs. paleodepth profiles from the 15, 12 and 6 Ma time periods, for both the Coryville and Mt. Grant blocks. An increase in the geothermal gradient since the Miocene is attributed to advection during rapid footwall exhumation throughout the Miocene. The most dramatic increase in geothermal gradient is from the Mt Grant block where large degrees of tilting exposed the deepest structural paleodepths in the study area. A second episode of rapid footwall exhumation (not shown here) initiated at ~4 – 5 Ma and likely raised the geothermal gradient to its present-day values. Also plotted are the modern regional geothermal gradient (35 ± 5 °C/km) and the bottom-hole temperature for the HWAAD-2A geothermal test hole in the Wassuk Range hanging wall.

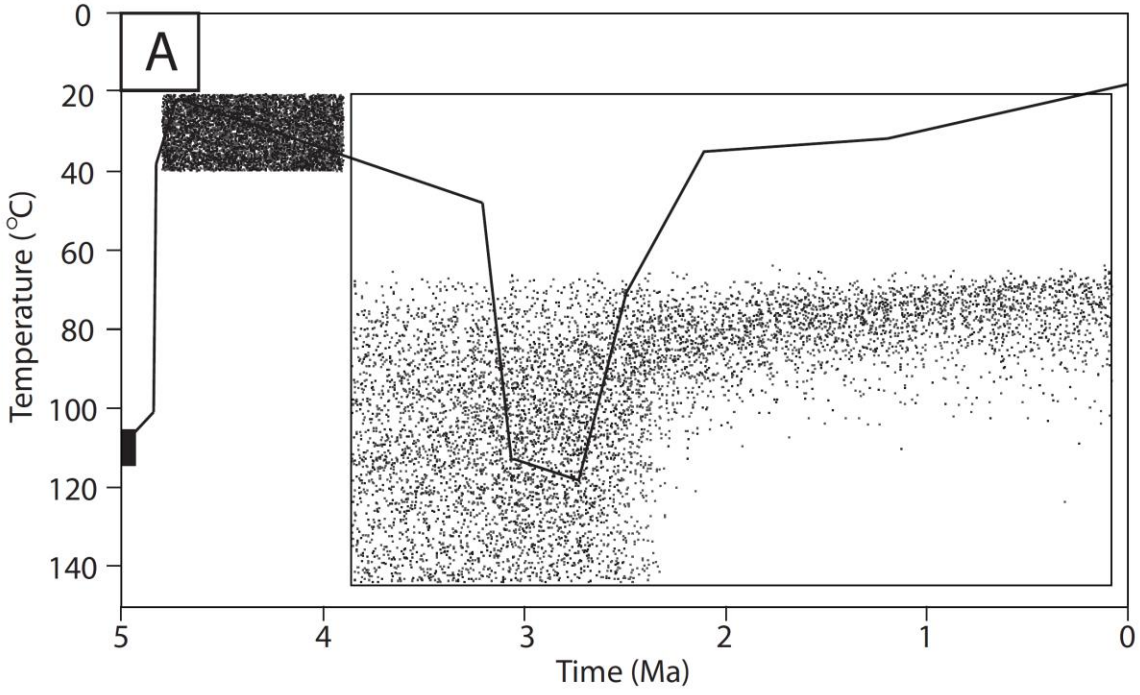
A
Temperature (°C)
0
20
40
60
80
100
120
140
5
4
3
2
1
0
Time (Ma)

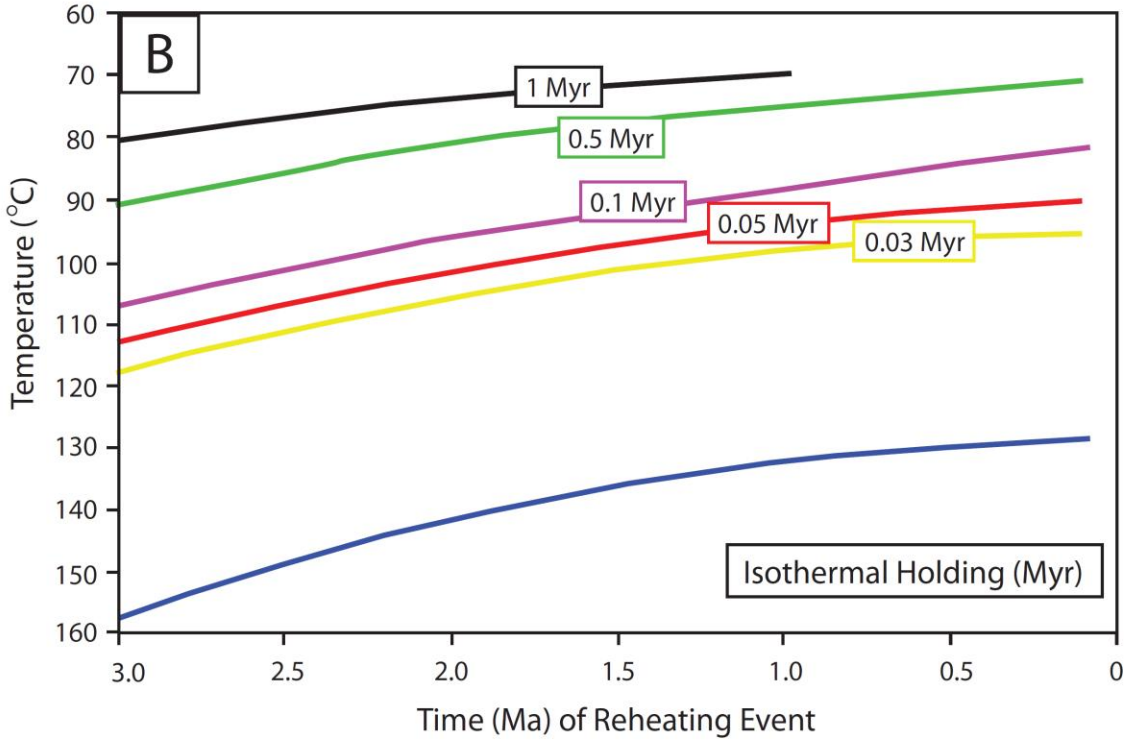
B
1 Myr
0.5 Myr
0.1 Myr
0.05 Myr
0.03 Myr
Isothermal Holding (Myr)
Temperature (°C)
60
70
80
90
100
110
120
130
140
150
160
3.0
2.5
2.0
1.5
1.0
0.5
0
Time (Ma) of Reheating Event

Figure 13. Inverse [A] and forward [B] models for sample 08WR17. Initial time-temperature constraints [A] were determined from the AHe vs. paleodepth profile from the Mt Grant block (Figure 5). Nodes from inverse modeled time-temperature histories are plotted and demonstrate a post- 3 Ma reheating event. A variety of isothermal reheating events were modeled in a forward sense, and plotted above [B]. These models predict that reheating resulted from interaction with temperatures ranging between ~70 and 160 °C, depending on the time and duration of an isothermal reheating event. Reheating for this sample was likely related to the migration of hot hydrothermal fluids along range-front structures. Based on the short-lived longevity of hydrothermal fluid pathways and the youthfulness of the Hawthorne geothermal system, temperature estimates for this reheating event (i.e., hydrothermal fluids) are between ~100 – 135 °C.

Sample	Latitude	Longitude	Elevation	Age [Ma]	± (6%) [Ma]	U [ppm]	Th [ppm]	Sm [ppm]	He [ncc]	F_T	ESR
08WR01	38.4291	-118.6311	1770	9.9	0.6	32	79	46	0.137	0.64	44
08WR02	38.4208	-118.6204	1812	8.2	0.5	26	72	29	0.204	0.68	84
08WR03	38.3883	-118.6319	2056	4.8	0.3	34	53	20	0.072	0.64	72
08WR04	38.3898	-118.6243	2011	4.6	0.3	13	33	93	0.020	0.61	62
08WR05	38.3909	-118.6156	1946	5.0	0.3	26	39	24	0.073	0.67	77
08WR06	38.3971	-118.6071	1870	5.1	0.3	22	42	40	0.073	0.65	76
08WR07	38.4023	-118.5995	1787	6.4	0.4	22	57	28	0.117	0.67	81
08WR08	38.5982	-118.7513	1666	4.2	0.3	4	6	1	1.516	0.67	46
08WR09	38.6022	-118.7480	1597	4.9	0.3	12	12	8	0.032	0.72	43
08WR10	38.6019	-118.7469	1555	5.9	0.4	17	17	44	0.009	0.56	33
08WR11	38.5837	-118.7501	1948	8.4	0.5	19	29	524	0.014	0.58	55
08WR12	38.5897	-118.7432	1886	11.4	0.7	9	22	39	0.017	0.61	39
08WR13	38.5937	-118.7409	1881	13.1	0.8	9	22	45	0.021	0.61	39
08WR14	38.5952	-118.7400	1788	12.1	0.7	13	31	50	0.036	0.63	41
08WR15	38.5969	-118.7373	1703	8.2	0.5	5	25	42	0.005	0.55	56
08WR16	38.5923	-118.7344	1593	8.3	0.5	9	18	35	0.105	0.65	44
08WR17	38.5734	-118.7126	1408	2.6	0.2	17	26	22	0.026	0.70	68
08WR18	38.5466	-118.7119	1500	4.5	0.3	20	3	67	0.031	0.67	72
08WR19	38.5452	-118.7012	1424	4.2	0.3	15	10	59	0.025	0.67	72
08WR20	38.5441	-118.6993	1412	4.4	0.3	19	19	70	0.014	0.62	39
08WR22	38.5214	-118.6795	1414	47.7	2.9	8	18	47	0.132	0.62	39
08WR23	38.5147	-118.7025	1728	14.2	0.9	25	47	76	0.211	0.66	75
08WR24	38.5150	-118.6979	1743	10.4	0.6	20	40	74	0.105	0.66	75
08WR25	38.5167	-118.6986	1664	13.3	0.8	19	41	78	0.090	0.61	66
08WR26	38.5237	-118.6927	1534	44.1	2.6	30	25	73	0.454	0.64	69

Sample	Latitude	Longitude	Elevation	Age [Ma]	± (6%) [Ma]	U [ppm]	Th [ppm]	Sm [ppm]	He [ncc]	F_T	ESR
08WR27	38.5223	-118.6850	1469	76.6	4.6	26	17	35	0.721	0.67	45
08WR28	38.4821	-118.7547	2084	11.3	0.7	30	52	44	0.164	0.64	70
08WR29	38.4872	-118.7419	1949	8.8	0.5	18	26	26	0.086	0.66	75
08WR30	38.4865	-118.7287	1873	5.4	0.3	19	33	28	0.068	0.66	44
08WR31	38.4866	-118.7143	1818	9.2	0.6	23	31	35	0.192	0.71	88
08WR32	38.4826	-118.7058	1744	4.2	0.3	32	41	32	0.083	0.69	79
08WR33	38.4844	-118.6980	1765	4.3	0.3	23	40	18	0.051	0.65	73
08WR34	38.4826	-118.6857	1656	3.6	0.2	82	72	38	0.214	0.70	86
08WR35	38.4845	-118.6739	1587	4.7	0.3	17	27	26	0.050	0.66	76
08WR36	38.4842	-118.6629	1525	42.7	2.6	10	8	22	0.076	0.66	48
08WR37	38.5685	-118.7911	3442	5.5	0.3	9	83	109	0.033	0.67	48
08WR42	38.5352	-118.8101	2791	56.4	3.4	19	55	45	0.229	0.58	36
08WR43	38.5081	-118.8076	2836	58.1	3.5	36	82	106	0.334	0.60	38
08WR46	38.4841	-118.8027	2936	55.6	3.3	20	50	93	0.340	0.65	41
08WR47	38.4788	-118.8033	2846	25.2	1.5	3	6	21	0.022	0.68	50
08WR48	38.4801	-118.7971	2728	42.5	2.5	12	13	63	0.091	0.65	42
08WR49	38.4766	-118.7836	2417	15.6	0.9	21	15	85	0.106	0.70	49
08WR54	38.5723	-118.7758	2797	15.6	0.9	25	27	8	0.057	0.63	42
08WR60	38.4407	-118.7461	2346	11.6	0.7	14	17	65	0.152	0.71	53
08WR61	38.4460	-118.7810	3117	15.7	0.9	25	29	47	0.065	0.59	36
08WR62	38.4617	-118.7585	2976	16.0	1.0	14	25	89	0.194	0.67	46
08WR63	38.4597	-118.7548	2847	14.3	0.9	27	48	33	0.422	0.69	48
08WR64	38.4545	-118.7514	2650	13.7	0.8	22	24	87	0.070	0.66	45
08WR65	38.4544	-118.7445	2553	12.5	0.8	23	37	74	0.205	0.69	50
08WR66	38.4540	-118.7403	2449	11.6	0.7	25	47	61	0.107	0.63	41

Sample	Latitude	Longitude	Elevation	Age [Ma]	± (6%) [Ma]	U [ppm]	Th [ppm]	Sm [ppm]	He [ncc]	F_T	ESR
08WR68	38.4600	-118.7226	2255	7.9	0.5	32	36	58	0.122	0.68	49
08WR69	38.4644	-118.7120	2136	5.9	0.4	85	71	45	0.294	0.68	47
08WR70	38.5334	-118.7138	1646	66.2	4.0	11	21	36	0.697	0.62	40
08WR71	38.5278	-118.7086	1662	44.5	2.7	14	28	36	0.438	0.64	42
08WR73	38.5040	-118.6854	1703	8.9	0.5	18	26	58	0.150	0.71	53
08WR74	38.5000	-118.6866	1797	7.8	0.5	35	41	47	0.149	0.68	47
08WR75	38.4938	-118.6782	1646	6.9	0.4	6	13	16	0.209	0.82	89
08WR76	38.4589	-118.6742	1792	3.1	0.2	9	10	13	0.061	0.79	75
08WR77	38.4443	-118.6548	1786	27.8	1.7	39	234	76	2.606	0.66	47
08WR78	38.4422	-118.6459	1709	33.0	2.0	7	12	13	0.567	0.79	74
08WR79	38.5892	-118.7233	1442	2.8	0.2	31	47	14	0.022	0.66	45
08WR80	38.5802	-118.7189	1422	4.3	0.3	5	2	12	0.057	0.81	81
08WR81	38.5118	-118.6831	1526	10.1	0.6	25	44	58	0.232	0.69	51
08WR82	38.4618	-118.6920	2034	4.5	0.3	25	33	18	0.084	0.69	50
08WR85	38.4673	-118.6694	1722	3.3	0.2	18	18	2	0.094	0.77	68
08WR87	38.4376	-118.6554	1752	4.0	0.2	8	12	13	0.084	0.79	76
08WR88	38.4322	-118.6628	1818	3.6	0.2	10	21	17	0.128	0.80	80
09WR90	38.6477	-118.7687	1339	11.8	0.7	27	55	24	0.050	0.59	36
09WR91	38.3679	-118.5920	1885	2.8	0.2	7	11	5	0.088	0.83	98
09WR92	38.3713	-118.6385	2332	5.3	0.3	32	48	21	0.076	0.63	41
09WR93	38.3678	-118.6262	2244	2.8	0.2	26	43	18	0.079	0.71	54
09WR94	38.3680	-118.6170	2547	3.2	0.2	29	49	15	0.115	0.73	58
09WR95	38.3688	-118.6068	2024	3.0	0.2	27	45	13	0.108	0.72	56
09WR101	38.5013	-118.6629	1476	6.3	0.4	16	19	22	0.053	0.67	46
09WR102	38.4996	-118.6633	1541	6.7	0.4	10	13	21	0.039	0.67	46

Sample	Latitude	Longitude	Elevation	Age [Ma]	± (6%) [Ma]	U [ppm]	Th [ppm]	Sm [ppm]	He [ncc]	F_T	ESR
03WL40	38.3442	-118.5994	1938	4.17	0.3						
03WL41	38.3606	-118.6105	2494	3.20	0.2						
03WL42	38.3554	-118.6063	2403	3.30	0.2						
03WL43	38.3527	-118.6053	2312	4.04	0.2						
03WL44	38.3513	-118.6018	2260	3.82	0.2						
03WL45	38.3498	-118.6002	2196	3.80	0.2						
03WL46	38.3467	-118.5992	2080	3.30	0.2						

Table 1. Wassuk Range footwall sample location and AHe age data.

Sample	Age [Ma]	± (6%) [Ma]	Depth [m]	U [ppm]	Th [ppm]	Sm [ppm]	He [nmol/g]	F_T	ESR	Temperature [°C]
09HW01-2	3.5	0.21	400	15	29	11	0.279	0.67	46	59
09HW01-3	4.4	0.26	400	13	30	37	0.349	0.72	55	59
09HW01-4	12.6	0.75	400	36	65	55	2.472	0.70	51	59
09HW01-5	5.0	0.30	400	16	22	10	0.452	0.77	69	59
09HW01-6	10.6	0.64	400	29	47	32	1.720	0.74	61	59
09HW06-1	3.7	0.22	674	19	25	26	0.294	0.59	35	80
09HW06-2	0.8	0.05	674	15	24	25	0.056	0.60	37	80
09HW08-1	7.1	0.43	766	19	36	35	0.647	0.61	38	85
09HW08-2	2.2	0.13	766	16	20	30	0.139	0.57	34	85
09HW08-3	6.2	0.37	766	23	42	40	0.752	0.67	46	85
09HW08-4	9.8	0.59	766	19	25	29	0.739	0.56	33	85
09HW08-5	19.0	1.14	766	12	5	11	0.837	0.63	38	85
09HW10-1	0.0	0.00	939	16	33	31	-0.001	0.59	36	88
09HW10-2	1.0	0.06	939	17	20	19	0.074	0.63	40	88
09HW10-3	0.1	0.01	939	21	30	29	0.012	0.61	38	88
09HW10-5	2.3	0.14	939	21	21	13	0.179	0.55	32	88
09HW10-6	0.0	0.00	939	36	58	47	0.002	0.55	33	88
09HW10-7	1.1	0.07	939	27	22	22	0.103	0.53	30	88
09HW10-8	0.5	0.03	939	27	41	39	0.050	0.51	29	88
09HW10-9	0.6	0.04	939	13	9	17	0.027	0.58	34	88
09HW10-4	0.3	0.02	939	24	18	21	0.028	0.54	31	88

Sample	Age [Ma]	± (6%) [Ma]	Depth [m]	U [ppm]	Th [ppm]	Sm [ppm]	He [nmol/g]	F_T	ESR	Temperature [°C]
09HW11-2	3.9	0.23	950	13	19	7	0.262	0.71	53	88
09HW11-3	14.4	0.86	950	24	41	17	1.747	0.67	46	88
09HW11-4	11.9	0.72	950	7	5	29	0.339	0.66	43	88
09HW11-6	6.0	0.36	950	34	35	20	1.020	0.75	62	88
09HW12-1	0.2	0.01	961	24	108	18	0.027	0.51	30	88
09HW12-2	10.1	0.60	961	16	32	33	0.919	0.72	56	88
09HW13-4	5.4	0.32	1040	20	9	16	0.378	0.57	33	90
09HW13-5	0.2	0.01	1040	31	24	23	0.022	0.53	30	90
09HW13-6	1.0	0.06	1040	33	51	48	0.147	0.61	38	90
09HW13-7	1.7	0.10	1040	21	11	13	0.129	0.61	37	90
09HW13-8	1.8	0.11	1040	17	18	26	0.130	0.62	39	90
09HW14-1	1.7	0.10	1132	25	46	32	0.200	0.61	39	91
09HW14-2	0.4	0.02	1132	9	9	8	0.012	0.54	31	91
09HW14-3	0.6	0.04	1132	25	33	41	0.065	0.61	38	91
09HW14-4	0.1	0.00	1132	13	12	8	0.004	0.57	33	91
09HW15-1	1.4	0.08	1223	21	35	22	0.114	0.52	30	92
09HW15-2	2.2	0.13	1223	14	12	16	0.123	0.61	37	92
09HW15-3	2.5	0.15	1223	30	36	27	0.304	0.59	36	92
09HW15-4	0.0	0.00	1223	16	26	27	0.003	0.56	33	92
09HW15-5	4.9	0.29	1223	62	74	40	1.293	0.62	39	92
09HW18-1	7.4	0.45	1435	8	9	24	0.319	0.75	60	95
09HW18-3	0.6	0.04	1435	13	14	16	0.035	0.62	39	95

Table 2. Sample depth, temperature and AHe age data from the HWAAD-2A borehole in the Wassuk Range hanging wall.